IAEA-TECDOC-1395

Intercomparison and Validation of computer codes for thermalhydraulic safety analysis of heavy water reactors

IAEA
International Atomic Energy Agency

August 2004

IAEA-TECDOC-1395

Intercomparison and Validation of computer codes for thermalhydraulic safety analysis of heavy water reactors

IAEA
International Atomic Energy Agency

August 2004

The originating Section of this publication in the IAEA was:

Nuclear Power Technology Development Section
International Atomic Energy Agency
Wagramer Strasse 5
P.O. Box 100
A-1400 Vienna, Austria

INTERCOMPARISON AND VALIDATION OF COMPUTER CODES FOR THERMALHYDRAULIC SAFETY ANALYSIS OF HEAVY WATER REACTORS

IAEA, VIENNA, 2004
IAEA-TECDOC-1395
ISBN 92–0–106004–1
ISSN 1011–4289

Printed by the IAEA in Austria
August 2004

FOREWORD

Activities within the frame of the IAEA's Technical Working Group on Advanced Technologies for HWRs (TWG-HWR) are conducted in a project within the IAEA's subprogramme on nuclear power reactor technology development. The objective of the activities on HWRs is to foster, within the frame of the TWG-HWR, information exchange and co-operative research on technology development for current and future HWRs, with an emphasis on safety, economics and fuel resource sustainability.

One of the activities recommended by the TWG-HWR was an international standard problem exercise entitled: "Intercomparison and validation of computer codes for thermalhydraulics safety analyses". Intercomparison and validation of computer codes used in different countries for thermalhydraulics safety analyses will enhance the confidence in the predictions made by these codes. However, the intercomparison and validation exercise needs a set of reliable experimental data. The RD-14M Large-Loss Of Coolant Accident (LOCA) test B9401 simulating HWR LOCA behaviour that was conducted by Atomic Energy of Canada Ltd (AECL) was selected for this validation project. This report provides a comparison of the results obtained from six participating countries, utilizing four different computer codes. General conclusions are reached and recommendations made.

The IAEA expresses its appreciation to the CANDU Owners Group (COG) for releasing the experimental data to the international community, and to D. Richards of AECL, Canada for leading the activity. The IAEA officer responsible for this publication was R. Lyon of the Division of Nuclear Power.

EDITORIAL NOTE

The use of particular designations of countries or territories does not imply any judgement by the publisher, the IAEA, as to the legal status of such countries or territories, of their authorities and institutions or of the delimitation of their boundaries.

The mention of names of specific companies or products (whether or not indicated as registered) does not imply any intention to infringe proprietary rights, nor should it be construed as an endorsement or recommendation on the part of the IAEA.

CONTENTS

CHAPTER 1. INTRODUCTION

Intercomparison and Validation of Computer Codes for Thermalhydraulics Safety Analyses is an International Atomic Energy Agency (IAEA) activity designed to facilitate international co-operative research and promote information exchange on computer codes for thermalhydraulic safety analyses. The objective has been to enhance the safety analysis capabilities of the participants and the effective use of their resources, through this international co-operation.

In the first meeting in November 1999, it was decided that the RD-14M experimental facility, a full vertical-scale representation of a CANDU® heat transport system, would be used as a benchmark data generating facility. Further, experimental data for RD-14M test B9401, a LOCA test, were selected as a benchmark data set for the intercomparison and validation exercise. This test was a large LOCA — one broken pass and one unbroken pass, conducted in the RD14M facility in Canada. For a break of this type, pump forces balance those of the break for the "broken" pass, and a flow split and low flows are obtained, resulting in fuel-element simulator heatup. Subsequently, the "RD-14M Facility Description" [1] along with the data set for the "RD-14M Test B9401" were distributed to the participating institutions in early summer of 2000. Since test B9401 was an integral test with over 558 variables measured, it was necessary to identify a much smaller subset of important variables for this intercomparison activity.

The purpose of the second meeting held in 2000 July was threefold. The document: "RD14M Facility Description" [1], was discussed together with the data set for the B9401 test which was selected at the first consultancy meeting. A detailed nodalization strategy and input data preparation for the CATHENA code was provided. Finally, guidance was provided by the representative from Italy for the preparation of the input data for other codes, and to discuss the theory behind detailed techniques for nodalization and error analysis.

The third meeting was held in 2001 May, with the objective of reviewing and discussing nodalizations, input data sets, steady state calculations and transient calculations that had been prepared by participants, and then to plan the completion of the activity, including finalization of the intercomparisons to be done and the structure of the final report.

The fourth meeting of this Group was held 2002 December. Prior to the meeting, a draft of the Comparison Report was generated by AECL, Canada, and distributed to participants. The purpose of the meeting was to discuss the comparisons, formulate conclusions and recommendations, and finalize the report. This was largely accomplished. However, when reviewing the calculations from each participant, a number of inconsistencies were identified in the calculations. Some were related to emergency core Cooling (ECC) flow, and after further investigation the cause was found to be an incorrect characterization of low-pressure ECC flow in [1]. It was agreed that participants would re-run their cases with a more accurate characterization (to be supplied by AECL) and re-submit. It was also agreed that the current case be modified to provide a more challenging additional problem for the codes, and that results also be reported for this comparison. AECL was tasked with proposing such a problem.

The fifth and final meeting took place in June 2003. The purpose of the meeting was to obtain any additional comments and to finalize the report.

CANDU® is a registered trademark of Atomic Energy of Canada Limited

CHAPTER 2. RD-14M EXPERIMENT LOOP

2.1. RD-14M Facility Description

The RD-14M facility, shown schematically in Figure 2.1, is a pressurised-water loop with essential features similar to the primary heat transport loop of a typical CANDU reactor. The facility is designed so that reactor typical conditions, such as fluid mass flux, transit time, pressure and enthalpy, can be achieved in the primary-side for both forced and natural circulation. The design incorporates the basic "figure-of-eight" geometry of a CANDU reactor, with five horizontal channels per pass and a 1:1 scaling of the vertical elevations throughout the loop. Each six-meter-long channel contains 7 electrically heated Fuel Element Simulators (FES), connected to end-fitting simulators. The feeder volumes, areas, and metal masses are appropriately scaled to the channels (7-pin FES). The thermal characteristics of the FES are similar to CANDU fuel in terms of power density, heat flux and heat capacity. The channel inlet and outlet-feeder piping arrangements are designed to represent Darlington Nuclear Generating Station (NGS) feeders.

Five reactor channel/feeder geometries were selected, representing three middle channels, one top channel, and one bottom channel. Preserving the 1:1 vertical scaling maintained similar hydrostatic pressures between RD-14M and a typical reactor. The inlet feeders are 1 –1.25" nominal schedule 40, while the outlet feeders are 1.25 –.50" nominal schedule 40. The above header piping is sized to give reactor-typical pressure drops.

A test section in RD-14M consists of an electrically heated section (fuel element simulators), inlet and outlet end-fitting simulators, a pressure tube, and a strongback to provide support for the test section.

The heated section is a 6-m long channel between the inlet and outlet end-fitting simulators, composed of a flow tube containing a 7-pin FES. Figure 2.2 is a cross-section of a typical RD-14M heated section. The FES pins are divided into 12 axial segments, each having a length of 495 mm and separated by short unheated sections to simulate fuel bundle spacers. The FES pins consist of a central core of magnesium oxide surrounded by an electrically heated Inconel 625 tube of 7.62 mm outside diameter. The tube is insulated from the 13.18 mm outside diameter stainless steel (type-304) sheath by a 2 mm thick annulus of boron nitride. The FES pins are surrounded by a 44.80 mm inside diameter, 57.20 mm outside diameter 316-type stainless steel flow tube that is surrounded by vermiculite insulation.

The RD-14M end-fitting simulators consist of a shield plug and liner tube contained within a flow tube. The RD-14M shield plug and liner tube annulus are sized to the reactor flow annulus using a 7:37 ratio. The end-fitting simulators are designed to reproduce the differential pressure and the thermal mass of typical reactor end-fittings.

The steam generators are scaled approximately 1:1 with typical CANDU steam generators, in terms of tube diameter, mass flux, and heat flux. The steam generators are 12 m in height and originally contained 44 U-tubes that have an outside diameter of 15.88 mm and a wall thickness of 1.13 mm. Over time, some U-tubes have developed leaks around the penetrations of instruments. These tubes have been plugged and are indicated in the electronic database. The secondary-sides of the steam generators contain an internal preheater and an external downcomer. Spiral-arm steam separators in the steam dome and flow restricting orifices in the external downcomer of the steam generators are used to produce reactor-typical recirculation

in the secondary-side. Sizing is based on the consideration of removing up to 5.5 MW from each of the steam generators.

Primary fluid circulation is provided by two centrifugal pumps. These deliver full reactor-typical head (about 225 m) at flowrates similar to a single reactor channel (about 24 kg/s). Primary circuit pressure is maintained by a loop pressuriser that contains an electrical heater.

Both inlet and outlet header breaks can be produced using the blowdown system. Replacing the end cap of the relevant header with a fast-acting ball valve simulates a break. A range of break sizes can be investigated by placing appropriately sized orifice plates immediately upstream of the fast-acting 6" ball valve leading to the blowdown stack. The coolant is discharged through the ball valve and into the blowdown stack (20" nominal pipe) that passes through the roof of the test facility.

The RD-14M facility is equipped with an Emergency Core Coolant (ECC) system that provides cooling to the FES under postulated LOCA conditions. The ECC system injects emergency coolant into the primary heat transport system through any combination of the four headers. The ECC system is controlled by the primary loop pressure at header 7 with the isolation valves automatically opening when header 7 pressure drops below a predetermined pressure.

Major loop parameters of the RD-14M facility are compared with a typical CANDU reactor in Table 2.1. More detailed information on the RD-14M facility can be found in [1].

2.2. Instrumentation

The RD-14M facility is extensively instrumented for data gathering during experiments. The data acquisition system consists of several input multiplexers each connected to an analog-to-digital converter, and a VAX 4000 Model 200 computer using a VMS 5.5-2 operating system capable of scanning up to 768 channels at a maximum rate of about 50 ms per scan (20 Hz). Data for RD-14M test B9401 was sampled every 100 ms (10 Hz). Parameters measured included fluid and FES temperatures, gauge and differential pressures, levels, flows, void fractions, power, and pump speeds. Over 400 temperatures at various locations around the primary and secondary loops were measured. Fluid and FES temperatures were measured using K-type thermocouples and resistance temperature detectors (RTDs). Gauge and differential pressures and levels were measured using Rosemount pressure transducers. Flowrates at the inlet and outlet of each test section, at the pump discharge, and the feedwater to each boiler were measured using turbine flow meters. The void fraction at the inlet and outlet of each boiler, at the pump discharge, and at the inlet and outlet of each test section was measured using three-beam, two-beam, and single-beam gamma densitometers, respectively. It should be noted that the void fraction at the inlet and outlet of each test section is measured approximately 2-m upstream and downstream of each test section. The locations of the gamma densitometers and turbine flow meters, in relation to test section 11, are shown in Figure 2.3 as an example. Table 2.2 lists the measurement uncertainties. More detailed information on the RD-14M instrumentation and control of the RD-14M facility can be found in [1].

Table 2.1. Comparison of RD-14M Loop Characteristics with a Typical CANDU Reactor

CHARACTERISTIC	RD-14M	Typical CANDU Reactor
Operating Pressure (MPa)	10	10
Loop Volume (m^3)	1.01	60
Heated Sections/Fuel Channels	1 indirectly heated 7-rod bundle	Nuclear fuel 37-rod bundle
Number of Channels Per Pass	5	95
Length (m)	6	12 x 0.5
Fuel Rod Diameter (mm)	13.1	13.1
Flow Tube ID (mm)	44.8	103.4
Power (kW/channel)	3x750 and 2x950	5410*
Pumps:	Single Stage	Single Stage
Impeller Diameter (mm)	381	813
Rated Flow (kg/s)	24	24*
Rated Head (m)	224	215
Rated Speed (rpm)	3560	1790
Specific Speed	565	2000
Steam Generators:	Recirculating U-tube	Recirculating U-tube
Tube Bundle Height (m)	9.42	9.42
Number of Tubes	44	37*
Tube ID (mm)	13.6	14.75
Tube OD (mm)	15.9	15.9
Secondary Heat Transfer Area (m^2)	41	32.9*
Secondary Volume (m^3)	0.9	0.131*
Recirculation Ratio at Full Power	6:1	5.7:1
Heat Flux (kW/m^2)	130	165
Elevation Difference (m) (bottom heated section to top of boiler U-tubes)	21.9	21.9

* average per channel

Table 2.2. Experimental Measurement Uncertainties

Measured Parameters	**Measurement Uncertainties**
Fluid and FES Sheath Temperatures	± 2.0^{o}C
Heated Section Power	± 1.5% of measured power
Pressures and Differential Pressures	± 0.5% of span*
Level	± 0.5% of span*
Flowrates	± 0.5% of span*
Break Orifice Size	± 0.1% of diameter (0.03 mm)

* The instrument range can be obtained from the scan list file (B9401B.DAT) on the CD-ROM

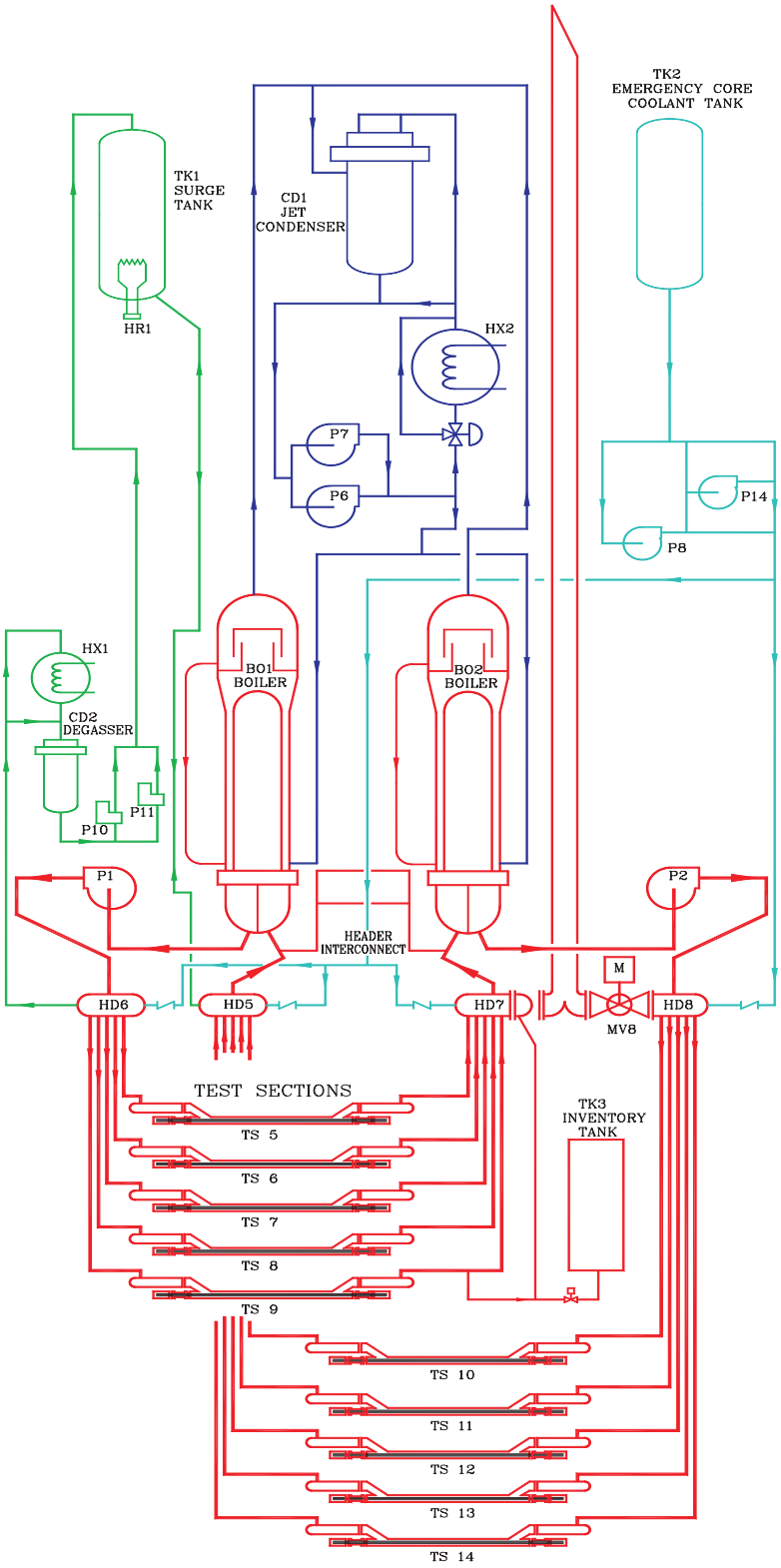

Fig. 2.1. Schematic of the RD-14M Facility.

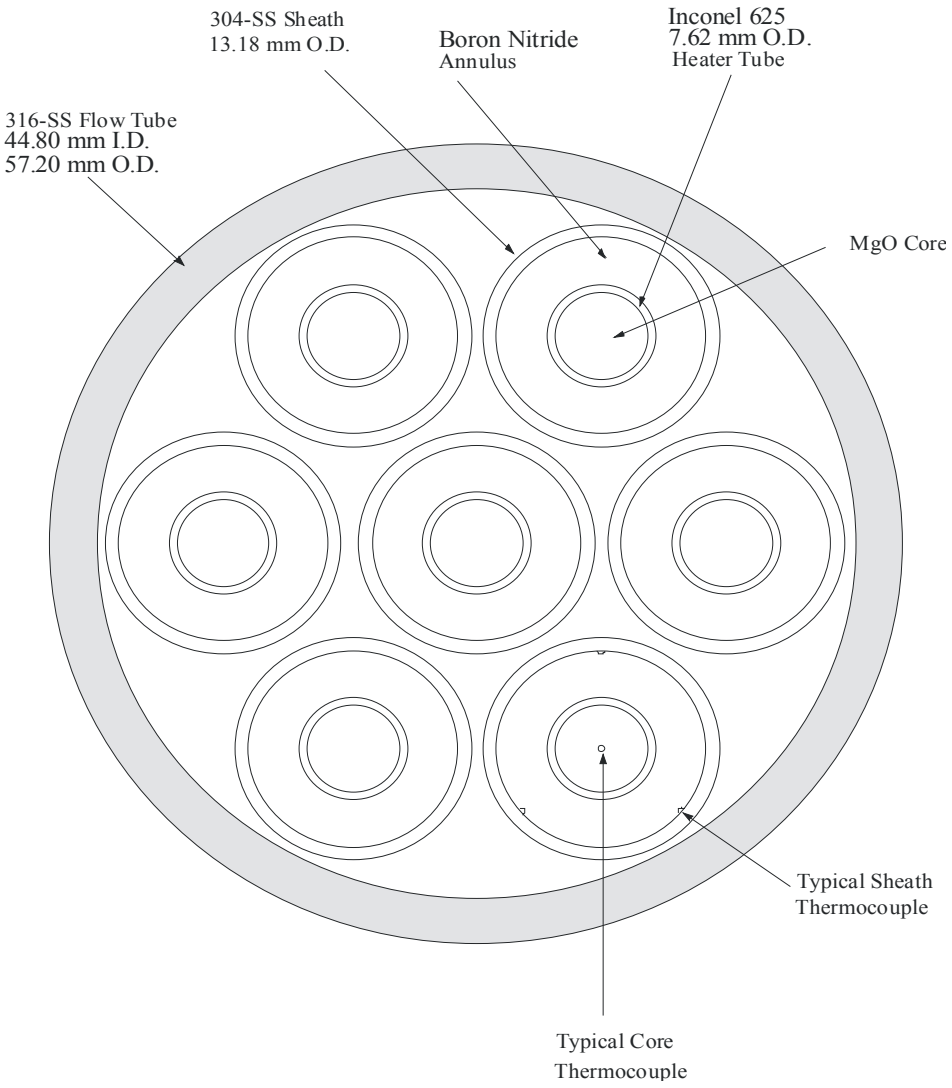

Fig. 2.2. Cross-Section of an RD-14M Heated Section.

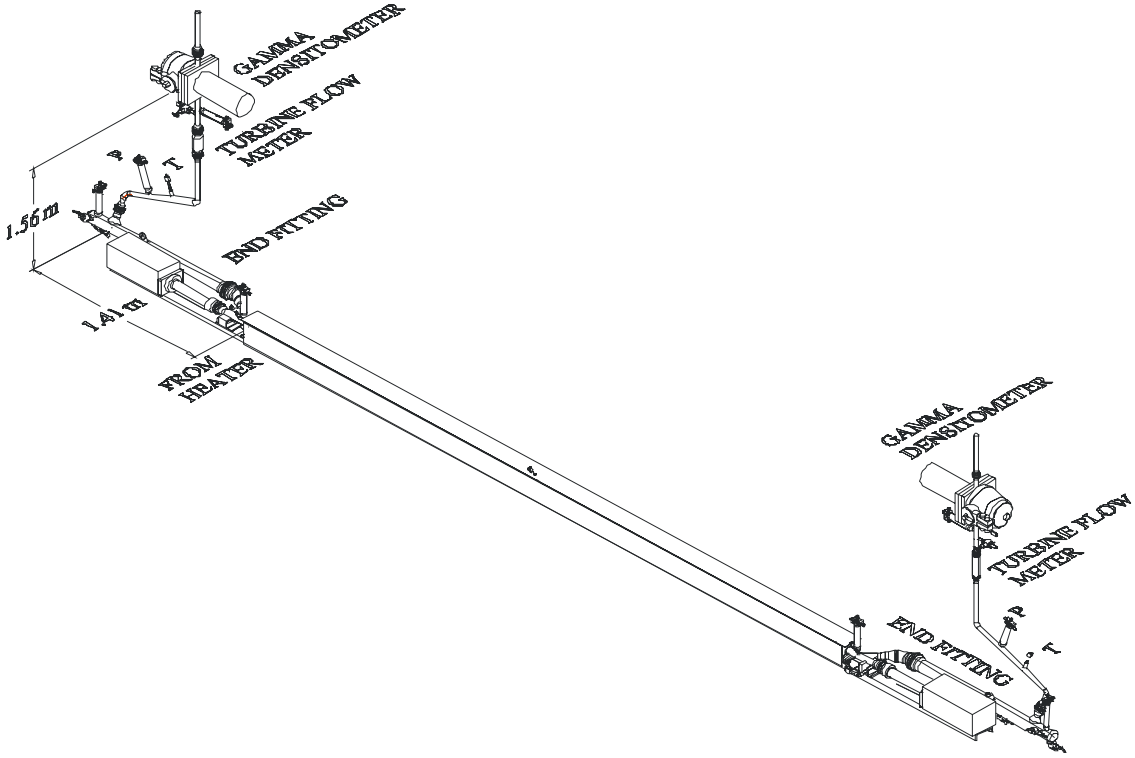

Fig. 2.3. Location of Instrumentation at the Inlet and Outlet of Test Section 11.

CHAPTER 3. RD-14M TEST B9401

3.1. Test Description

RD-14M test B9401 was a 30-mm diameter inlet-header break test with a high pressure pumped emergency coolant injection available. The test was conducted in 1994. The purpose of the test was to investigate the primary loop response to a 30-mm break with emergency coolant injection.

3.2. Initial Conditions

The nominal initial conditions for the test B9401 were as follows:

Primary System:	outlet header pressure	10.0 MPa(g)
	nominal input power	4.0 MW per pass
Secondary System:	steam drum pressure	4.4 MPa(g)
	steam separator level	55%
	feedwater temperature	186°C
ECC System	mode	pumped
	Temperature	30°C

3.3. Test Procedure

The loop was operated until the required single-phase, steady state conditions were achieved and then scanning of the experimental data was started. The blowdown valve was opened at inlet header 8 to simulate the break approximately 10 s after data sampling started. About two seconds after break initiation, the power (Table 3.1) was decreased to represent decay power levels and the primary loop pump speeds were exponentially decreased to simulate the loss of class IV power. The ECC isolation valves were opened at 20.6 s and the Pressurizer was manually isolated at 22.8 s. The test was terminated after an extended period at decay power levels. A summary of the significant events in test B9401 is shown in Table 3.2.

3.4. Experimental Measurements

Five hundred fifty-eight (558) channels of data were scanned and collected during test B9401. Detailed test information can be found in Appendix B of [1], and the electronic version of the data was provided on CD-ROM. A subset of the measured variables was used for the inter-comparison activity.

Table 3.1. Input Power for B9401

HEATED SECTION	POWER (kW)	
	Full	Decay
5	772 kW	28 kW
6	775 kW	29 kW
7*	819 kW	36 kW
8	954 kW	42 kW
9	786 kW	29 kW
10	761 kW	29 kW
11	765 kW	30 kW
12*	797 kW	33 kW
13	940 kW	40 kW
14	771 kW	29 kW

* Pin #5 in heated section 7 and pin #7 in heated section 12 were disconnected in this test.

Table 3.2. Significant Events in RD-14M Experiment B9401

SIGNIFICANT EVENTS	TIME OF EVENTS FOR TEST B9401 (s)
Data gathering started	0.0
Initiation of blowdown valve opening	10.0
Initiation of power ramp	12.0
Initiation of primary pump rundown	12.0
ECC isolation valves open and high pressure ECC injection started	20.6
Pressurizer (TK1) isolated	22.8
High pressure pumped ECC terminated, low pressure ECC started	116.2
Primary pumps off	213.2
Low pressure ECC terminated	350.7

CHAPTER 4. PARTICIPANTS, CODES, AND IDEALIZATIONS

A list of participants, along with the computer code used by each participant is provided in the following Table:

Participant	*Code Used*
Argentina (CNEA)	FIREBIRD-III MOD1-77
Canada (AECL)	CATHENA MOD 3.5d
India (BARC)	RELAP5/MOD3.2
Italy (U. of Pisa)	RELAP5 Mod3.2.2g
Republic of Korea (KINS)	RELAP5/CANDU
Romania (CNPP)	FIREBIRD-III MOD1-77

In the following Sections each participant's code and idealization are described.

4.1. Argentina

4.1.1. The FIREBIRD Code

The FIREBIRD III MOD1-77 digital computer program [2] is a general network code developed primarily for predicting the thermalhydraulic behaviour of a CANDU power reactor plant during a postulated loss of coolant accident and the subsequent emergency coolant injection.

- Because of its generality, the code can also be used to solve a large variety of general two-phase flow problems.
- The code models the physical system in terms of a set of interconnecting nodes. A node corresponds to a user-defined segment of pipe, a component, or a boundary condition in the system. The geometrical parameters required for a node are volume for the hydraulic calculation, and pipe mass, pipe inside diameter and pipe thickness for the thermal calculation.
- The connection between two nodes is defined as a link. A link has geometrical parameters of length, hydraulic diameter, pipe roughness, elevation, and flow area.
- The mass and energy conservation equations are solved for nodes. Quantities such as pressure, density, internal energy, temperature, void fraction, static quality and enthalpy, pipe and fuel temperature distribution, heat transfer and heat transfer coefficient, and pump heat are node properties.
- The momentum equation is solved for links. Quantities such as flow, drift flow, flow quality and enthalpy, friction factor, two-phase multiplier, pump head, pump speed, and pump torque are link properties.

The core of FIREBIRD III MOD1-77 contains generalized algorithms for solving the mass, momentum and energy conservation laws associated with mass and heat transfer in a piping network, as well as constitutive relationships such as slip and drift and heat transfer coefficient correlations.

In order to model particular systems and event sequences, FIREBIRD III MOD1-77 code is structured to include a set of user subroutines which a user adapts to provide specific component models, control logic or boundary conditions for a given problem.

- The code couples these boundary conditions and control logic with its fluid flow conservation equations, fluid state equation, and constitutive relationships to form the governing equations for the system being analyzed.
- Since the problem-dependant programming is transferred to the user routines, different sets of user routines for various problems can be handled with a single reference code.
- The boundary conditions and control logic could be in the form of pressure-enthalpy boundary conditions, flow-enthalpy boundary conditions, breaks in pipes, valve actions, pump condition changes, and fuel power variations.

In the hydraulic calculations, an implicit numerical integration technique is used to solve the one-dimensional three-equation fluid flow conservation equations together with the fluid state equation.

- In the code, both light water and heavy water properties are available, and the two-phase fluid is assumed to be in thermal equilibrium. However, to account for the effects of the relative phase velocity, a drift-flux model with several slip and drift correlations is included in the code. The thermal non-equilibrium effect is accounted for in the pressure calculation through an adjustment of fluid property derivatives.
- In the thermal calculations, a one-dimensional heat conduction equation is solved implicitly to obtain the heat transfer to the coolant and the temperature distribution within the pipe and the fuel. The resulting heat transfers to the fluid are then coupled explicitly with the hydraulic calculations.

Some additional data about the program:

Program version
FIREBIRD-III MOD1-77 VER 0.131

Restrictions of the complexity of the problem
Maximum number of nodes: 400
Maximum number of links: 400

Program language used
FORTRAN-77

Other programming and operating information
FIREBIRD-III MOD1-77 has built in-restart capabilities.
It also outputs data for plotting.

The program uses the Atomic Energy of Canada Limited library routines SORTAG, XTIME, MFID, JOBNAME, TRIEQN, AND CHNGFX.

Name and establishment of authors

M.R. Lin, et al, Atomic Energy of Canada Limited, CANDU Operations, Sheridan Park Research Community, Mississauga, Ontario L5K 1B2.

4.1.2. The FIREBIRD Idealization

The FIREBIRD idealization of RD-14M for modelling Test B9401 consisted of a nodalization briefly described in the following sub-sections.

Some of its relevant dimensions are summarized in Table 4.1.

Figure 4.1 shows a global sketch of the primary system nodalization.

Below header model

Feeders

Observing actual feeders shape led to a different number of nodes for representing each pair of them (see Figure 4.1):

	Number of Nodes	
	Inlet Feeder	Outlet Feeder
HS 5 – HS 10	4	4
HS 6 – HS 11	4	5
HS 7 – HS 12	6	7
HS 8 – HS 13	5	7
HS 9 – HS 14	7	7

End-fitting simulators

Geometrical parameters were observed as far as possible. The model consisted of 3 nodes: one for the annulus, one for the stagnant volume, and one for the lateral pipe. The way in which these three volumes were configured is shown in Figure 4.2.

Fuel Element Simulators

Each fuel element simulator was modelled with 12 nodes, one per heated section (Figure 4.2).

Power generation

A power transient was defined as a boundary condition for each individual test section, applying a “decay factor” obtained by dividing total power at present time step by initial total power.

Headers

Each of them was represented by 4 nodes.

All pipes connected to headers (feeders, pump discharge, ECC pipes, pressurizer line) were linked to the corresponding node, as it is shown in Figure 4.3.

Above header piping

Steam generator inlets; pump suctions and pump discharges were represented by one node each (Figure 4-1)

Steam generators

The steam generators' primary side was represented as follows (Figure 4.1):

The U-tubes were divided in 7 nodes, one of them corresponding to the preheater zone.
The boiler inlet and outlet plena consisted of 1 node each.

Pressurizer

This component was implemented in this model as a boundary condition for its interaction with the primary system.

Secondary side

The secondary side of the steam generator was included as a boundary condition, where pressure and temperature evolution were defined.

Feedwater flow and steam flow were also treated as boundary conditions.

Emergency coolant injection system

The emergency coolant injection system model is shown in Figure 4.4.

Sixteen nodes were used for representing the operation of both phases of the ECC system: high-pressure pumped ECC and low-pressure recovery phase ECC.

ECC tank TK2 and water proceeding from distilled water tanks were considered as boundary conditions, as well as the return line to TK2.

Pump 8 and Pump 14 were implemented in the subroutine USPUMP.

FIREBIRD Subroutines Modified for Modelling RD-14M Test B9401

User subroutines

The following user subroutines were modified in order to complete the simulation model:

USBCL3	Feedwater flow Vapor flow	
USBCN7	Steam generator pressure Pressurizer pressure	
USQG	Heated sections power	
USPUMP	P14 head P8 head	
USCOVAL	Pressurizer isolation valve	
	ECC valves	MV 22
		MV4, MV5, MV6, MV7
		CV10
		MV12
USPTRP	Primary pumps rundown	
USPOS	Secondary side boundary conditions	
USMODL	Control variables calculation	

Reference code subroutines

Subroutine PUMPAN (which belongs to the group of reference code subroutines) was also modified for modelling primary pumps during rundown.

Break Model

Three discharge models are used:

(1) The orifice discharge model for subcritical flow

(2) The Henry-Fauske two-phase critical flow model for a sharp edge orifice

(3) Critical discharge through a sharp edge orifice for superheated steam

Heat storage and release from heated sections:

FIREBIRD is mainly intended to be used for modeling heat storage and release from the core of a nuclear reactor. The model available in the code can simulate fuel and sheath temperature transients in what is referred to as a *fuel model*.

However, the RD14-M heaters have a heat capacity close to that of CANDU reactor fuel and therefore the FIREBIRD fuel model was applied for the simulation, with the heaters treated as if they were actual fuel elements.

Fuel model

The code solves the fuel dynamics equation by an implicit finite-difference method.

These calculations are explicitly coupled with the hydraulic calculations.

Mathematical model

Cylindrical co-ordinates (r,θ,z) with the Z axis (r=0) placed at the fuel centerline are considered. Neglecting all axial and angular non-uniformities, the governing transient heat conduction equation becomes:

$$C \cdot \frac{\partial T}{\partial t} = \frac{1}{r} \cdot \frac{\partial}{\partial r} \cdot \left(k \cdot r \cdot \frac{\partial T}{\partial r} \right) + Q$$

Numerical technique

The temperature field is represented by a set of discrete values defined at some fixed radial positions:

$$T_i(t) = T(r_i, t) \quad i = 1,2,....$$

Each temperature, $T_{i,}$ is associated with a ring of material extending from $r_{i-1/2}$ to $r_{i+1/2}$.

Current capabilities

Nodalization

- The maximum number of fuel rings allowed is 6.
- The thickness of each fuel ring must be the same
- A single ring for the sheath is used.

Average pin and hot pin level calculations

In this model, two types of calculations are performed:

- **Average pin calculation**

  Average pin power and heat transfer coefficient based on homogeneous coolant.

  The resulting total power to coolant provides the coupling between the fuel dynamics and hydraulics.

- **Hot pin calculation**

  Fuel behaviour under stratified flow conditions.

  This effect is estimated by calculating the temperatures of a hot pin located at each of the user specified elevations (levels).

  No thermohydraulic feedback from this calculation.

Data for fuel heat calculation

- Number of vertical regions of each fuel node for *hot pin level fuel* calculation.
- Number of regions of equal radial thickness.
  One region is assumed for the sheath.
- Thermal properties
  Constant
  Variable: determined dynamically by the code

Initial and boundary conditions

The initial conditions for Test B9401 simulation are presented in Table. 4.2. These are the results of a *steady state* calculation that implied 2 consecutive runs: an actual *steady state* run followed by a *"do nothing" transient* run (transient calculation without any perturbation). This table lists some calculated variables as well as some quantities that were imposed as boundary conditions. The experimental values are included for comparison (measured quantities at time = 10 s, before experiment initiation).

Table 4.3 shows the sequence of events imposed for the transient calculation.

Table 4.1. Main Dimensions of the FIREBIRD Nodalization Developed for RD-14M

No	QUANTITY		VALUE
1	Total number of nodes		372
2	Total number of links		375
3	Number of nodes for each feeder		4 - 7
4	Number of nodes for end-fitting simulators		3
5	Number of nodes for each fuel element simulator		12
6	Number of nodes for each header		4
7	Number of nodes for above header piping	Steam generator inlet	1
		Pump suction	1
		Pump discharge	1
8	Number of nodes for steam generators (primary side)	Inlet plenum	1
		U-tubes	7
		Outlet plenum	1
9	Number of nodes for Emergency coolant injection system		16

Table 4.2. List of Relevant Initial Conditions for Test B9401 Simulation

No	QUANTITY	UNIT	EXP	CALC
1	Pressurizer pressure *	MPa	10.0	10.0
2	HD5 pressure	MPa	10.1	10.1
3	DP (HD8-HD5)	MPa	1.52	1.57
4	DP (HD6-HD7)	MPa	1.56	1.57
5	SGs pressure *	MPa	4.5	4.5
6	MCP1 flowrate	L/s	27.9	27.9
7	MCP2 flowrate	L/s	27.4	27.9
8	HS5 mass flowrate	L/s	5.0	5.2
9	HS6 mass flowrate	L/s	5.1	5.2
10	HS7 mass flowrate	L/s	–	6.1
11	HS8 mass flowrate	L/s	–	6.2
12	HS9 mass flowrate	L/s	5.1	5.1
13	HS10 mass flowrate	L/s	5.0	5.1
14	HS11 mass flowrate	L/s	5.1	5.2
15	HS12 mass flowrate	L/s	–	6.1
16	HS13 mass flowrate	L/s	–	6.3
17	HS14 mass flowrate	L/s	5.0	5.2
18	SG1 SL flowrate *	kg/s	1.9	1.9
19	SG1 FW flowrate *	kg/s	1.9	1.9
20	SG2 SL flowrate *	kg/s	2.0	2.0
21	SG2 FW flowrate *	kg/s	2.0	2.0
22	HD5 fluid temperature	°C	296.1	297.8
23	HD7 fluid temperature	°C	296.7	299.2
24	HD8 fluid temperature	°C	263.5	262.8
25	HD6 fluid temperature	°C	262.2	263.7
26	FW temperature *	°C	187	187
27	Void fraction at HS5 outlet	–	–	0
28	Void fraction at HS8 outlet	–	–	0
29	MCP speed *	RPM	3400	3400
30	Core total power *	Mw	8.13	8.13

* Imposed as a boundary condition

Table 4.3. Sequence of Events Imposed for the Transient Calculation

No	EVENT	TIME [s]
1	Simulation beginning	0.0
2	Open MV8 (break)	10.0
3	Step power down to decay levels Start primary pump rundown	12.0
4	ECC high pressure injection initiated	20.6
5	Pressurizer isolated	22.8
6	High Pressure ECC terminated Low Pressure ECC initiated	350.7
7	End of calculation	400.0

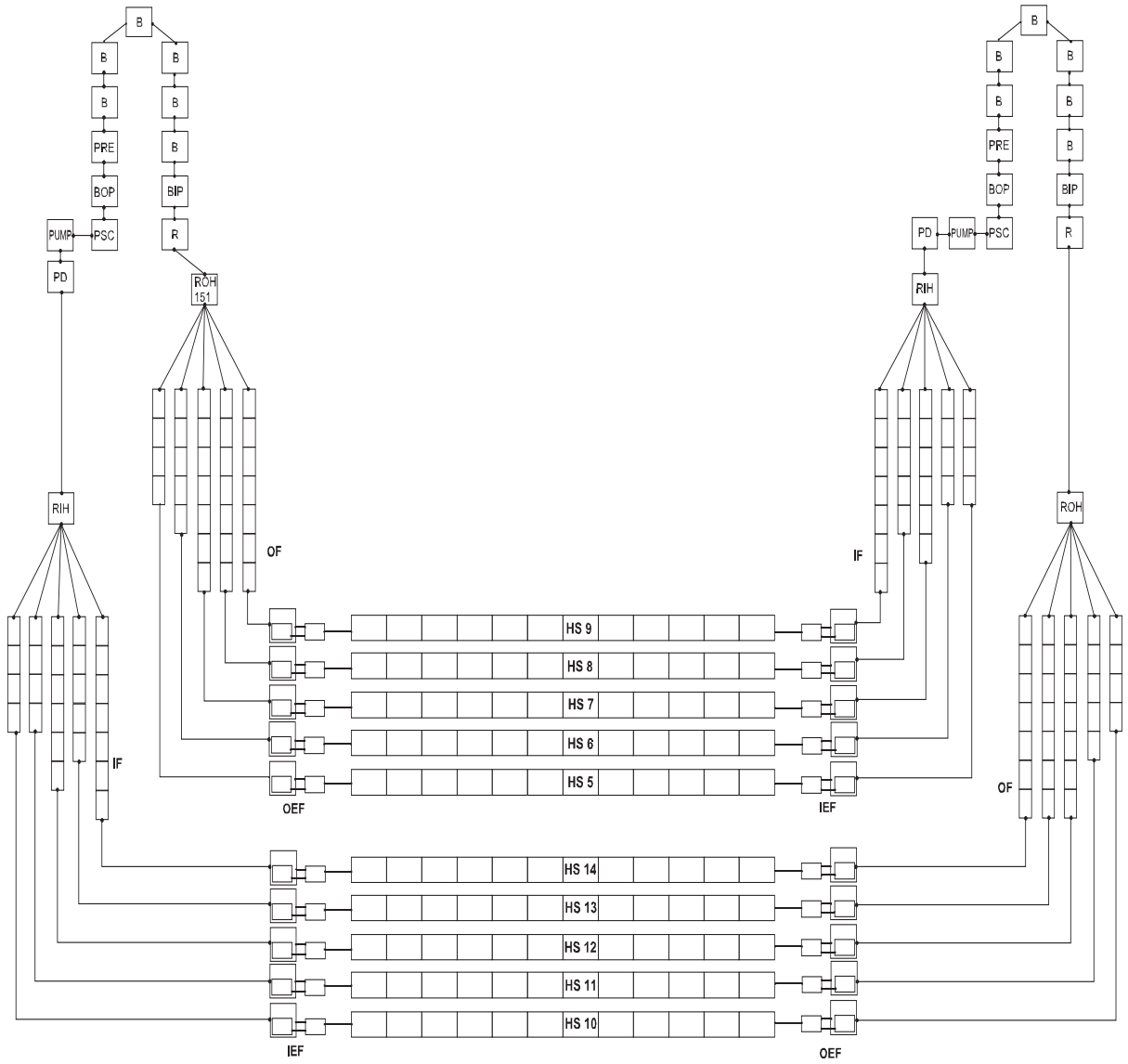

Fig. 4.1 Primary System Model.

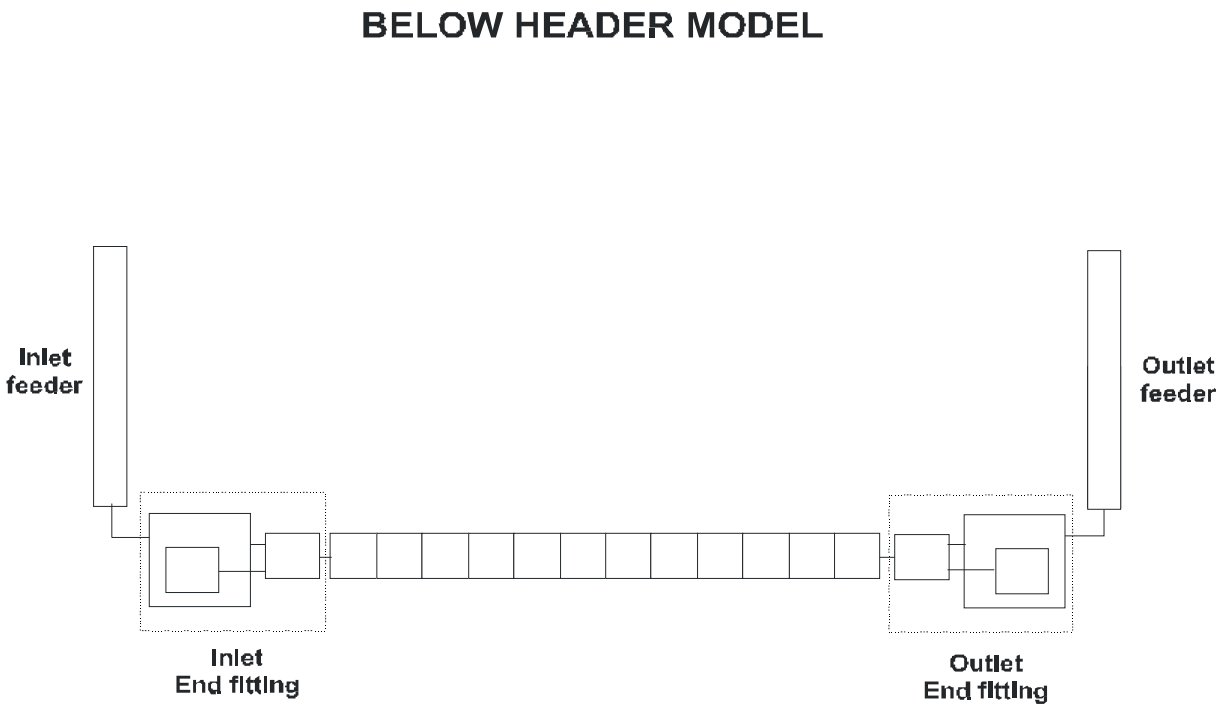

Fig. 4.2. Below Header Model.

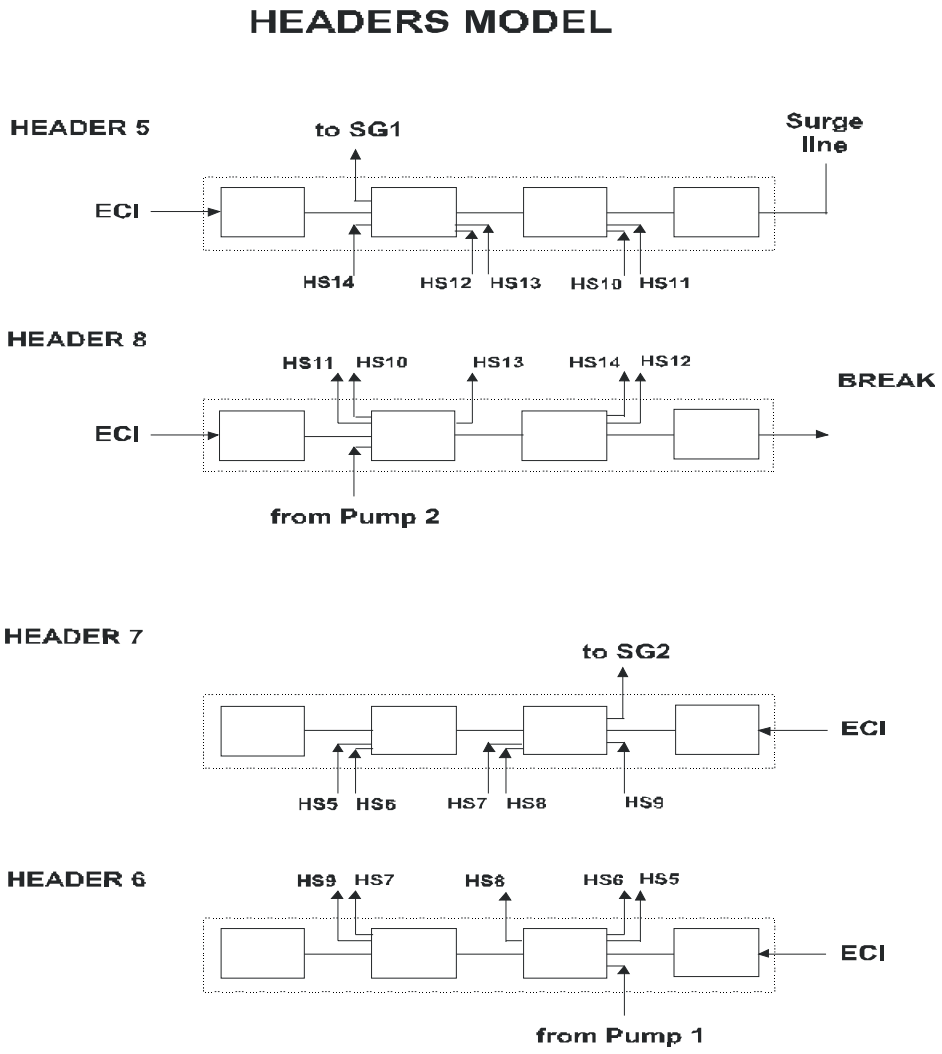

Fig. 4.3. Headers Model.

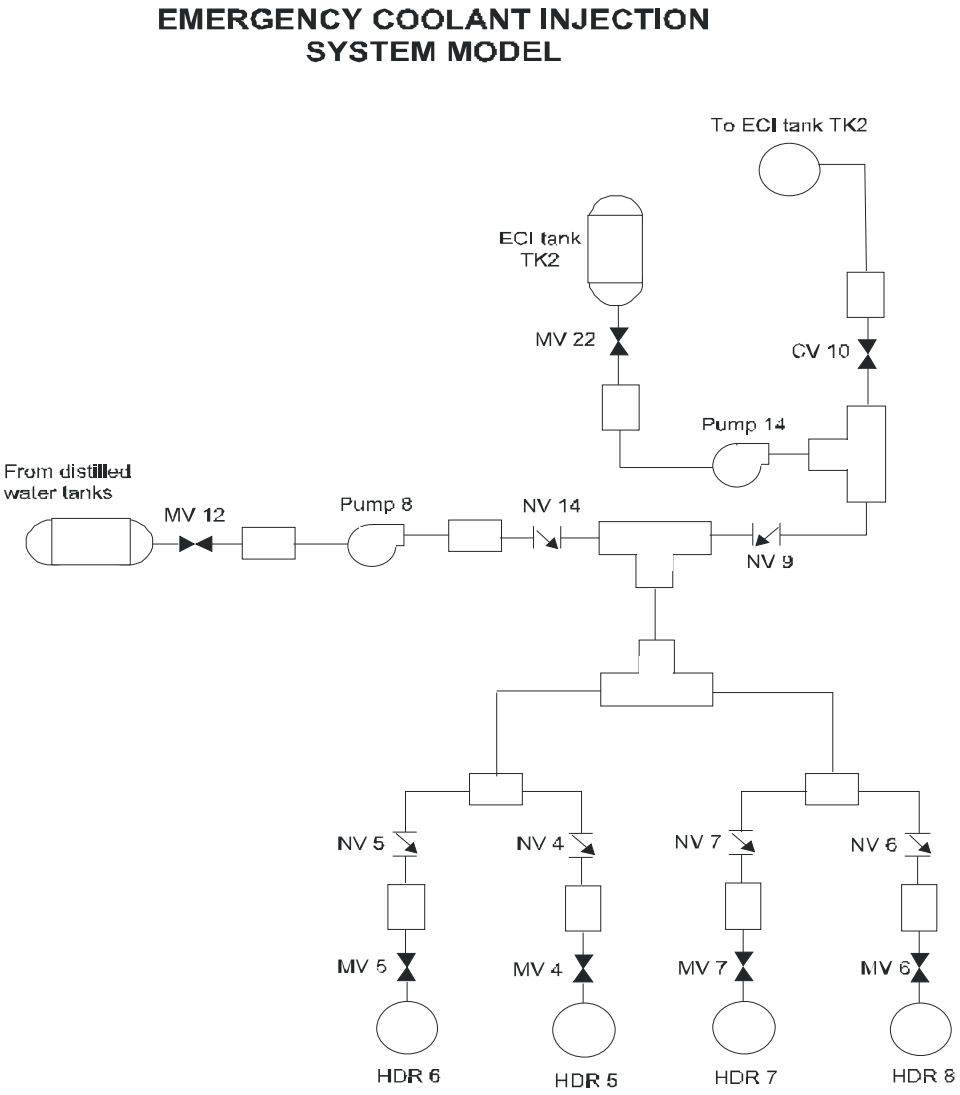

Fig. 4.4. Emergency Coolant Injection System Model.

4.2. Canada

4.2.1. The CATHENA Code

The acronym CATHENA stands for **C**anadian **A**lgorithm for **The**rmalhydraulic **N**etwork **A**nalysis. The CATHENA code was developed by Atomic Energy of Canada Limited (AECL) [3].

CATHENA uses a transient, one-dimensional, two-fluid representation of two-phase flow in piping networks. In the thermalhydraulic model, the liquid and vapour phases may have different pressures, velocities, and temperatures. In addition, up to four noncondensable gases may be included in the vapour phase. The thermalhydraulic model consists of solving six partial differential equations for the conservation of mass, momentum and energy for each phase. If noncondensable gases are included in a simulation, an additional mass conservation equation for the mass fraction of each noncondensable gas component is solved simultaneously with the two-fluid model conservation equations.

Interface mass, energy and momentum transfer between the liquid and vapour phases are specified using constitutive relations obtained either from the literature or developed from separate-effect experiments.

The code uses a staggered-mesh, one-step, semi-implicit, finite-difference solution method, that is not transit time limited. In the numerical solution method used, a system of finite-difference equations is constructed. These equations result from the linearization after integration of the partial differential mass, momentum and energy conservation equations over finite time and finite spatial (nodes for mass and energy and links for momentum) steps. In the CATHENA numerical method, the timestep is selected based on the rate of change of a set of parameters including pressure and void fraction.

The thermalhydraulic model in CATHENA includes pipe, volume, T-junction, reservoir and tank components. The pipe component is the main thermalhydraulic component and consists of one or more "nodes" where volume-related dependent variables (void fraction, pressure, phase enthalpy and noncondensable mass fractions) are calculated. These nodes are connected by "links" where the phase velocities are calculated. Volume components are used at the connection of multiple pipe components to more accurately calculate the pressure and flow distribution through the junction. T-junctions are used at the junction of three pipe components to calculate pressure loss coefficients that are dependent on the flow distribution (splitting or combining). Reservoir components are used to establish boundary conditions for a simulation. Tank components were developed to model pressurizers, Pressurizers and other vessels. The model assumes the tank can be divided into upper and lower regions. A two-fluid model is used to represent mass and energy conservation in each region and as a result non-equilibrium conditions can be modelled. The fluid (both vapour and liquid) momentum within the tank, however, is neglected and the pressure difference between the upper and lower regions is represented by a hydrostatic pressure balance.

The CATHENA code includes thermophysical properties for both light water (H_2O) and heavy water (D_2O). The pressure range of application of the fluid properties is from the triple-point pressure (611.73 and 660.1 Pa for H_2O and D_2O, respectively) to the critical pressure (22.0 and 21.66 MPa for H_2O and D_2O, respectively). The temperature range of light water properties is from 0°C to 2000°C and the temperature range of the heavy water properties is from 0°C to 800°C. The thermodynamic properties for light water are within 1.5% of values

obtained from the US National Bureau of Standards (NBS) steam table generating functions, Kestin *et al.* [4], and the property derivatives are within 5%. For vapour temperatures above 2000°C, the properties are obtained using the ideal gas approximation. The thermodynamic properties for heavy water are within 1.5% of the values obtained from the generating functions of Hill *et al.* [5] and the property derivatives are within 5%. For temperatures above 800°C, the ideal gas approximation is used.

Noncondensable gas properties for H_2, He, N_2, Ar, CO_2 and air are available in CATHENA. The thermodynamic properties for the noncondensable gases are assumed to obey the ideal gas law. The vapour-noncondensable gas mixture is assumed to obey Gibbs-Dalton thermodynamic relationships.

The comprehensive solid heat-transfer package used to model pipes or fuel in contact with the fluid has been given the acronym GENHTP; which stands for GENeralized Heat Transfer Package. The heat transfer package includes radial and circumferential conduction, thermal radiation and contact conduction between solid surfaces. The zirconium-steam reaction is included as a heat source (the H_2 resulting from the reaction is also calculated). The heat transfer package also includes a pressure-tube deformation model to account for expansion of a pressure tube resulting in either rupture or contact with the calandria tube. The heat-transfer package allows the connection of multiple solid surfaces of a heat transfer model to a single thermalhydraulic node or multiple thermalhydraulic nodes. As a result, very detailed modelling of a CANDU channel containing horizontal fuel bundles can be performed. Testing of CATHENA/GENHTP has shown high computational efficiency, as well as the advantage of closely coupling thermalhydraulic and fuel/channel behaviour. Heat transfer in deformed geometries (pressure tube/calandria tube/moderator, fuel element/pressure tube, etc.) may be modelled. One code, CATHENA, may be used for modelling the system thermalhydraulics, as well as detailed heat transfer modelling of a CANDU fuel channel.

The CATHENA code also includes system models for components like tanks, pumps, valves, emergency coolant injection accumulator, user definable junction resistances, and separators. Also included in the set of system models is a point-reactor kinetics model, a break-discharge model and a heat-balance calculation model. An extensive control system modelling capability is also provided for complete loop simulations (i.e. regulation and safety shutdown systems).

The thermalhydraulic code CATHENA was developed primarily for the analysis of postulated upset conditions in CANDU reactors; however the code has found a wider range of applications for the modelling of thermalhydraulic test facilities such as RD-14M, the Blowdown Test Facility and the CHAN Thermal-Chemical Test Facility, as well as research reactors such as MAPLE, NRU and McMaster Research Reactor.

4.2.2. The CATHENA Idealization

The CATHENA idealizations of the RD-14M facility primary and secondary side are shown in Figures 4-5 to 4-8. The CATHENA idealizations of the RD-14M facility ECC system common piping, and Darlington NGS modes are shown in Figure 4-8. A brief description of the primary side, secondary side and the ECC systems are presented in the following sub-sections.

Overview

The CATHENA idealization used to simulate test B9401 consisted of 530 thermalhydraulic nodes, 546 links and 179 wall heat transfer models. The calculation was performed with CATHENA MOD 3.5d/Rev 0, required approximately 17,000 simulation time steps for the 400 s transient, and took 1.0 hrs CPU time (PC Pentium III, 1063 Mz.).

The Henry-Fauske discharge model was used to simulate the break. In these simulations, a mixed flow regime was specified at the headers, the primary pumps discharge, and the secondary-side of the steam generators using the 'FIX-MIXED' option. The CATHENA flow regime map was developed primarily for fully developed flow along the axis of open pipes and pipes containing fuel bundles. At these locations, this is not the case and mixed flow conditions are expected for most of the transient.

Primary-Side Idealization

The RD-14M primary side consists of all piping connecting the headers, heated sections, steam generators, pumps and pressurizer. The idealization used to model the primary-side piping is shown in Figures 4-5 and 4-6.

In developing the primary-side idealization, the volume, length, flow area and elevation change of each CATHENA pipe component resembled, as closely as possible, the RD-14M test facility. This ensured that the fluid transit time and hydrostatic pressure changes around the loop were represented accurately in the simulation. Since CATHENA is a two-fluid code, horizontal and vertical sections of piping were not combined as one inclined pipe component, unless the horizontal or vertical sections were very short. The principal reason for the segregation between horizontal and inclined pipe sections was that the flow regime map used in each is quite different. Sections of piping that were inclined, but varied in the degree of inclination, were combined to simplify the idealization. The total volume of the primary-side idealization, excluding the pressurizer and the line connecting it to the primary loop, has been compared with the volume of the facility and found to be within 1 %.

The flow area of complicated geometries, such as the end fittings, boiler plenums and primary pumps were determined by dividing the volume of the component by the flow path length. This method proved to be acceptable provided the fluid velocities were not significantly different from those in the facility. Modelling of headers, using this procedure to account for the dead-end volumes, was not acceptable for this reason. Therefore, the dead volumes at the ends of the headers were modelled as separate pipe components with one closed end. Complicated geometries and intrusions into the fluid flow path of temperature measurement devices caused difficulties in determining values for the minor loss coefficients.

The heat transfer models in the GENeralized Heat Transfer Package (GENHTP) were used to model all solid components in contact with the fluid. They also account for the heat transfer from the primary fluid to the pipe walls and from pipe walls to the environment, or in the case of the steam generator tubes, to the secondary side. Pipe radii (inner and outer) were used in defining the metal mass and heat transfer area in contact with the primary fluid. The thermal properties used for the piping materials were obtained from CATHENA's internally stored temperature-dependent thermal properties. Heat losses to the environment were modelled by applying heat transfer coefficients, and a reference temperature of 20°C to the outside of piping components.

The heated section was modelled using a single pipe component divided into 6 equal length thermalhydraulic nodes. The 7-element FES bundle was represented by 3 "cylinder groups" to model the heat transfer split between the liquid and vapour phases under stratified flow conditions. The power distribution in the axial direction was assumed to be constant in the CATHENA model.

The CATHENA thermalhydraulic code provides a number of "system control" models that can be configured to perform the measurement and control functions of a reactor or the RD-14M test facility. System control models were used in these simulations to control the opening of the break, pressurizer isolation, heated section power rundown, primary pump speeds rundown and opening of the four ECC isolation valves. Opening of the break and closing of the pressurizer and ECC isolation valves was assumed to occur over a 0.1 s time span. Heat section power and pump speeds were extracted from experimental data.

A trip model was used to simulate the switch from high pressure ECC to low pressure pumped ECC. These functions are used to isolate the high pressure ECC line, open the pumped ECC isolation valve and startup the low-pressure ECC pump.

Secondary Side Idealization

The secondary-side idealization that was used to simulate these tests is shown in Figure 4-7. This idealization includes the steam generators up to the steam nozzle and that part of the feeder water line from the thermocouple location measuring the feedwater temperature to the steam generator feedwater inlets. The portion of the feedwater lines, upstream of this location was represented by flow and enthalpy boundary conditions. The secondary side steam generator outlet pressures were modelled using the pressure boundary conditions obtained from boiler steam dome pressures. Time varying feedwater flowrates, extracted from the experimental results, were imposed as the flow boundary conditions.

Junction resistance models were used to account for head losses in the contraction at the top of the riser section to the steam separator, expansion/contraction losses at the connection between the external downcomer and the hot leg of the steam generator, the expansion/contraction losses at the connection between the external downcomer and the steam drum and the resistance of the steam generator. Separator models were used to simulate the liquid separation at the bottom of the steam drum, and steam separation in the spiral-arm separator at the top of the steam drum. Valve/orifice models were used to account for the orifice in the external downcomers and the flow resistance through the hole in the longitudinal baffle box in the centre of the steam generators.

ECC System Idealization

The CATHENA idealization of the ECC configurations is shown in Figure 4-8. The idealizations of the ECC system included provision for both the high pressure ECC phase (high pressure ECC tank or high pressure pump) and low pressure ECC phase (low pressure pump) injection modes used in these experiments.

In the high pressure ECC phase, a polynomial pump head relation was used to characterize the high pressure pump (pump 14) behaviour in the Darlington NGS injection mode. A flow boundary condition was used to simulate the low pressure pumped ECC phase since it was suspected that the low pressure pump (pump 8) cavitated during these experiments. In these idealizations, the total predicted ECC flowrates were used to calculate a level in the ECC tank. Once the calculated level reached the ECC tank low level point, (-0.27 m), a switchover to

low pressure pumped ECC was initiated as in the experiments. A trip model was used to initiate the operation of the isolation valve in the main high-pressure line to accomplish the switchover to low pressure pumped ECC mode.

Tables 4-4, 4-5, and 4-6 give the main dimensions of the CATHENA nodalization, a comparison of experimental and predicted initial conditions, and the boundary conditions applied to the calculation.

Table 4.4. Main Dimensions of the CATHENA Nodalizations Developed for the RD-14M

No	QUANTITY	VALUE	NOTES
1	No of Hydraulic Nodes	530	
2	No of Links	546	
3	No of nodes for piping heat calculation	368	
4	No of nodes in the channel	6	
7	No of cards of the input deck (including comments and blank lines)	8620	

Table 4.5. List of Relevant Initial Conditions Measured and Calculated for the RD-14M, B9401 Experiment

No	QUANTITY	UNIT	EXP	CALC	NOTES
1	Pressurizer pressure	MPa	9.9	10.10	
2	HD5 pressure	MPa	10.0	10.10	
3	DP (HD8-HD5)/(HD6-HD7)	MPa	1.3-1.5	1.49 / 1.55	
4	SGs pressure	MPa	4.5	4.52	
5	MCP1 flowrate	Kg/s	21.9	21.81	
6	MCP2 flowrate	Kg/s	21.6	22.13	
7	HS5 mass flowrate	Kg/s	4.0 – 4.1	4.10	
8	HS6 mass flowrate	Kg/s	4.0 – 4.1	4.03	
9	HS7 mass flowrate	Kg/s	4.5 – 4.8	4.94	Fed by MCP1
10	HS8 mass flowrate	Kg/s	4.5 – 4.8	4.93	
11	HS9 mass flowrate	Kg/s	4.0 – 4.1	3.90	
12	HS10 mass flowrate	Kg/s	3.9 – 4.0	4.02	
13	HS11 mass flowrate	Kg/s	4.0 – 4.0	3.99	
14	HS12 mass flowrate	Kg/s	4.5 – 4.8	5.08	Fed by MCP2
15	HS13 mass flowrate	Kg/s	4.5 – 4.8	4.89	
16	HS14 mass flowrate	Kg/s	3.9 – 4.0	3.92	
17	SG1 SL flowrate	Kg/s	1.9	1.91	
18	SG1 FW flowrate	Kg/s	2.1	1.91	
19	SG2 SL flowrate	Kg/s	2.0	2	
20	SG2 FW flowrate	Kg/s	2.5	2	
21	SG1 DC flowrate	Kg/s	-	-	
22	HD5 / HD7 fluid temperature	°C	295	297 / 296	
23	HD8 / HD6 fluid temperature	°C	262	261 / 260	
24	SG1 fluid temperature	°C	-	257.3	
25	FW temperature	°C	187	187	
26	Void fraction at HS5 outlet	-	-	0.	
27	Void fraction at HS8 outlet	-	-	0.	

Table 4.6. List of Relevant Boundary Conditions Measured and Adopted in the Calculation of the RD-14M, B-9401 Experiment

No	EVENT/QUANTITY	UNIT	VALUE	NOTES
1	Test start	s	0	Transient steady state was run before this time. Steady state data for 10 seconds are added before this time in the results.
2	Break opening	s	0.	
3	Power ramp down	s	2.	Channels are grouped in accordance with Table 1 of App. B, Report RC-2491 by R.S. Swartz (AECL, June 2000) to 4 channel groups. Power is decreased in 40 steps in accordance with data provided by test records.
4	SGs SL flowrate	-	-	SL flowrate has been imposed as a function of time following relevant experimental signal.
5	SGs FW flowrate	-	-	FW flowrate is calculated by code in order to maintain boiler level.
6	MCP coast-down start	s	2.	Pump speed versus time was imposed in accordance with test data.
7	ECC-HPIS start	s	10.6	The HPIS 'P14' pump characteristic (G vs P) has been taken from Figure 8.10 of the report at item 3 above (dotted line with ▲).
8	PRZ isolation	s	12.8	
9	Isolation of ECC-HPIS	s		Based on the HP–ECC tanks depletion
10	ECC-LPIS start	s	106.2	The LPIS 'P8' pump characteristic (G vs P) has been taken from Figure 8.11 of the report at item 3 above (dotted line with □).
11	MCP coast-down end	s	205.6	
12	Isolation of ECC-LPIS	s		Based on LP-ECC tanks depletion
13	End of calculation	s	400.0	

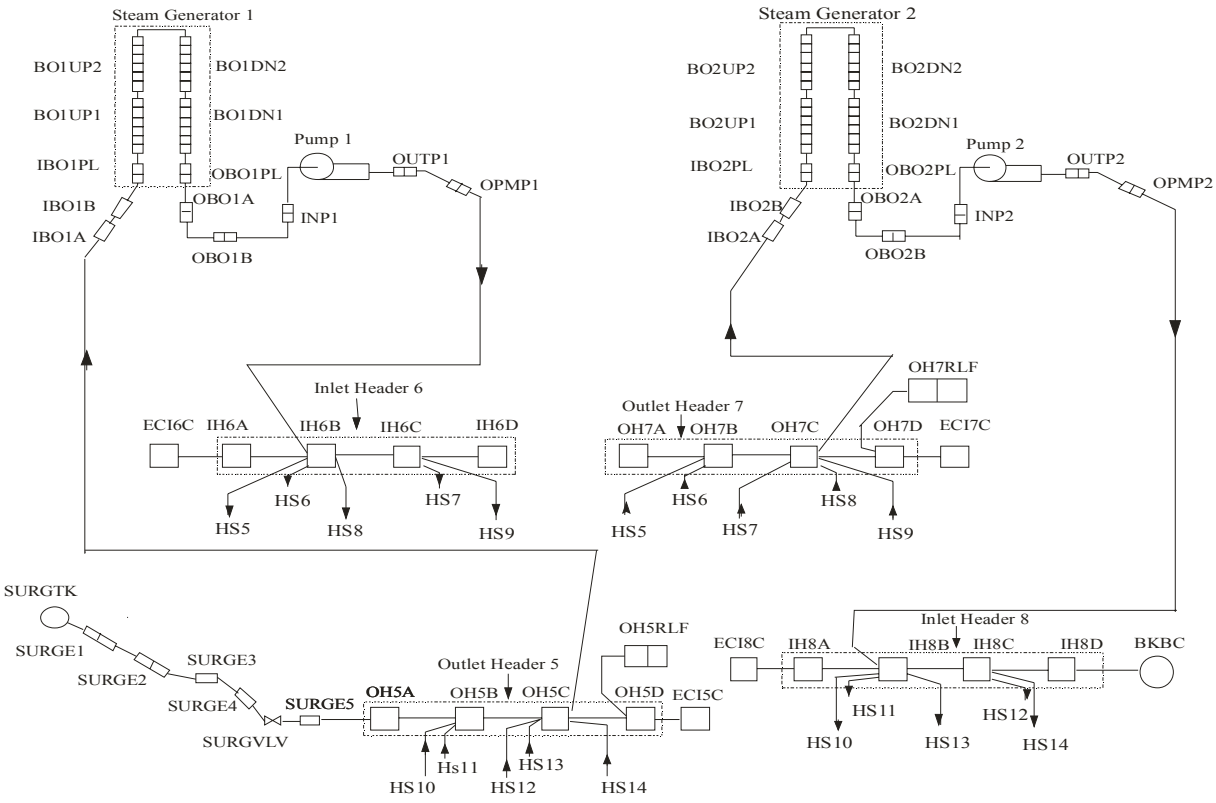

Fig. 4.5. CATHENA Idealization — Primary System, Above Headers.

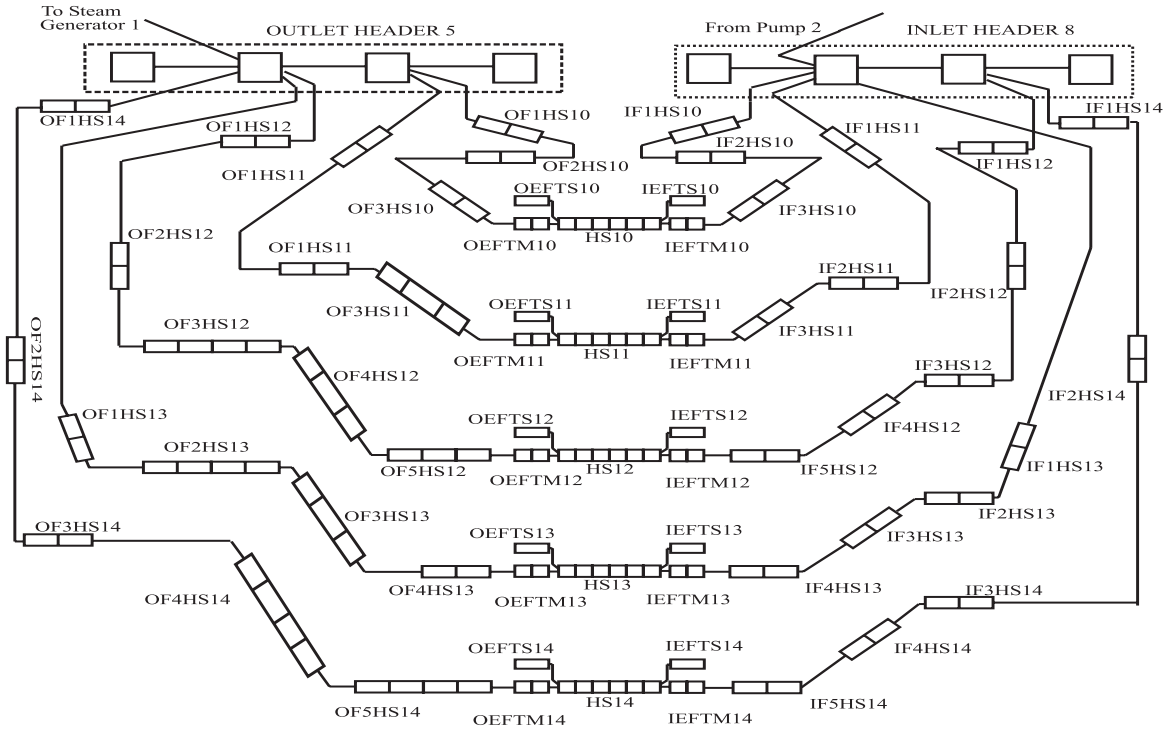

Fig. 4.6. CATHENA Idealization — Primary System, Below Headers.

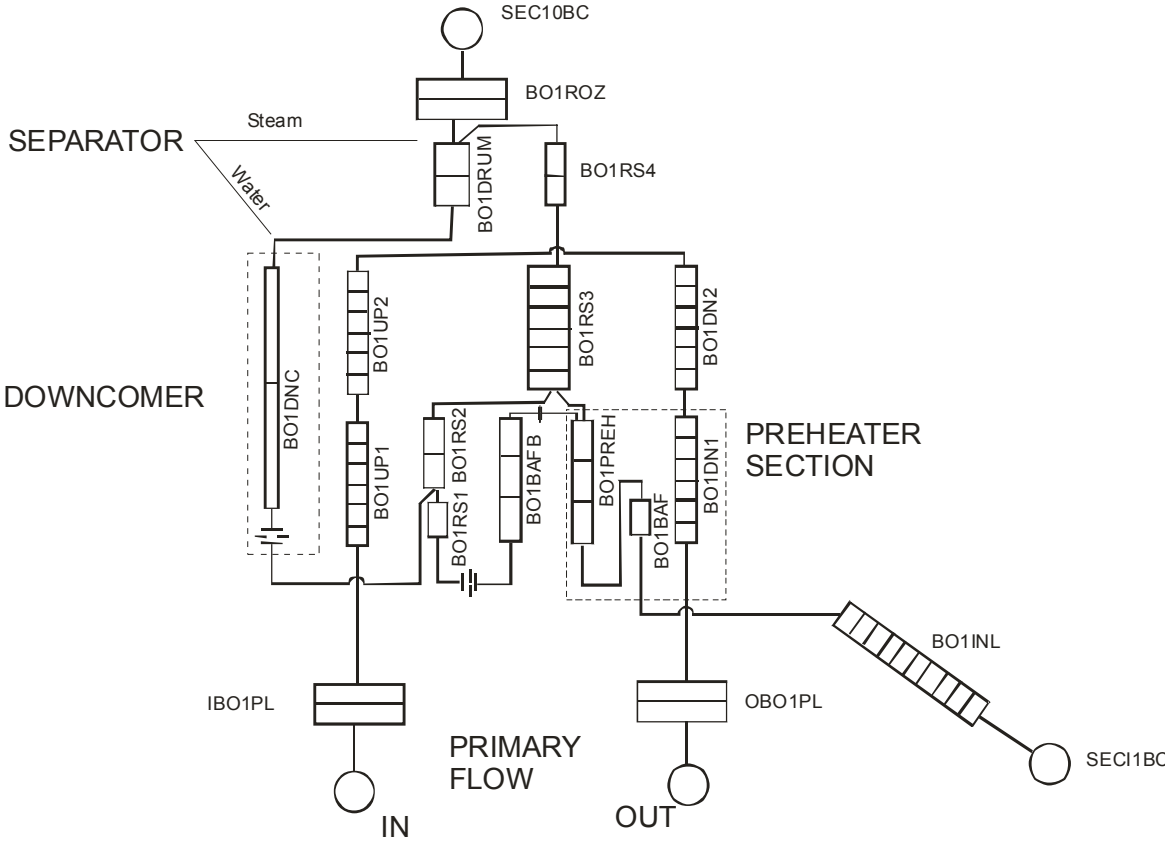

Fig. 4.7. CATHENA Idealization – Secondary Side.

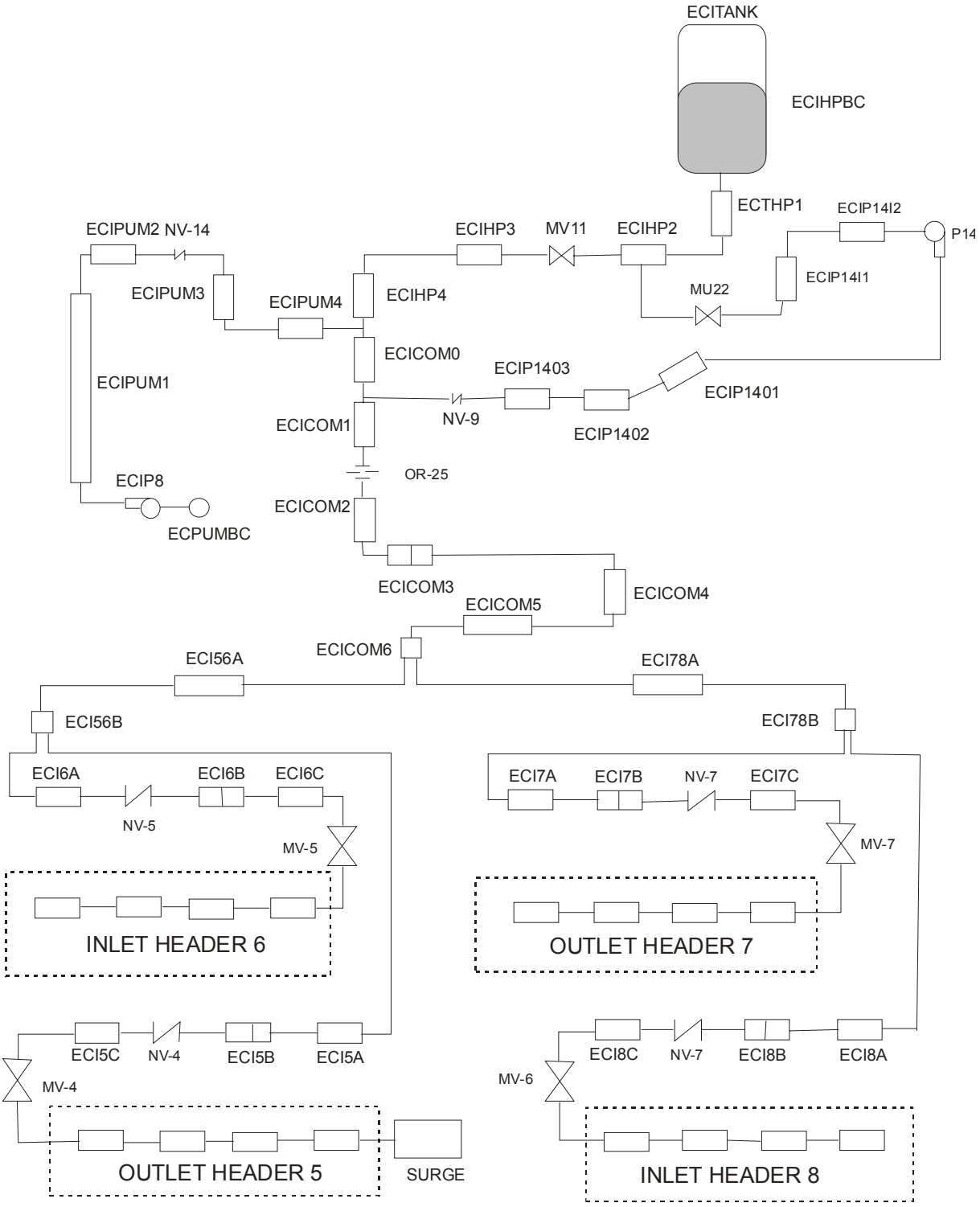

Fig. 4.8. CATHENA Idealization – ECC Delivery System.

4.3. India

4.3.1. RELAP5 / MOD3.2 CODE

DESCRIPTION OF CODE AND MODELLING FOR B9401 EXPERIMENT

RELAP5 was developed at the Idaho National Engineering Laboratory for the U.S. Nuclear Regulatory Commission (NRC). RELAP is basically developed for LWR transient analysis. However, the code's generalization has enabled its application to both nuclear and non-nuclear fields, horizontal and vertical types of reactors, and light and heavy water reactors. Its nuclear specific applications include simulations of transients such as loss of coolant accidents, anticipated transients without scram (ATWS) and operational transients such as loss of feedwater, loss of offsite power etc.

The RELAP5/MOD3 code is based on a nonhomogeneous and nonequilibrium model for the two-phase system. It solves unsteady and one-dimensional mass, energy and momentum equations for each phase based on a fast and partially implicit finite-difference numerical scheme. The code includes many generic component models such as pumps, valves, pipes, heat releasing or absorbing structures, reactor point kinetics, electric heaters, jet pumps, turbines, separators, accumulators, and control system components. In addition, special process models are included such as form loss, flow at an abrupt area change, branching, choked flow, boron tracking, and noncondensable gas transport.

The difference equations are based on the concept of a control volume (or mesh cell) in which mass and energy are conserved. This results in defining mass and energy volume-average properties and requires knowledge of velocities at the volume boundaries. The velocities at boundaries are obtained through the use of momentum control volumes (cells) centered on the mass and energy cell boundaries. Therefore, the scalar properties (pressure, energies, and void fraction) of the flow are defined at cell centers, and vector quantities (velocities) are defined on cell boundaries.

Heat structures represent the solid structures bounding hydrodynamic volumes (i.e. pipe walls) or structures internal to the volumes (fuel pins). The one dimensional heat conduction equation is used to compute temperature distributions within heat structures. Hydrodynamic volumes and heat structure conditions are coupled through heat structure boundary conditions.

The constitutive relations include models for defining flow regimes and flow-regime-related models for interphase drag and shear, the coefficient of virtual mass, wall friction, wall heat transfer, and interphase heat and mass transfer. Heat transfer regimes are defined and used for wall heat transfer.

The basic approach to pump modeling is to superimpose a quasi-static model for pump performance on the RELAP5 volume-junction flow path representation. The pump is a volume-oriented component, and the head developed by the pump is apportioned equally between the suction and discharge junctions that connect the pump volume to the system. The pump model is interfaced with the two-fluid hydrodynamic model by assuming the head developed by the pump is similar to a body force. The pump head is coupled implicitly to the volumetric flow rate.

4.3.2. The RELAP Idealization

DESCRIPTION OF MODELLING

The experimental and the auxiliary loop have been modelled in the RELAP5/MOD3.2 code. It necessitates nodalization of the total system into a number of volumes and inter-connecting junctions, valves, heat slabs and component-specific models such as pump, separator etc. The system controls are modelled through trip cards, which accept logical inputs based on time, pressure and other thermal-hydraulic parameters. The power trip, pump coast down, break initiation, ECC pump activation etc are controlled through the trip cards.

Header, Feeder and Channel Modelling

Headers, Feeders and Channel discretization are shown in Figure 4.9. Each of the ten channels is discretised into three axial volumes to obtain the axial distribution of thermal-hydraulic parameters. Feeders are nodalised such that sections of the pipes having similar inclination and cross-sectional area are combined. Each feeder has 13 to 14 volumes maintaining the pipe length and elevation. In the setup, the intake and off-take branches such as ECC injection, feeder connection, break valve, instrument inserts etc. are connected to the header at different axial locations. Accordingly the header is discretised into three axial volumes (Figure 4.10).

Fuel Element Simulation

Each fuel element consisting of center core of MgO, Inconel 625 heater tube, Boron Nitride and outer S.S. Sheath, which transfers heat to the coolant, is modelled with a RELAP specific heat generating Heat Structure Component. The seven fuel pins are combined into a single fuel pin heat structure maintaining the surface area, mass and equivalent heated perimeter. Axially, the fuel bundle is divided into three in accordance with the number of channel volumes. The fuel pin is radially discretised into five regions simulating the different layers. These fuel pins generate heat corresponding to each channel power. The power ramp down during the transient is given in a tabular form in the code as reported in the experiment.

Steam Generator (SG) Modelling

The primary side steam generator path in both the loops is shown in Figure 4.11 and Figure 4.12. The Steam Generating U-Tubes are segregated into six volumes including two inlet and outlet plenum volumes. Four of the U-Tube volumes are attached with four heat slabs, forming the thermal linkage between the primary and secondary system. The secondary system consists of riser, drum and downcomer volumes. A RELAP specific separator component, attached with the drum volume, is used to separate out steam and water. The drum volume is modeled using a pipe component having 10 volumes. The U-Tube heat slabs are connected to the two volumes of the riser portion. One single volume downcomer connects the drum inlet to the secondary riser inlet. The feed from a time-dependent volume is injected into the riser portion and mixes with the saturated water from the downcomer. It picks up heat from the U-tubes, converts into a two-phase mixture and rises in the riser volume. At the exit of the riser this two-phase mixture enters the separator volume. Steam from the separator moves to the upper portion of the drum volume and the saturated liquid falls back into the lower portion of the drum volume. The bottom volume of the drum is connected to the downcomer. The feed flow and temperature are given as a time dependent boundary condition, as obtained in the experiment.

Pump Modelling

The primary pump is modelled using the RELAP in-built Bingham Pump characteristic. The rated flow, speed and head are provided as given in the report. ECCS pumps of stage 1 and 2 are simulated using time-dependent junctions whose flow characteristics are given as functions of downstream discharge pressure. This characterization is obtained from the report. Pump coast down is simulated through a time vs. pump velocity lookup table as reported during the transient.

ECC System Modelling

Nodalization of the ECC system is shown in Figure 4.13. Only the high-pressure phase and the recovery phase of the system are modelled as no gravity phase activation is observed during the transient. Both the pumps are modelled as described in the previous section. The number of volumes and junctions used closely simulate the experimental setup. The total integrated ECC flow is used to calculate the accumulator inventory and level. As the level decreases below 10 % in the accumulator tank, the low-pressure phase is activated.

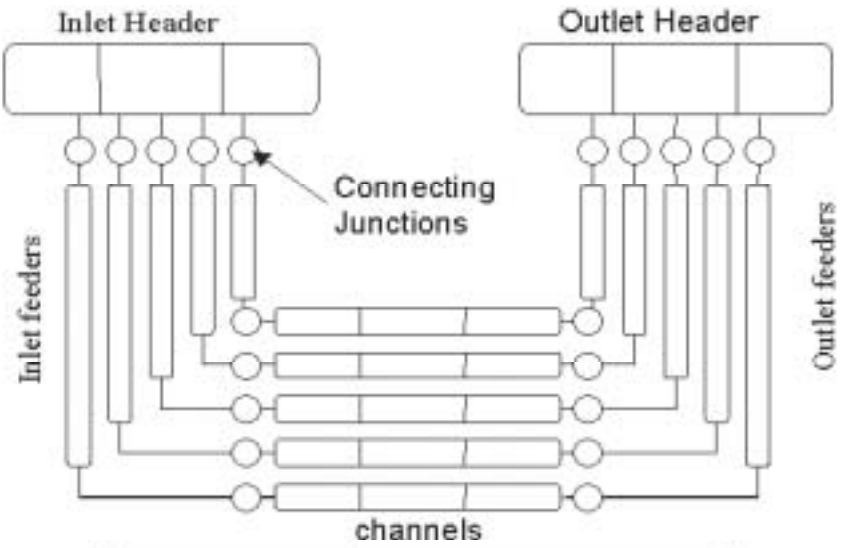

	Number of volumes
Each Header	3
Each Feeder	13 - 14
Each Channel	3

Fig. 4.9. Channel and Feeder Discretization in RELAP5.

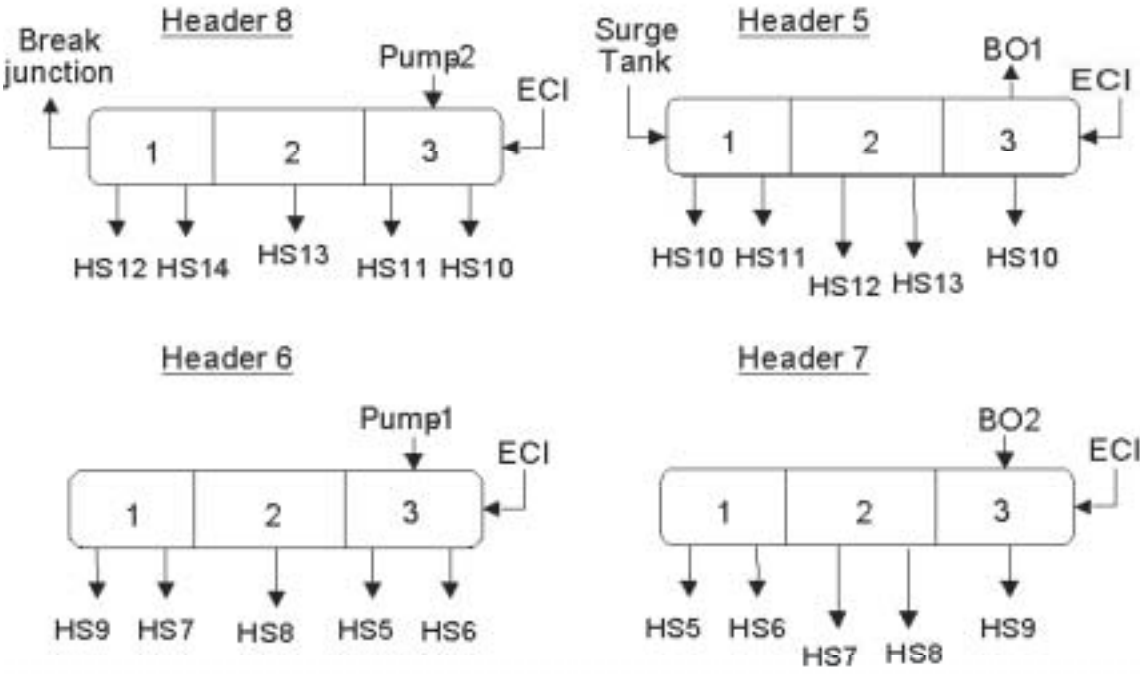

Fig. 4.10. Header Discretization in RELAP5.

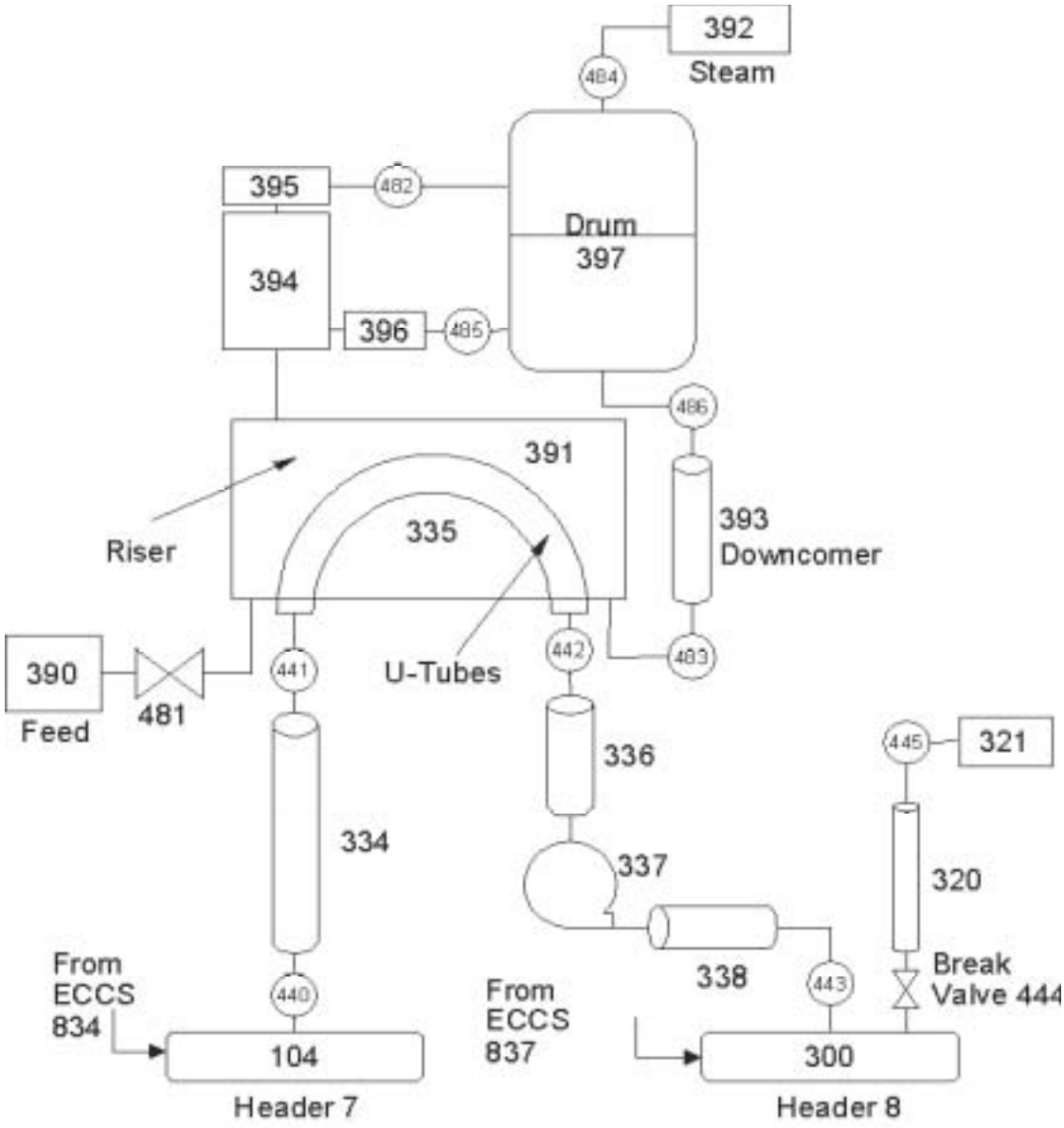

Component	No. of Volumes
334	3
335, U-Tubes	6
336	4
337, Pump-2	1
338	6
391, Riser	2

Component	No. of Volumes
393, Downcomer	1
397, Drum	10
394, Separator	4
392, 390, 321, TDV	1 each
395, 396	1 each
320, Blowdown pipe	2

Fig. 4.11. PHT Discretisation between HDR7 and HDR8 in RELAP5.

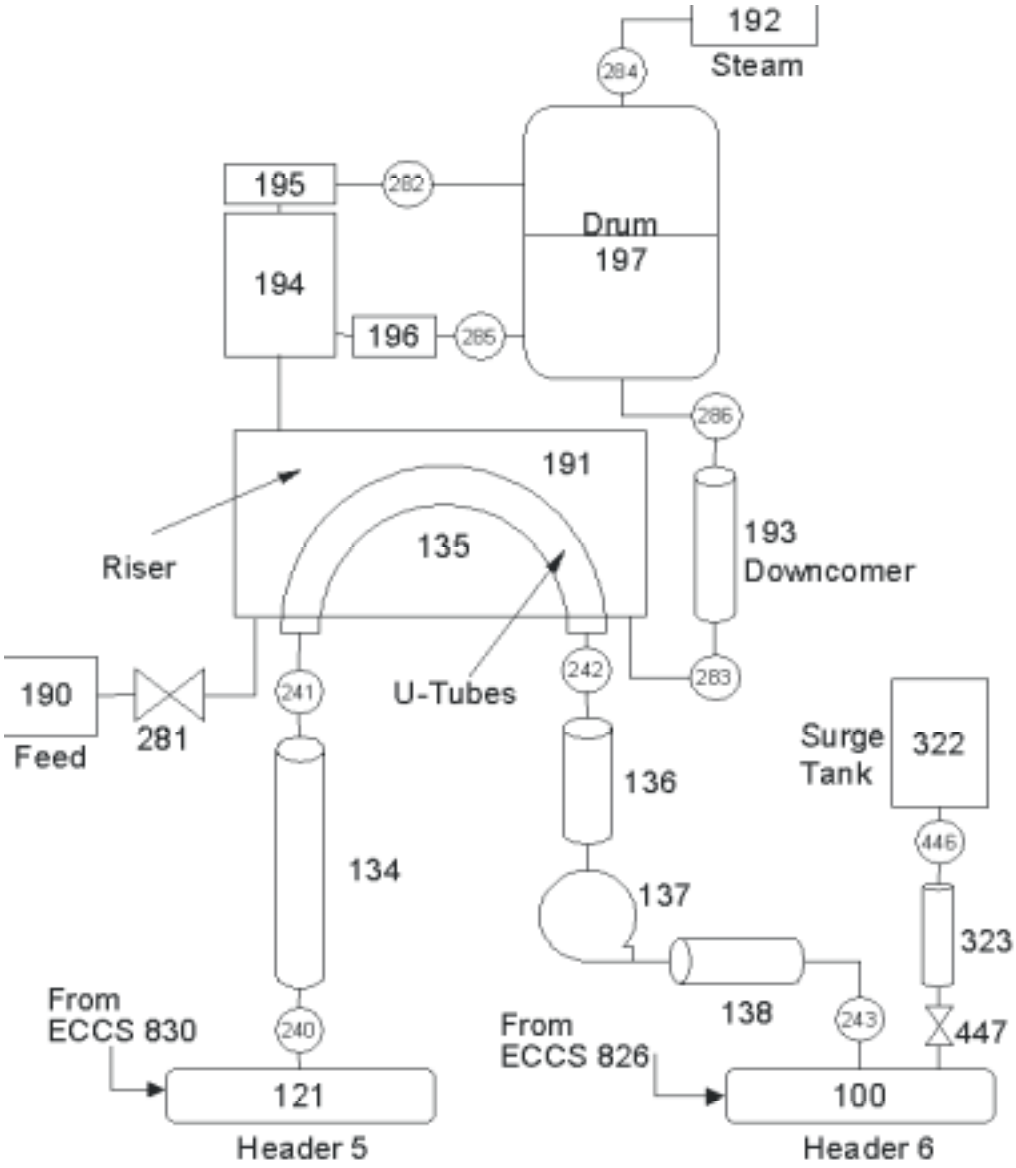

Component	No. of Volumes
134	3
135, U-Tubes	6
136	4
137, Pump1	1
138	6
191, Riser	2

Component	No. of Volumes
193, Downcomer	1
197, Drum	10
194, Separator	4
192, 190	1 each
195, 196	1 each
323, surge line	12
322, surge tank	6

Fig. 4.12. PHT Discretisation between HDR5 and HDR6 in RELAP5.

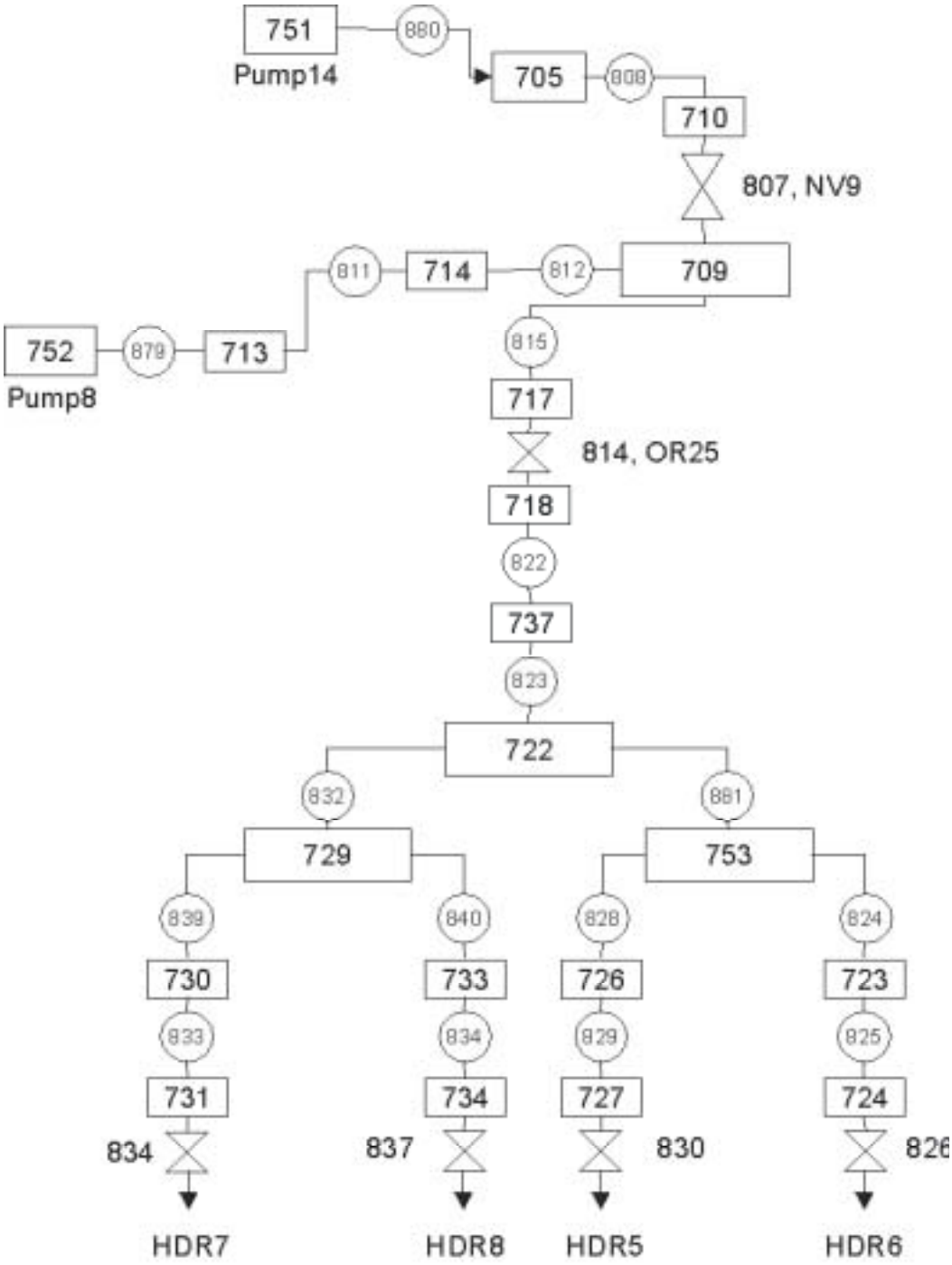

Fig. 4.13. ECCS Discretization in RELAP5.

4.4. Italy

4.4.1. The RELAP Code

The US NRC version of the RELAP5/mod3.2, ref. [6], is used for the post-test analysis of the B-9401 LBLOCA experiment performed in the RD-14m test facility simulating a CANDU reactor. RELAP5, together with TRAC, Cathare and Athlet is one of the four widely diffused system codes available to the scientific community for transient analysis for the LWR. The code solves six 1-D balance equations for mass momentum and energy, separately for the steam and the liquid phases. It has the capability to model any complex thermalhydraulic system including primary loop, secondary loop and Balance of the Plant systems in an LWR. Control systems can also be simulated together with the 0-D neutron kinetics performance of the core. The main reasons for the selection of the code can be stated (or repeated) as:

- diffusion of the code, i.e. interest from the scientific community;
- experience in its use at University of Pisa, including the 'independent' achievement of quality proofs, e.g. refs. [7-12];
- quality of the produced results as demonstrated by various international organizations;
- flexibility in developing nodalizations that also makes easy the transfer of expertise gathered from studying ITF phenomena to NPPs.

4.4.2. The RELAP Idealization

The 'idealization' is the result of a wide range brainstorming processes where the user capabilities, the available computational power and the resources for the analysis, together with the code features, play a fundamental role. Here the word 'idealization' is used as a synonym of 'nodalization' that appears to have a broader diffusion within the international community.

Two main nodalizations have been developed at the University of Pisa within the framework of the participation to the analysis of the B-9401 RD-14m LBLOCA experiment. Their main features as well as the differences are outlined in the two reports listed as refs. [13] and [14].

The first nodalization has been derived from the standard criteria proposed by the University of Pisa for nodalization development and qualification as outlined in ref. [7]. Those criteria, validated for PWR, BWR and VVER situations have been 'adapted' to the CANDU system configuration.

The second nodalization, utilized for producing the reference RELAP5 code calculation results by UNIPI, differs from the first one, owing to the following items:

A. The heated channel HS13 has been sub-divided into two hydraulic channels including '5 bottom' pins and '2 top' pins, respectively. These are connected by 'cross-junctions' and allow the simulation of stratification inside the channel.

B. The ECCS lines have been simulated: in the first nodalization (available from April 2001, ref. [13]), ECC flow-rates were imposed as a function of time at each individual ECC port in each header. In the present nodalization flowrate versus pressure is imposed at the location where the high and the low pressure ECC system pumps are installed in the RD-14M loop.

C. Flow-rates in the primary loop available from the experimental database have been correctly interpreted (in the nodalization of April 2001, 'l/s' were interpreted as 'kg/s').

D. As a consequence of the above, MCP speed has been correctly set at 350 rpm (it was 372.6 rpm in the first nodalization).

E. One node has been added per SG to take into account the volume of the steam line between each SG vessel and the main steam isolation valve location.

F. The 'pin 5' in heated section 7 and the 'pin 7' in heated section 12 were disconnected, according to Table 3 of the document of H. Q. Zhou [15] discussed during the meeting held in Vienna in May 2001.

G. Minor changes have been introduced to the SG level control to stabilize the initial steady state.

H. The experimental value of the pressure drops between headers has been 'better matched' by the calculated results, by increasing the pressure loss coefficients through the channels and connected piping.

I. The 'heat transfer' surfaces "110" and "134" for the calculation of the heat transfer coefficient have been adopted in the heated section. However, further analyses may be needed related to this user option.

The main dimensions of the two nodalizations can be found in Table 4.7 and the sketch of the second nodalization is given in Figures from 4.14 to 4.17.

The boundary and initial conditions and the imposed sequence of main events adopted for the final calculation, i.e. second nodalization, are given in Tables 4.8 and 4.9, respectively, where a comparison is made with experimental data as applicable. It must be noted that the calculated values in Table 4.8 are related to the end of the 100 s transient-steady-state calculation. In addition, input power for individual heated sections are those reported in Table 3 of reference [15]. In the case of the heated section 13, 2/7 and 5/7 power applicable for that channel, are generated in the hydraulic channels 760 and 260 of Figure 4.16, respectively.

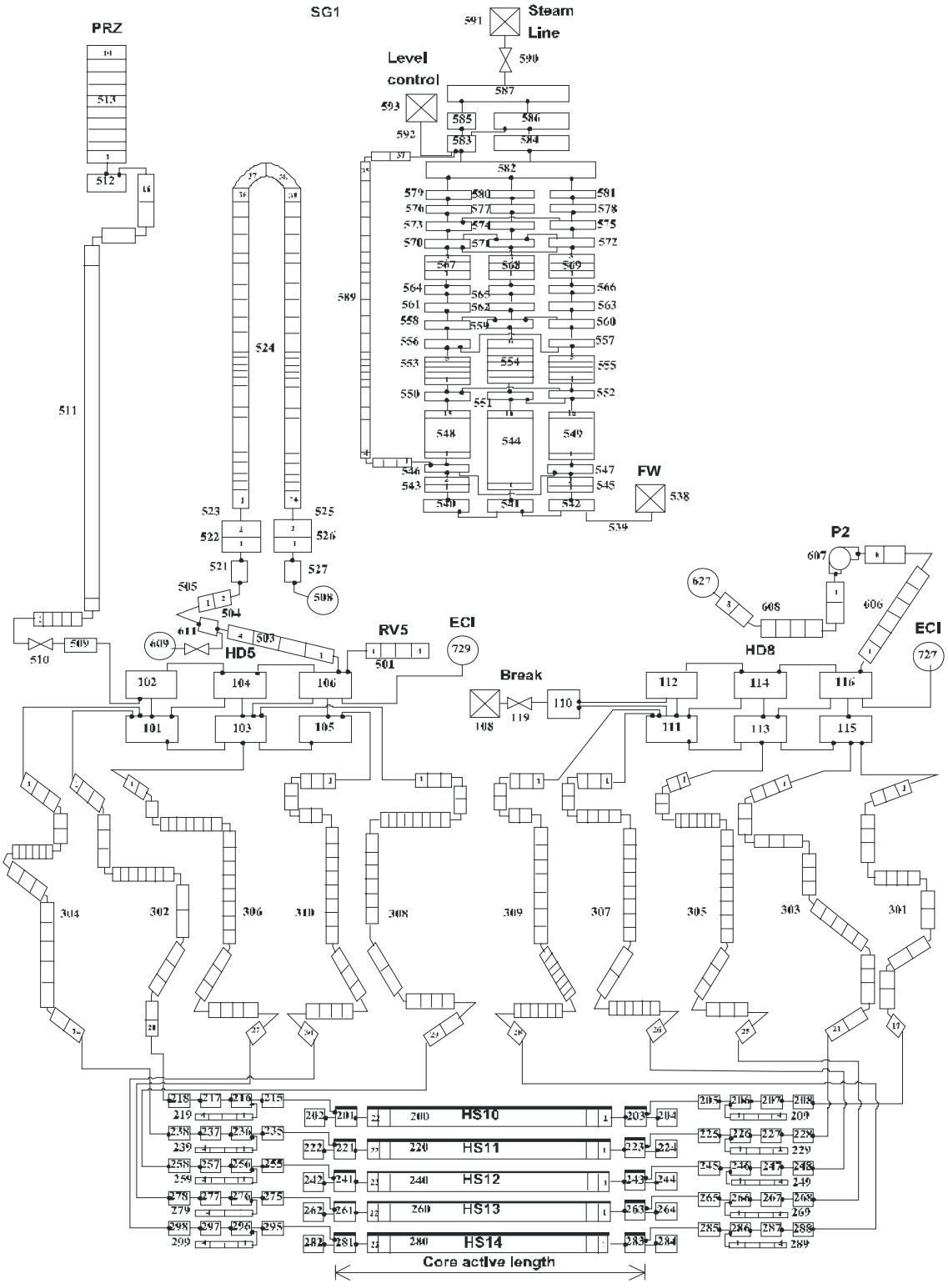

Fig. 4.14. UNIPI Nodalization of RD-14M Suitable for RELAP5/MOD3.2 Code, Overall System, Part I.

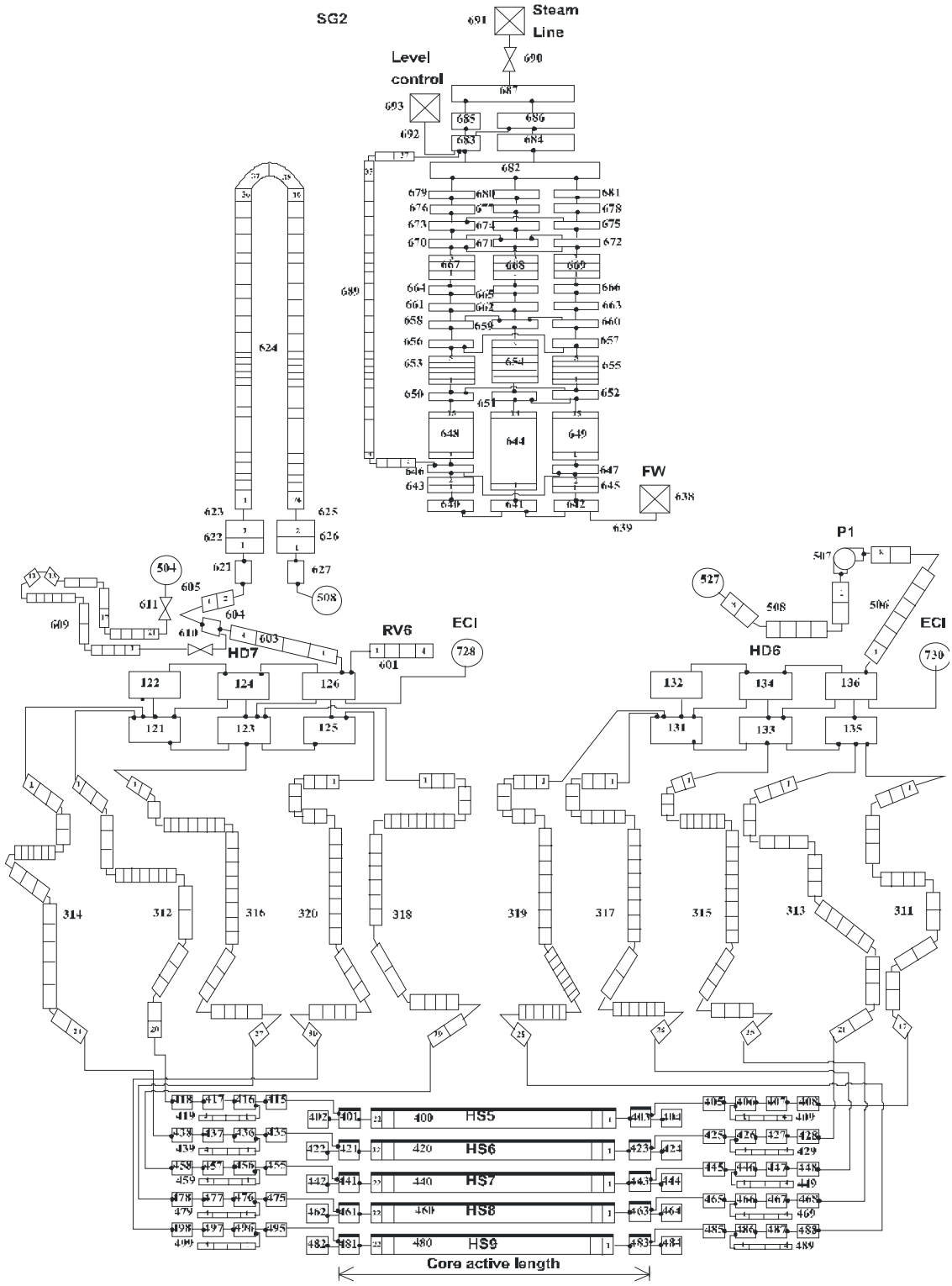

Fig. 4.15. UNIPI Nodalization of RD-14M Suitable for RELAP5/MOD3.2 Code, Overall System, Part II.

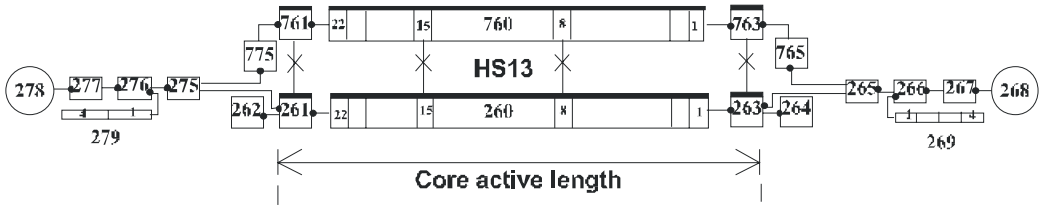

Fig. 4.16. UNIPI Nodalization of RD-14M Suitable for RELAP5/MOD3.2 Code, Detail of the HS13.

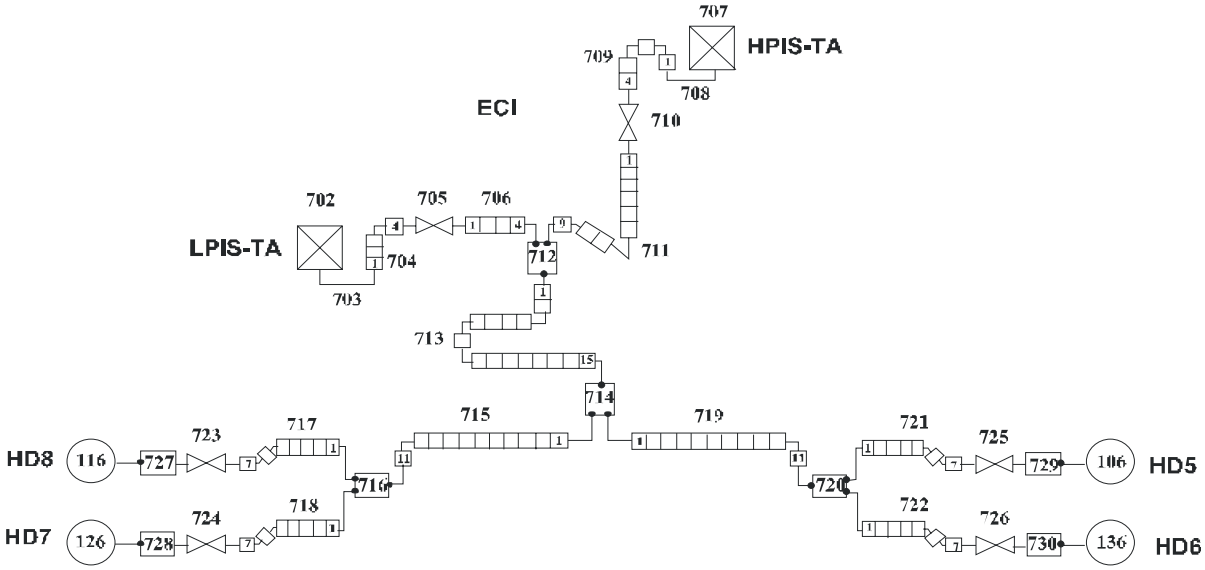

Fig. 4.17. UNIPI Nodalization of RD-14M Suitable for RELAP5/MOD3.2 Code, Detail of the ECC System.

Table 4.7. Main Dimensions of the RELAP5/MOD3.2 Nodalizations Developed for the RD-14M by UNIPI

No	QUANTITY	VALUE rm12	VALUE rm35	NOTES
1	No of Hydraulic Nodes	1517	1636	
2	No of Junctions	1572	1699	
3	No of structures for conduction heat transfer	2119		
4	No of mesh points for conduction heat transfer	10885	11788	
5	No of hydraulic channels for the active core	10		Each of the HS5 to HS14 is simulated.
6	No of structures and of hydraulic nodes belonging to a horizontal stack per each hydraulic channel of the active core	24		
7	No of cards of the input deck	8440	9331	

Table 4.8. List of Relevant Initial Conditions Measured and Calculated for the RD-14M, B-9401 Experiment

No	QUANTITY	UNIT	EXP	CALC	NOTES
1	Pressurizer pressure	MPa	9.9	10.2	
2	HD5 pressure	MPa	10.0	10.3	
3	DP (HD8-HD5)/(HD6-HD7)	MPa	1.3-1.5	1.4/1.46	
4	SGs pressure	MPa	4.5	4.4	
5	MCP1 flowrate *	Kg/s	21.9	22.7	
6	MCP2 flowrate	Kg/s	21.6	22.7	
7	HS5 mass flowrate	Kg/s	4.0 – 4.1	4.3	Fed by MCP1
8	HS6 mass flowrate	Kg/s	4.0 – 4.1	4.0	
9	HS7 mass flowrate	Kg/s	4.5 – 4.8	5.1	
10	HS8 mass flowrate	Kg/s	4.5 – 4.8	4.9	
11	HS9 mass flowrate	Kg/s	4.0 – 4.1	4.5	
12	HS10 mass flowrate	Kg/s	3.9 – 4.0	4.3	Fed by MCP2
13	HS11 mass flowrate	Kg/s	4.0 – 4.0	3.9	
14	HS12 mass flowrate	Kg/s	4.5 – 4.8	5.1	
15	HS13 mass flowrate	Kg/s	4.5 – 4.8	3.7+1.5	
16	HS14 mass flowrate	Kg/s	3.9 – 4.0	4.1	
17	SG1 SL flowrate	Kg/s	1.9	2.0	
18	SG1 FW flowrate	Kg/s	2.1	1.95	Unreliable signal in ‘exp’ database
19	SG2 SL flowrate	Kg/s	2.0	2.0	Unsteady situation from ‘exp’ database
20	SG2 FW flowrate	Kg/s	2.5	1.95	
21	SG1 DC flowrate	Kg/s	-	9.8	Unsteady quantity in ‘calc’ database
22	HD5 / HD7 fluid temperature	°C	295	293-295	
23	HD8 / HD6 fluid temperature	°C	262	260-261	
24	SG1 DC bottom fluid temperature	°C	-	256	
25	FW temperature	°C	187	187	
26	Void fraction at HS5 outlet	-	-	0.	
27	Void fraction at HS8 outlet	-	-	0.	
28	MCP speed	rpm	350	350.	
29	SG1 DC level	m	8.7	9.9	Unsteady quantity in ‘exp’ and ‘calc’ database. Reference ‘0’ position not identified in ‘calc’.
30	PRZ level	m	1.27	1.32	Reference ‘0’ position not identified in ‘calc’.
31	Core total power	MW	8.14	8.14	

* Related to the Table 3A of the report DIMNP NT 432(01), experimental flowrate values of primary and secondary loop quantities have been multiplied by 0.787 and 0.881 (kg/l), respectively, because original experimental data were given in l/s (and not, as previously interpreted, in kg/s).

Table 4.9. List of Relevant Boundary Conditions Measured and Adopted in the Calculation of the RD-14M, B-9401 Experiment

No	EVENT/QUANTITY	UNIT	VALUE	NOTES
1	Test start°	s	0	Data gathering start
2	Break opening	s	10.	
3	Power ramp down	s	12.	Electrical power is stepwise decreased to the value reported in the last column of the Table 1 of App. B of report RC-2491 by R.S. Swartz (AECL, June 2000).
4	SGs SL flowrate	-	-	SL flowrate has been imposed as a function of time following relevant experimental signal.
5	SGs FW flowrate	-	-	FW flowrate has been imposed as a function of time following relevant experimental signal.
6	MCP coast-down start	s	12.	
7	ECC-HPIS start	s	20.6	The HPIS 'P14' pump characteristic (G vs P) has been taken from Figure 8.10 of the report at item 3 above (dotted line with ▲).
8	PRZ isolation	s	22.8	
9	Isolation of ECC-HPIS	s	116.2	
10	ECC-LPIS start	s	116.2	The LPIS 'P8' pump characteristic (G vs P) has been taken from Figure 8.11 of the report at item 3 above (dotted line with □).
11	MCP coast-down end	s	213.2	The curve MCP speed vs time has been arbitrarily imposed (typical exponential decay).
12	Isolation of ECC-LPIS	s	350.7	
13	End of calculation	s	924.	Results of code run RD-14M 35 are given up to 900 s in Annex 1, where they are compared with the experimental data and up to 400 s in Annex 2 with reference to the variables requested in Table 5 of [15].

° 100 s of "transient steady-state" calculation has been performed before this time

4.5. Republic of Korea

4.5.1. The RELAP5/CANDU Code

As the RELAP5 code was described in another section, the focus here is on the differences between RELAP5 and RELAP5/CANDU. Several earlier assessment results of the RELAP5 code in the RD-14 tests indicated some deficiencies in the prediction of the heated section sheath temperatures, etc. Therefore, the development of RELAP5/CANDU code was initiated by the Republic of Korea Institute of Nuclear Safety in cooperation with the Republic of Korea Atomic Energy Research Institute, to reduce the identified deficiencies. The RELAP5/CANDU code is currently under development and until now, modifications have been performed for the following areas:

(1) Critical Flow Model
(2) Nuclear Kinetics Model
(3) Critical Heat Flux Model
(4) Reactor Core Control Model
(5) Valve and Spray Model
(6) Improvement of Horizontal Flow Regime Map
(7) Heat Transfer Model in Horizontal Channel

Some of the above modifications had already been adopted in the RELAP5/MOD3.2 version.

4.5.2. The RELAP/CANDU Idealization

Basically, in view of hydrodynamic model (fluid control volumes and junctions), a relatively fine nodalization scheme is adopted for the components where two-phase phenomena and system functions play important roles, and cross flow junctions are modeled where the flow direction is vertically linked to the main flow direction such as at end fitting connections. The system model was developed following reference to the various nodalizations in the references and reflected experience in determining the nodalization of the systems. Also, RELAP5 User's Guidelines were followed as closely as possible. In a heat structure, heat flow paths modeled in a one-dimensional sense, and radial meshes are divided in order to get the accurate temperature distribution. Heat structures were modeled for pipe walls, nuclear-fuel pins simulator, heat exchanger surfaces, etc.

With the above general nodalization philosophy, the RD-14M facility was modeled. System models for the RELAP5/CANDU calculation are shown in Figures 4.18 and 4.19, which are basically similar to those found in the CATHENA model and therefore may help reduce the effect of nodalization. The system model comprises the primary heat transport system including heaters, pumps, secondary system, ECC system, and break model. The test section was modeled in each channel and each steady state channel flowrate was tuned up.

The forward/backward junction loss coefficients were used to simulate pressure loss and in the case of orifices, a junction abrupt area change model was used. High and low ECC pumps were modeled as time-dependent junctions in which mass flow was controlled by discharge pressure. In particular, the ECC piping was modeled in order to simulate the ECC flow-splitting behavior. The break model was single normal junction and the discharge volume was simulated by a time-dependent volume.

Table 4.10. Main Dimensions of the RELAP5/CANDU Nodalizations Developed for RD-14M by KINS

No.	QUANTITY	RELAP5/ CANDU	NOTES
1	No of Hydraulics Nodes	450	
2	**No of Junctions**	461	
3	No of structures for conduction heat transfer	716	
4	No of mesh points for conduction heat transfer	2160	
5	No of hydraulics channels for active core	10	
6	No of structures and of hydraulic nodes belonging to a horizontal stack per each hydraulic channel of the active core	N/A	
7	No of cards of the input deck	7404	

Table 4.11. List of Relevant Initial Conditions Measured and Calculated for the RD-14M, B9401 Experiment

No	QUANTITY	UNIT	EXP	CALC	NOTES
1	Pressurizer pressure	MPa	9.9	10.05	
2	HD5 pressure	MPa	10.0	10.0425	
3	DP (HD8-HD5)/(HD6-HD7)	MPa	1.3-1.5	1.5/1.52	
4	SGs pressure	MPa	4.5	4.4	
5	MCP1 flowrate *	Kg/s	21.9	21.6	
6	MCP2 flowrate	Kg/s	21.6	21.7	
7	HS5 mass flowrate	Kg/s	4.0 – 4.1	4.07	FED BY MCP1
8	HS6 mass flowrate	Kg/s	4.0 – 4.1	3.9	
9	HS7 mass flowrate	Kg/s	4.5 – 4.8	5.1	
10	HS8 mass flowrate	Kg/s	4.5 – 4.8	4.9	
11	HS9 mass flowrate	Kg/s	4.0 – 4.1	4.0	
12	HS10 mass flowrate	Kg/s	3.9 – 4.0	4.16	FED BY MCP2
13	HS11 mass flowrate	Kg/s	4.0 – 4.0	4.02	
14	HS12 mass flowrate	Kg/s	4.5 – 4.8	5.00	
15	HS13 mass flowrate	Kg/s	4.5 – 4.8	4.98	
16	HS14 mass flowrate	Kg/s	3.9 – 4.0	3.9	
17	SG1 SL flowrate	Kg/s	1.9	2.7	
18	SG1 FW flowrate	Kg/s	2.1	2.7	Unreliable signal in ‘exp’ database
19	SG2 SL flowrate	Kg/s	2.0	2.7	Unsteady situation from ‘exp’ database
20	SG2 FW flowrate	Kg/s	2.5	2.7	
21	SG1 DC flowrate	Kg/s	-	13.3	Unsteady quantity in ‘calc’ database
22	HD5 / HD7 fluid temperature	°C	295	295-296	
23	HD8 / HD6 fluid temperature	°C	262	261-262	
24	SG1 DC bottom fluid temperature	°C	-	255	
25	FW temperature	°C	187	183	
26	Void fraction at HS5 outlet	-	-	0.	
27	Void fraction at HS8 outlet	-	-	0.	
28	MCP speed	rpm	350	372	
29	SG1 DC level	m	8.7	9.2	Unsteady quantity in ‘exp’ and ‘calc’ database. Reference ‘0’ position not identified in ‘calc’.
30	PRZ level	m	1.27	1.31	Reference ‘0’ position not identified in ‘calc’.
31	Core total power	MW	8.14	8.14	

* Related to the Tab. 3A of the report DIMNP NT 432(01), experimental flowrate values of primary and secondary loop quantities have been multiplied by 0.787 and 0.881 (kg/l), respectively, because original experimental data were given in l7s (and not, as previously interpreted, in kg/s).

Table 4.12. List of Relevant Initial Conditions Measured and Calculated for the RD-14M, B-9401 Experiment

No	EVENT/QUANTITY	UNIT	VALUE	NOTES
1	Test start°	s	0	Data gathering start
2	Break opening	s	10.	
3	Power ramp down	s	12.	Electrical power is stepwise decreased to the value reported in the last column of the Tab. 1 of App. B of report RC-2491 by R.S. Swartz (AECL, June 2000).
4	SGs SL flowrate	-	-	SL flowrate has been imposed as a function of time following relevant experimental signal.
5	SGs FW flowrate	-	-	FW flowrate has been imposed as a function of time following relevant experimental signal.
6	MCP coast-down start	s	12.0.	
7	ECI-HPIS start	s	20.6	The HPIS 'P14' pump characteristic (G vs P) has been taken from Fig. 8.10 of the report at item 3 above (dotted line with ▲).
8	PRZ isolation	s	22.8	
9	Isolation of ECI-HPIS	s	116.2	
10	ECI-LPIS start	s	116.2	The LPIS 'P8' pump characteristic (G vs P) has been taken from Fig. 8.11 of the report at item 3 above (dotted line with □).
11	MCP coast-down end	s	213.2	The curve MCP speed vs time has been arbitrarily imposed (typical exponential decay).
12	Isolation of ECI-LPIS	s	350.7	
13	End of calculation	s	924.0	Results of code run rd14m35 are given up to 900 s in Annex 1, where they are compared with the experimental data and up to 400 s in Annex 2 with reference to the variables requested in Table 5 of [15].

° 100 s of "transient steady-state" calculation has been performed before this time

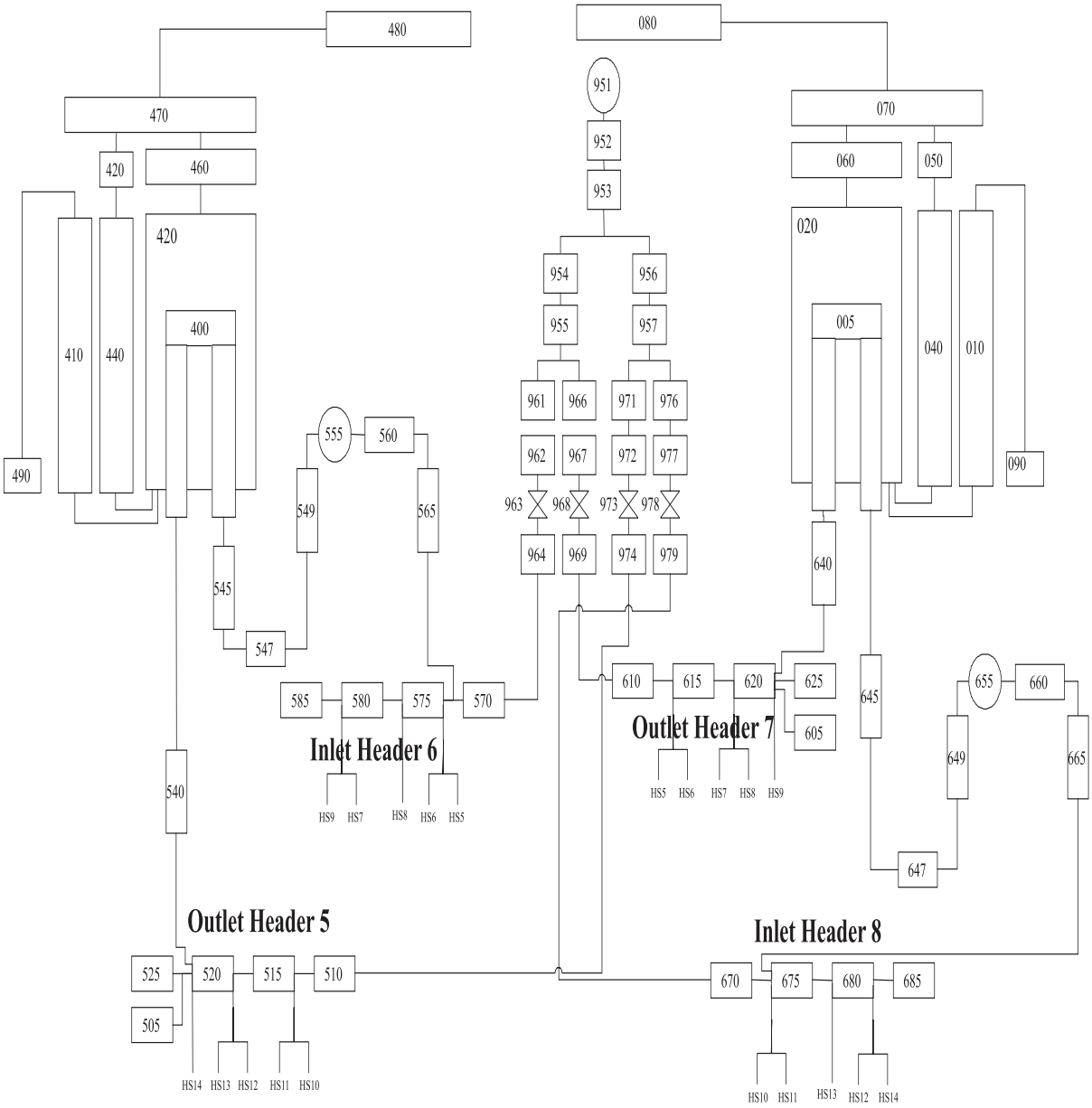

Fig. 4.18. RD-14M RELAP5/CANDU Nodalization.

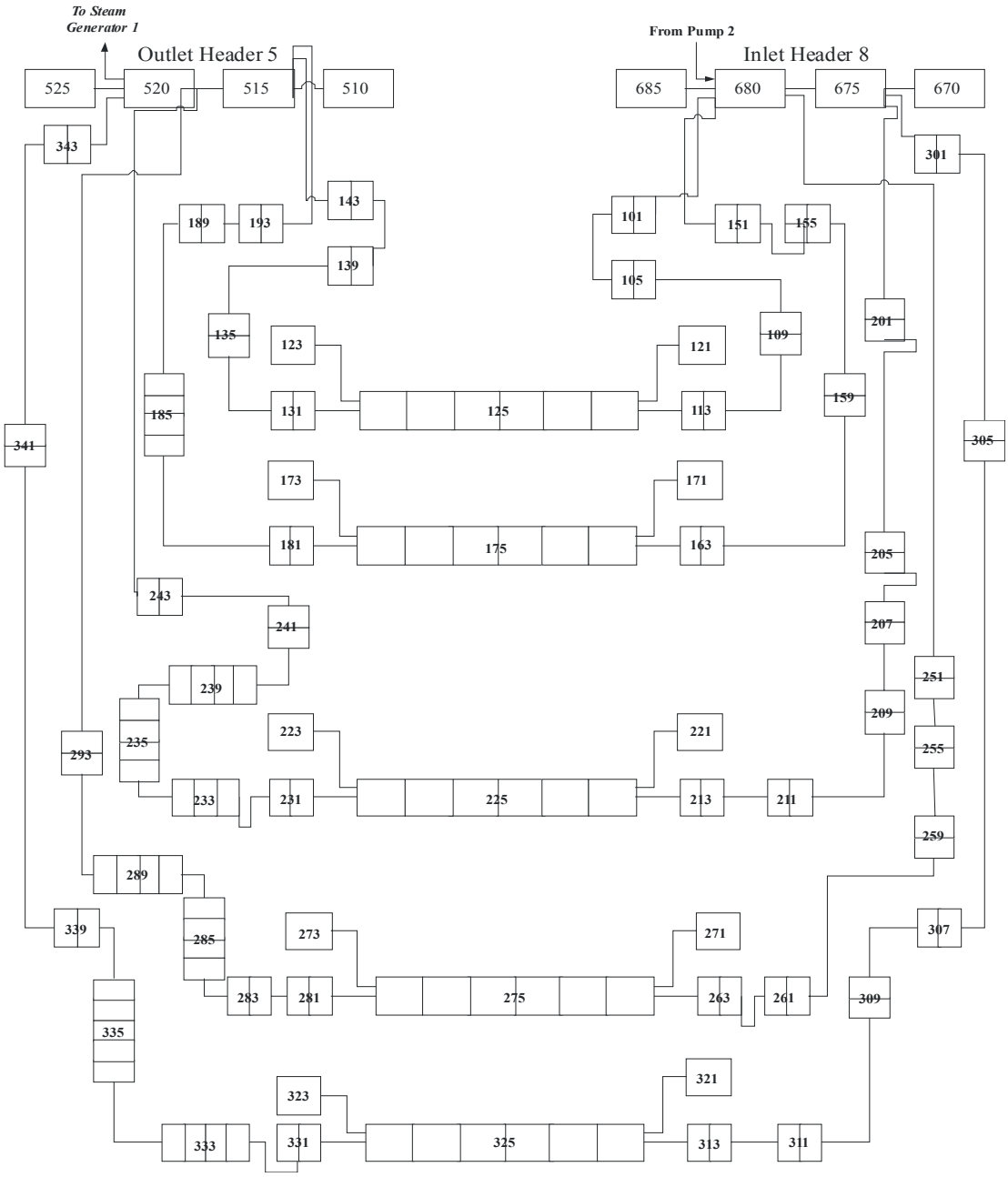

Fig. 4.19. RD-14M Below Header RELAP5/CANDU Nodalization.

4.6. Romania

4.6.1. The FIREBIRD Code

The FIREBIRD-III MOD 1-77 was developed by Atomic Energy of Canada Limited [2].

The FIREBIRD-III MOD 1-77 program is a general network code developed primarily for predicting the transient thermalhydraulic behaviour of CANDU reactor power plants during a postulated loss of coolant accident with subsequent emergency coolant injection.

The code models the physical system in terms of a set of interconnecting nodes. A node corresponds to a user-defined segment of a pipe, a component, or a boundary condition in the system. Each node is specified by a label and by the following geometric parameters: volume of coolant for the hydraulic calculation, and mass, pipe inside diameter, and thickness for the thermal calculation. The connection between two nodes is defined as a link. A link is characterized by the geometrical parameters of hydraulic length, hydraulic diameter, flow area, elevation change (terminal node relative to initial node), absolute pipe roughness, and loss coefficient. The mass and energy conservation equations are solved for nodes. Quantities such as pressure, density, internal energy, temperature, void fraction, static quality and enthalpy, pipe and fuel temperature distribution, heat transfer and heat transfer coefficient, and pump heat are node-dependent. The momentum equation is solved for links. Quantities such as flow, drift flow, flow quality and enthalpy, friction factor, two-phase multiplier, pump head, pump speed, and pump torque are link-dependent.

In the code, a set of user routines is provided which allows the user to program various boundary conditions and control logic for a given problem. The code will couple these boundary conditions and control logic with its fluid flow conservations equations, fluid state equation, and heat conduction equation to form the governing equations for the system being analyzed. Since the problem-dependent programming is transferred to the user routines, different set of user routines for various problems can be handled with a single reference code.

The boundary conditions and control logic could be in form of pressure-enthalpy boundary conditions, flow-enthalpy boundary conditions, breaks in pipes, valve actions, pump condition changes, and fuel power variations.

In the hydraulic calculations, an implicit numerical integration technique is used to solve the one-dimensional three-equation fluid flow conservation equations together with the fluid state equation. In the code, both light water and heavy water properties are available, and the two-phase fluid is assumed to be in thermal equilibrium. However, to account for the effects of the relative phase velocity, a drift-flux model with several slip and drift correlations is included in the code. The thermal non-equilibrium effect is accounted for in the pressure calculation through an adjustment of fluid property derivatives.

In the thermal calculations, a one-dimensional heat conduction equation is solved implicitly to obtain the heat transfer to the coolant and the temperature distribution within the pipe and the fuel. The resulting heat transfers to the fluid are then coupled explicitly with the hydraulic calculations.

4.6.2. The FIREBIRD Idealization

The FIREBIRD idealization of the RD-14M facility primary and secondary side is shown in Figures 4-20 to 4-21. The FIREBIRD idealization of the RD-14M facility ECC system

common piping is shown in Figure 4-22. A brief description of the primary side, secondary side and the ECCS models developed are presented in the following sub-sections.

4.6.2.1. Overview

The FIREBIRD idealization used to simulate test B9401 consisted of 387 thermalhydraulic nodes and 399 links because the code is limited to a maximum number of nodes of 400. The RD-14M idealization is presented from the perspective of the way the specific node and link parameters were calculated.

The following options have been used: Bryce indicator for slip option and RELAP-UK indicator for drift option. For all links in the model, the Martinelli-Nelson-Jones correlation is used.

The calculation was performed on HP-UNIX 9000.

4.6.2.2. Primary Side Idealization

The RD-14M primary side idealization is shown in Figure 4-20.

Fuel Channel Modeling

Nodes data were calculated as follows:

- Each heated section is split in twelve nodes, corresponding to the 12 bundle positions.
- The volume of coolant in one channel node is equal to one-twelfth of the empty channel volume, minus the volume of the fuel bundles. The water volume for the outer nodes is bigger due to a longer zone at the end of the channels.
- The metal mass for the outer nodes is bigger due to a longer zone at the end of the channels and due to the end caps.

Link data were calculated as follows:

- The cross-sectional flow area is estimated by dividing the cooling volume by the core length associated to a node. This method is used to maintain consistency with coolant volume and pressure tube length. It leads to a more representative calculation of coolant transit time across the core.
- The value for each link segment between core nodes is simply the core length divided by the number of link segments.
- An effective hydraulic diameter is defined as four times the ratio of flow area to wetted perimeter. The flow area used is the value calculated above. The wetted perimeter used is the sum of that of the flow tube and the 7 fuel element simulators.

End Fitting Modeling

The inlet and outlet fittings are split in three nodes. Inside the end fitting, the coolant flows around a liner tube. Coolant enters the shield plug via holes at the inboard end of the liner tube, then either by the annulus outside the shield plug (stagnant volume) or through the shield-plug holes to the flow tube. The reverse flow path is followed in the outlet end fitting. A large volume of coolant in the dead space near the shield plug is normally stagnant. To model flow in and out of the dead volume, a nodalization scheme, which uses a node to model

the dead space inside a node representing the end fitting body, is used. This node can act very similar to a boiler node with calculations being made for heat transfer between the dead space and the end fitting body. This representation incorporates the thermalhydraulic characteristics associated with flowing and stagnant coolant, and the entire coolant volume.

There are four inputs in FIREBIRD-III MOD1-77 that determine the thermal properties of the end fitting representation. These inputs are pipe inside diameter, pipe mass, pipe density, and pipe thickness. From these input data, an effective heat transfer area is calculated.

Each end fitting is divided into 3 nodes as follows:

- node 1, between end fitting outer body and liner tube (annular zone)
- node 2, inside liner tube, between coupling and shield plug (stagnant zone)
- node 3, between shield plug and pressure tube.

Nodes data were calculated as follows:

- The water volumes for nodes 1 and 3 were calculated as the product between cross-sectional area and length. The water volume for node 2 is 3 liters.
- The metal masses for nodes 2 and 3 were calculated as the product between density and metal volume. The metal volume for node 2 was calculated as a sum between liner tube volume, shield plug volume and end-fitting body volume behind the coupling minus the holes volume inside the shield plug. The metal volume for node 3 was calculated as a product between the pipe metal-sectional area and length. The metal mass for node 1, was calculated as a difference between the total metal mass of 33.1 kg and the sum of nodes 1 and 2 metal masses.
- The diameter for the piping heat calculation is: end-fitting body inner diameter for node 1; liner tube inner diameter for node 2; and the pipe average inner diameter for node 3.
- The appropriate thickness was determined by the other specified variables, using the expression for effective heat transfer area.

Link data were calculated as follows:

- The hydraulics of the end fitting divide naturally into two groups: the hydraulics associated with the normal flow path of fluid, and the hydraulics associated with the shield plug and the stagnant water.

There are 6 link segments in the inlet and outlet end fitting, since each FIREBIRD-III MOD 1-77 link is subdivided into two segments. However, since one of the nodes represents the dead volume, there are actually only four link segments on the normal flow path.

Normal flow path:

- The flow area for the link segments connected to node 1 is equal to the annular area between the end-fitting body and the liner tube.
- The flow area for the link segments connected to node 3 is equal to the cross-sectional area, taking into account pipe inner diameter.

- The hydraulic length for the link segments connected to node 1 is equal to half of annular zone length. The hydraulic length for the link segments connected to node 3 is equal to the pipes length from node 3.
- An effective hydraulic diameter is defined as four times the ratio of flow area to wetted perimeter.

Flow path from stagnant volume to the flow tube:

- The flow area for the link segment connected to node 2 is equal to the cross-sectional area corresponding to the liner tube inner diameter.
- The flow area for the link segment connected to node 3 is equal to the annular-sectional area, between shield plug and liner tube.
- The hydraulic length for the link segment connected to node 2 is equal to half of the stagnant zone length.
- The hydraulic length for the link segment connected to node 3 is equal to the shield plug length.
- An effective hydraulic diameter is defined as four times the ratio of flow area to wetted perimeter.

Feeder Modeling

Each feeder was split in vertical and horizontal pipes and each pipe was modelled like a node.

Node data were calculated as follows:

- The water volume was calculated as the product between the cross-sectional area and pipe length.
- The metal mass was calculated as the product between density and metal volume. The metal volume was calculated as the product between the metal annular-sectional area and the pipe length.
- The diameter is equal to the pipe inner diameter or average pipe average inner diameter (for pipes with different inner diameters)
- The thickness was calculated as half of the difference between outer and inner diameter.

Link data were calculated as follows:

- The flow area was calculated as pipe cross-sectional area.
- The hydraulic length is equal to half of the pipe length.
- The hydraulic diameter is equal to the pipe inner diameter.

Reactor Headers Modeling

Each reactor header was split in three nodes to take into account pump/boiler and feeders connection. The heat transfer area was calculated taking into account the end caps mass (where applicable) and boiler/pump/ECCS/feeder connections.

For the links between two nodes of the inlet/outlet header the flow area, hydraulic length, and hydraulic diameter were provided. The value considered for loss coefficient was zero.

The following data is provided for the header section of the links between inlet/outlet header node and inlet/outlet feeder node or boiler/pump connections node:

- The flow area is assumed to be equal to the pipe cross-sectional area connecting feeder/pump/boiler to inlet/outlet header.
- Hydraulic length is the header radius.
- The hydraulic diameter is assumed to be equal to the pipe diameter connecting feeder/pump/ boiler to inlet/outlet header.
- The elevation difference is equal to the header radius corrected with the pipe angle.
- A loss coefficient of 0.5 is assumed for pipe entrance and 1.0 for pipe exit.

The following data is provided for the header section of the links between inlet/outlet header node and pressuriser/ECCS connection node:

- The flow area is equal to the pipe cross-sectional area of the reactor header.
- The hydraulic length is equal to the length between end cap and the first inlet/outlet feeder connections to the reactor header.
- The hydraulic diameter is equal to the reactor header inner diameter.
- The elevation difference is zero.
- The loss coefficient is zero.

Pressurizer Modeling

A single node is used to model the pressurizer. The piping connecting the pressuriser to the RD-14M loop (pressurizer line) is modelled as one node.

Node data were calculated as follows:

- The coolant volume in the pressurizer node is equal to the product between the cross-sectional area and the length pipe.
- The diameter used in the thermal calculation was taken equal to inner pipe/pressuriser diameter.
- Because there are pipes with different thickness in the pressurizer node, it is quite difficult to estimate the thickness. Therefore, the thickness was calculated from the heat transfer area equation. For the pressuriser node, it is equal to the pressuriser thickness.

Link data were calculated as follows:

- The flow area is estimated as being the pipe cross-sectional area.
- The length value for each link segment corresponds to the pipe length.
- An effective hydraulic diameter is defined as four times the ratio of flow area to wetted perimeter.

Heat Transport Pump and Associated Piping Modelling

In the RD-14M loop, there are two heat transport pumps. The standard data specified in Reference 18 have been used.

Separate nodes are used to model the pump suction line (PS1/2), pump bowl (PM) and pump discharge line (PD1/2). The node-link arrangement is shown in Figure 4-20. The pump is modelled in the link between the pump suction and pump bowl nodes.

Node data were calculated as follows:

- The coolant volume in nodes 1 and 3 is equal to the product between the cross-sectional area and the pipe length.
- The diameter used in the thermal calculation was taken equal to the inner pipe diameter or the average inner pipe diameter (for different pipes in the same node).
- Due to the irregular shape of the pump bowl and because there are pipes with different thickness in the same node, it is quite difficult to estimate the thickness. Therefore, the thickness was calculated from the heat transfer area equation.

Link data were calculated as follows:

- The flow area is estimated as being the pipe cross-sectional area. The flow area for a pump was taken the same as the neighbouring pipes.
- The length value for each link segment corresponds to the pipe length. For a pipe node, the hydraulic length was taken equal to the difference between the pump inlet/outlet elevation and the pump core elevation.
- An effective hydraulic diameter is defined as four times the ratio of flow area to wetted perimeter. For pump links, the same hydraulic diameter as for neighbouring links was taken into account.

Pipes Between Outlet Header and Boiler

In the model, the pipe between outlet header and boiler was split in three nodes to take into account the angle of inclination of the pipe.

Node data were calculated as follows:

- The water volumes were calculated as the product between the pipe cross-sectional area and the length associated to the node.
- The metal mass was calculated as the product between density and metal volume. The metal volume was calculated as a product between the pipe metal-sectional area and length.
- The diameter for the piping heat calculation is the inner pipe diameter.

Link data were calculated as follows:

Pipes between outlet header and boiler

- The flow area for the link segments is equal to the product between the tube cross-sectional area and the length associated to each node.
- The hydraulic length is equal to half of the length associated to each node.
- An effective hydraulic diameter is defined as four times the ratio of flow area to wetted perimeter.

Boiler inlet/outlet plenum

- The flow area was calculated by dividing the cooling volume by the length between pipe connection to boiler plenum and tubesheet. This maintains consistency with coolant volume and length and leads to a more representative calculation of cooling transit time across the core.
- The hydraulic length was calculated as the difference between tubesheet elevation and pipe connection elevation to boiler plenum.
- An effective hydraulic diameter is defined as four times the ratio of flow area to wetted perimeter (near tubesheet).
- Minor losses are negligible, hence the loss coefficient in the connecting link sections is taken to be equal to zero.

Boiler Tubes

- The flow area for the link segments is equal to the product between the tube cross-sectional area and the length associated to each node.
- The hydraulic length is equal to half of the length associated to each node.
- An effective hydraulic diameter is defined as four times the ratio of flow area to wetted perimeter.
- The height is equal to the length for vertical portions. For U-bend portions, the total U-bend length of all boiler tubes was calculated based on Reference 3 for each boiler.
- Minor losses are negligible, hence the loss coefficient in the connecting link sections is taken to be equal to zero.

4.6.2.3. Secondary Side Idealization

The secondary side idealization is presented in Figure 4-21.

Primary Side Boiler Modelling

Only unplugged tubes are taken into account and they are modelled as one "average" tube. Six nodes can be identified:

- Vertical portion from inlet plenum through the tubesheet to the preheater end elevation,
- Four portions of equal length:
  one vertical portion starting from the preheater end elevation,
  one vertical portion followed by a U-bend portion, ended by the U-bend top,
  one U-bend portion starting from the U-bend top, followed by a vertical portion,
  one vertical portion ended by the preheater end elevation,
- Vertical portion from preheater end elevation through tubesheet to outlet plenum.

Node data were calculated as follows:

- The water volumes were calculated as the product between the number of unplugged tubes, the tube cross-sectional area and the length associated with each node.
- The boiler tube total length of one boiler was calculated as the sum of the product between the number of tubes of each type and the tube length for that tube type.

- The metal mass was calculated as the product between density and metal volume. The metal volume was calculated as a product between the pipe metal-sectional area and length.
- The diameter for the piping heat calculation is the inner tube diameter.

Secondary Side Boiler Modelling

Each of two boilers is modelled as a single node. Each node is a lumped heat transfer node, incorporating the downcomer, riser, internal preheater, and steam drum portion of the boiler. Specific modelling of each of these components is contained in the user subroutines. The steam pipes between each boiler and the steam balance header are each represented by one node, as is the steam balance header itself. All flows into and from this system (boiler feedwater, jet condenser steam flow), are modelled as flow-enthalpy boundary conditions. Hence node and link geometrical data are only needed for the two boilers, the two steam pipe nodes, and the single steam balance header node.

Node data were calculated as follows:

The parameters specified for nodes are coolant volume, and the three effective values for the piping heat calculation -inner diameter of a representative cylinder, its thickness, and piping mass.

Boiler node:

- Volume: It includes the riser volume, downcomer volume, the volume above the bottom of the separators, and the steam drum. These volumes are not modelled individually in the one-node boiler model.
- Metal mass: It was calculated as the sum of the shell metal mass, longitudinal baffle metal mass and downcomer metal mass.
- The heat transfer area was calculated as the sum of the heat transfer areas of the shell, longitudinal baffle and downcomer.
- The thickness was calculated from the heat transfer area equation.

Steam pipe node:

- This volume was calculated as a product between cross-sectional area and length.
- Metal mass: It was calculated as the product between the pipe metal area and the pipe length.
- The diameter is equal to the pipe inner diameter.

Steam balance header node:

- Volume: This volume was calculated as a product between cross-sectional area and length.
- Metal mass: It was calculated as the product between the pipe metal area and the pipe length.
- The diameter is equal to the average pipe inner diameter.

Link data were calculated as follows:

All flows into and from this system (boiler feedwater, jet condenser steam flow) are modelled as flow-enthalpy boundary conditions. Hence link geometrical data is only needed for the link between the boiler node and the steam pipe node and between the steam pipe node and the steam balance header node.

Between the boiler node and the steam pipe node:

- The flow area is estimated as being the steam pipe cross-sectional area.
- The length for the link segment connected to the boiler node is equal to the steam space height of the boilers. The length for the link segment connected to the steam pipe node is equal to the pipe length.
- The hydraulic diameter for the link segment connected to the boiler node was assumed to be equal to the steam drum inner diameter. The hydraulic diameter for the link segment connected to the steam pipe node was assumed to be equal to the pipe inner diameter.

Between the steam pipe node and the steam balance header node:

- The flow area is estimated as being the pipe cross-sectional area.
- The length is equal to the pipe length.
- The hydraulic diameter was assumed to be equal to the pipe inner diameter.

The steam line connecting the balance header to the jet condenser is modeled by one link. Since this link is connected to a flow-enthalpy boundary condition node, only the flow area and the hydraulic diameter are specified for the terminal section. The pipe hydraulic parameters are similar to the link segment parameters connected to the steam balance header, on the link between the steam pipe and the steam balance header.

4.6.2.4. ECC System Idealization

Figure 4-22 shows the nodalization for the ECCS model. The emergency core coolant system is divided into two phases: high pressure injection and low pressure injection. During both phases, the water is supplied by ECCS pumps. The high pressure injection will end when the water level in the ECC tank TK2 reaches 10%. The low pressure pumped ECC phase ends when the level in the distilled water tank falls below 50%.

Figure 4-22 also identifies the relevant control valves. All valve control logic is modelled in the user subroutine USCOVL.

The ECC pumps head is calculated as a function from a flow versus head table, built on the pump P14/8 performance curve (See Reference 3).

No piping heat calculations are performed for ECCS piping. Hence, the only node geometric parameter input is volume.

Link data were calculated as follows:

- The flow area is estimated as being the pipe cross-sectional area.
- Hydraulic Length — The length value for each link segment corresponds to the pipe length.
- An effective hydraulic diameter is defined as four times the ratio of flow area to wetted perimeter.

Table 4.13. Main Dimensions of the FIREBIRD III MOD 1 Nodalizations Developed for RD-14M

No	QUANTITY	VALUE	NOTES
1	No. of Hydraulic Nodes	387	
2	No. of Links	399	
3	No. of nodes for piping heat calculation	368	
4	No. of nodes for fuel heat calculation	120	
5	No. of hydraulic channels for the active core	10	Each of the HS5 to HS14is simulated.
6	No. of structures and of hydraulic nodes belonging to a horizontal stack per each hydraulic channel of the active core	12	
7	No. of cards of the input deck	3183	

Table 4.14. List of Relevant Initial Conditions Measured and Calculated for the RD-14M, B-9401 Experiment

No	QUANTITY	UNIT	EXP	CALC	NOTES
1	Pressurizer pressure	MPa	9.9	10.02	
2	HD5 pressure	MPa	10.0	10.02	
3	DP (HD8-HD5)/(HD6-HD7)	MPa	1.3-1.5	1	
4	SGs pressure	MPa	4.5	4.52	
5	MCP1 flowrate	Kg/s	21.9	21.81	
6	MCP2 flowrate	Kg/s	21.6	22.13	
7	HS5 mass flowrate	Kg/s	4.0 – 4.1	3.98	
8	HS6 mass flowrate	Kg/s	4.0 – 4.1	4.05	
9	HS7 mass flowrate	Kg/s	4.5 – 4.8	5.09	Fed by MCP1
10	HS8 mass flowrate	Kg/s	4.5 – 4.8	4.97	
11	HS9 mass flowrate	Kg/s	4.0 – 4.1	4.04	
12	HS10 mass flowrate	Kg/s	3.9 – 4.0	3.91	
13	HS11 mass flowrate	Kg/s	4.0 – 4.0	4.04	
14	HS12 mass flowrate	Kg/s	4.5 – 4.8	4.93	Fed by MCP2
15	HS13 mass flowrate	Kg/s	4.5 – 4.8	4.99	
16	HS14 mass flowrate	Kg/s	3.9 – 4.0	3.95	
17	SG1 SL flowrate	Kg/s	1.9	1.91	
18	SG1 FW flowrate	Kg/s	2.1	1.91	
19	SG2 SL flowrate	Kg/s	2.0	2	
20	SG2 FW flowrate	Kg/s	2.5	2	
21	SG1 DC flowrate	Kg/s	-	-	
22	HD5 / HD7 fluid temperature	°C	295	295.2 / 296.8	
23	HD8 / HD6 fluid temperature	°C	262	261.3 / 261.4	
24	SG1 fluid temperature	°C	-	257.3	
25	FW temperature	°C	187	187	
26	Void fraction at HS5 outlet	-	-	0.	
27	Void fraction at HS8 outlet	-	-	0.	
28	MCP speed	rpm	3400	3549	
29	SG1 level	m		10.23	
30	PRZ level	m	1.31	1.31	
31	Core total power	MW	8.14	8.14	

Table 4.15. List of Relevant Boundary Conditions Measured and Adopted in the Calculation of the RD-14M, B-9401 Experiment

No	EVENT/QUANTITY	UNIT	VALUE	NOTES
1	Test start	s	0	Transient steady state was run before this time. Steady state data for 10 seconds are added before this time in the results.
2	Break opening	s	0.	
3	Power ramp down	s	2.	Channels are grouped in accordance with Table 1 of App. B of Report RC-2491 by R.S. Swartz (AECL, June 2000) to 4 channel groups. Power is decreased in 40 steps in accordance with data provided by test records.
4	SGs SL flowrate	-	-	SL flowrate has been imposed as a function of time following relevant experimental signal.
5	SGs FW flowrate	-	-	FW flowrate is calculated by code in order to maintain boiler level.
6	MCP coast-down start	s	2.	Pump speed versus time was imposed in accordance with test data.
7	ECC-HPIS start	s	10.6	The HPIS 'P14' pump characteristic (G vs P) has been taken from Figure 8.10 of the report at item 3 above (dotted line with ▲).
8	PRZ isolation	s	12.8	
9	Isolation of ECC-HPIS	s		Based on the HP–ECC tanks depletion.
10	ECC-LPIS start	s	106.2	The LPIS 'P8' pump characteristic (G vs P) has been taken from Figure 8.11 of the report at item 3 above (dotted line with □).
11	MCP coast-down end	s	205.6	
12	Isolation of ECC-LPIS	s		Based on LP-ECC tanks depletion.
13	End of calculation	s	400.0	

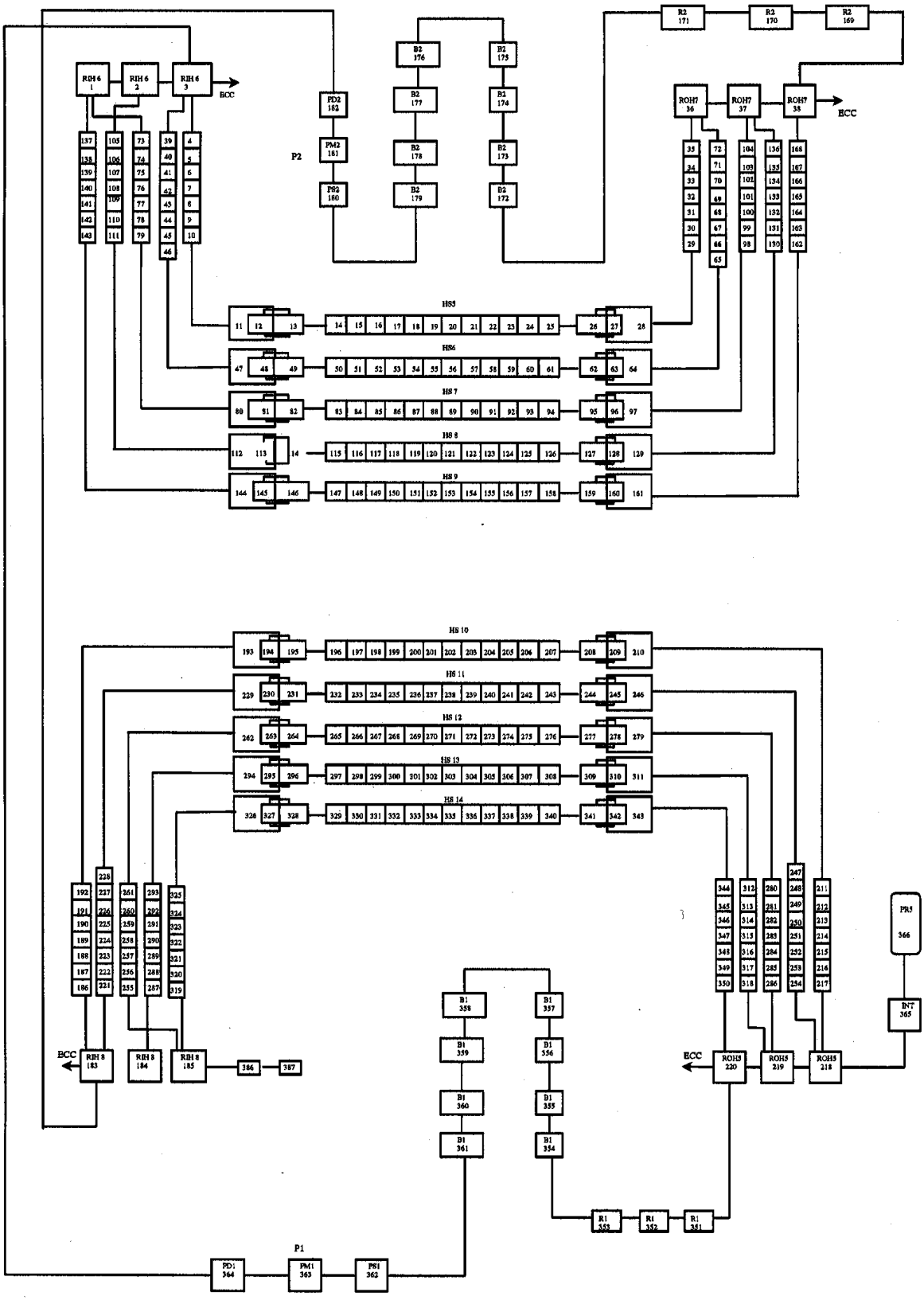

Fig. 4.20. Primary Side Idealization.

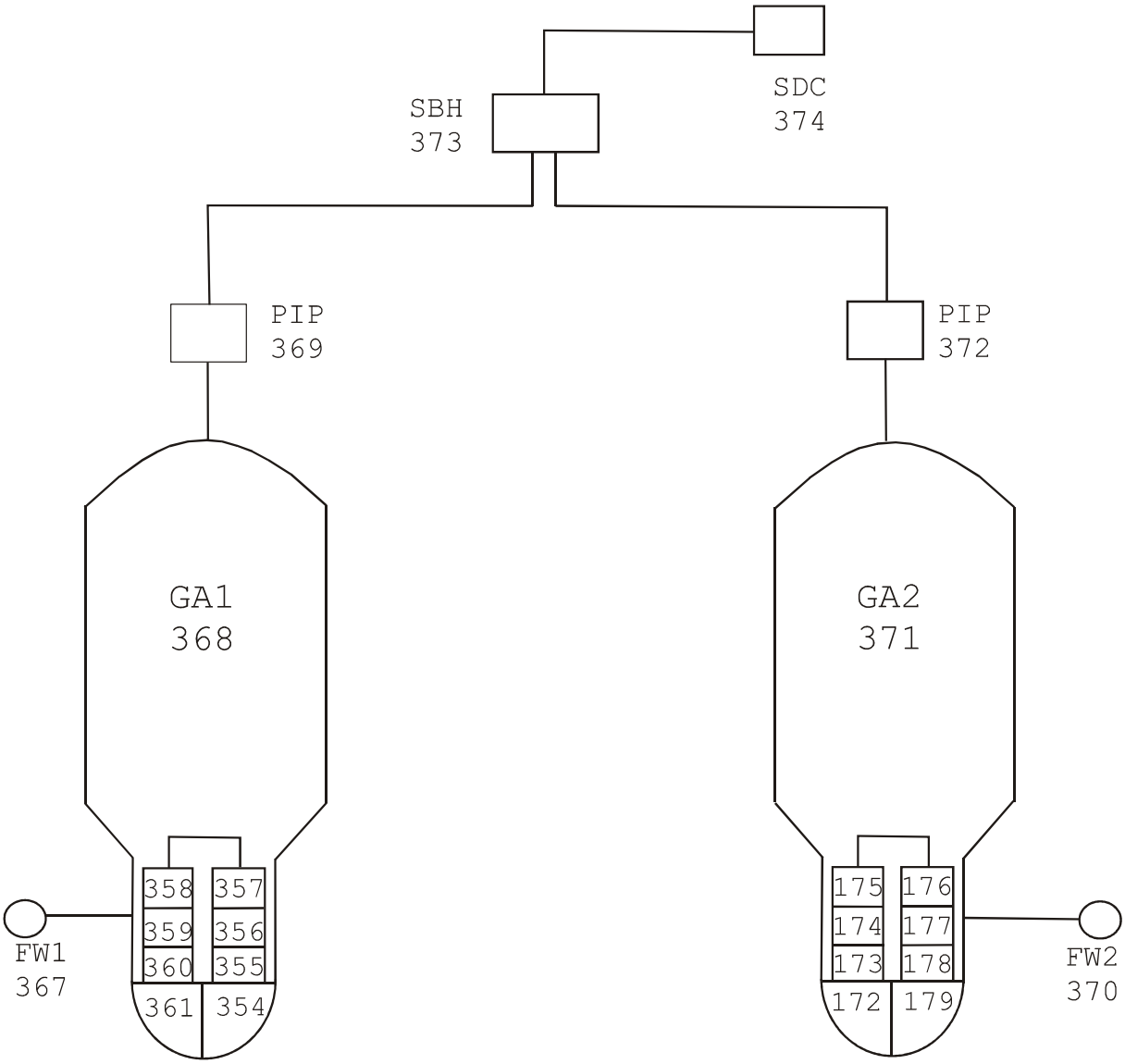

Fig. 4.21. Secondary Side Idealization.

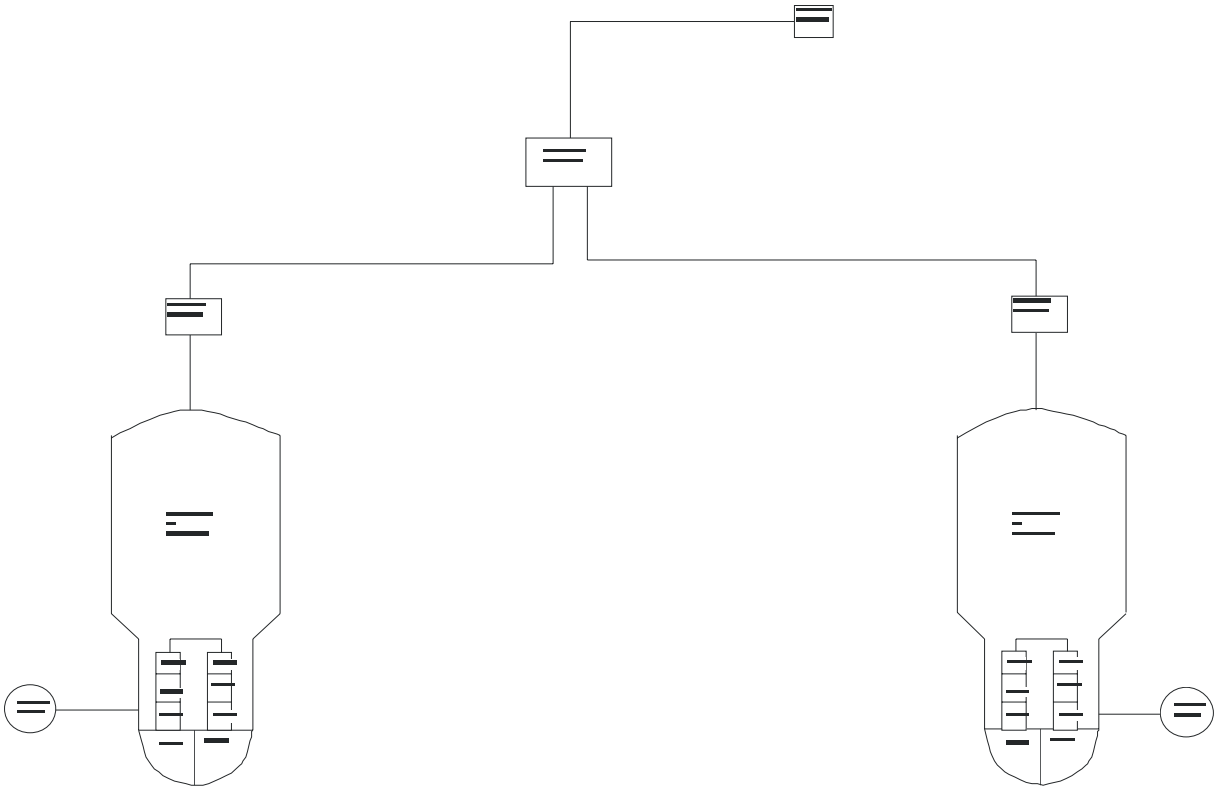

Fig. 4.22. Secondary side Idealization.

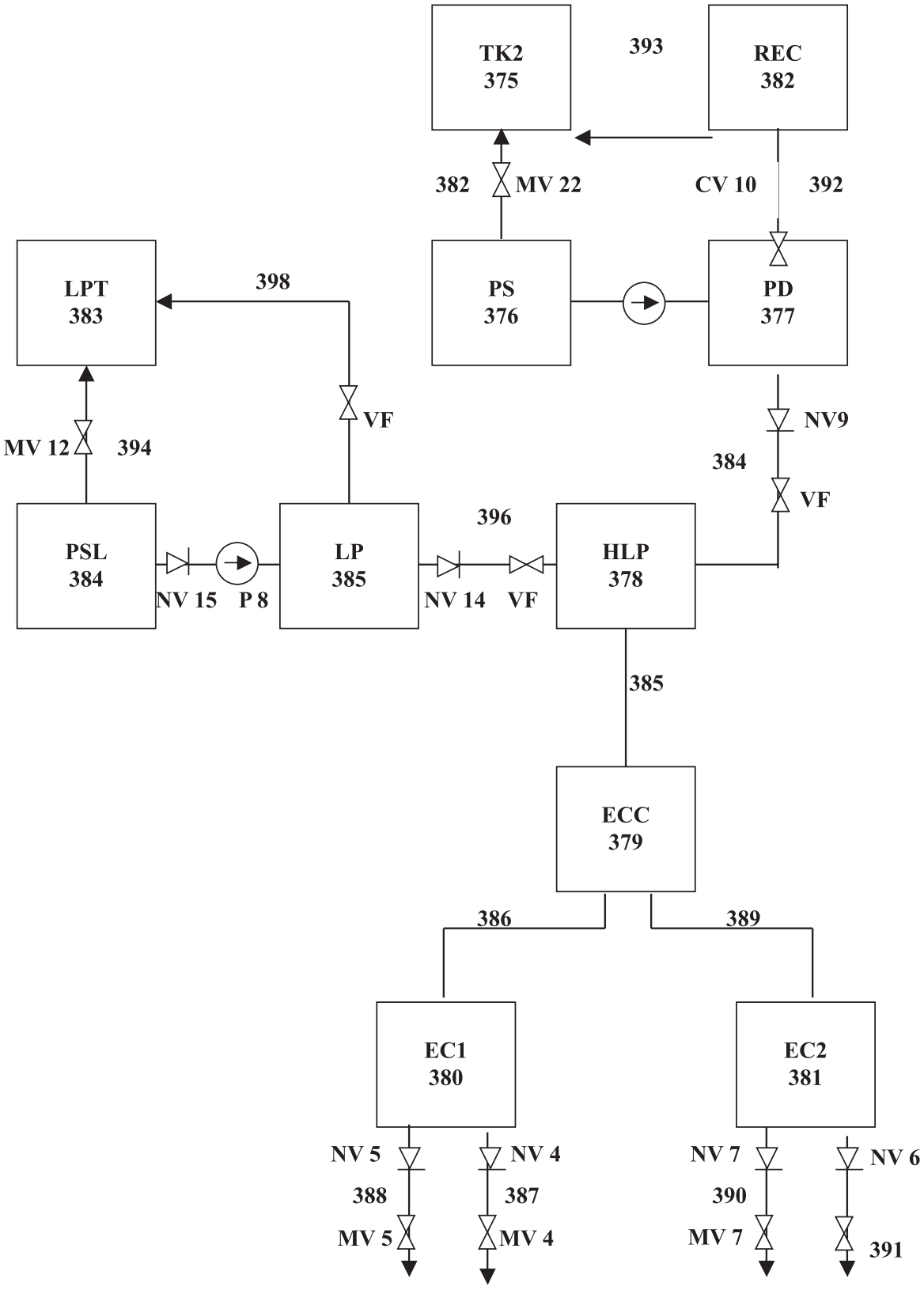

Fig. 4.23. ECCS Idealization.

CHAPTER 5. CODE COMPARISONS WITH EXPERIMENT

As discussed previously, test B9401 was characterized with over 558 measurements over the duration of the experiment. A subset is required to make a meaningful comparison. A proposed list of variables to be compared was prepared by Canada, and distributed to participants in 2002 April, prior to the third meeting. Based on detailed discussions during this meeting, a revised list was generated, and documented in [15]. Table 5-1 lists these selected variables for the code intercomparison and validation. Exact locations of the measurement for these variables can be found in [1] based on the "Device Code" given in Table 5. Data were collected for 924 s in the experiment. However, *only the first 400 s of the transient is used for the intercomparison* since the significant events occur in the first 400 s of the test B9401.

In the following sections the rationale for the selection of these variables is given followed by a discussion of participant's results compared to experiment.

5.1. Primary Pump Differential Pressures, ΔP_{P1} and ΔP_{P2}

Primary loop coolant circulation is provided by two high-head centrifugal pumps. In test B9401, the break occurred at inlet-header 8 at 10 s, and the primary pumps were ramped down starting at 12 s. The histories of ΔP_{P1} and ΔP_{P2} are a good indication of flow directions across the pumps during the blowdown transient. Since the break occurred at the inlet-header 8, which is close to pump 2 outlet, ΔP_{P1} and ΔP_{P2} should demonstrate different behaviours.

Figures 5.1 and 5.2 provide the code comparison to experiment. In Figure 5.1 all calculations show the proper trends. The peak differential pressure around 30 seconds is thought due to the flow stagnation location. The flow stagnation location is a function of break flow, pump forces and system hydraulic losses. In Figure 5.2 it is noted that Republic of Korea and Argentina calculate a higher (and more correct) negative DP at about 30 s.

5.2. Header Differential Pressures, ΔP_{HD8-5} and ΔP_{HD6-7}

During the break, the primary pump speeds are reduced and ECC flow is initiated causing flows to change dramatically in the primary heat transport system. Header differential pressures (DP) provide an overall indication of flow directions in the below-header portion of the loop (inlet feeders, outlet feeders and heated sections) during the blowdown transient.

Figures 5.3 and 5.4 provide the code comparison to experiment. In both Figures 5.3 and 5.4, all calculations show the correct timing and trend, with the differential pressures being under-predicted by some participants and over-predicted by others. It is noted that this DP will drive the FES heatup in channels connected to these headers, with a smaller DP resulting in higher temperatures.

Table 5.1. Selected Variables for Intercomparison

Selected Variables	Variable Description	RD-14M Channel	Device Code	Var. Units	Order of Var.
	Time			s	1
ΔP_{P1}	Pump 1 Differential Pressure (DP)	341	5Q-D1	kPa(a)	2
ΔP_{P2}	Pump 2 DP	348	12Q-D1		3
ΔP_{HD8-5}	DP from HDR8 to HDR5	336	35Q-D1	kPa(a)	4
ΔP_{HD6-7}	DP from HDR6 to HDR7	338	36Q-D1		5
P_{HD8}	Header 8 Pressure	179	10P-D1	MPa(a)	6
P_{HD6}	Header 6 Pressure	323	4P-D1		7
P_{HD7}	Header 7 Pressure	178	6P-D1		8
Q_{P1}	Pump 1 Discharge Flowrate	78	1F	L/s	9
Q_{P2}	Pump 2 Discharge Flowrate	79	2F		10
Q_5	ECC to Header 5 Flowrate	235	231F-D1	L/s	11
Q_6	ECC to Header 6 Flowrate	237	232F-D1		12
Q_7	ECC to Header 7 Flowrate	236	233F-D1		13
Q_8	ECC to Header 8 Flowrate	238	234F-D1		14
Q_{INT}	Integral of ECC Flows	92	1H	L	15
α_1	Boiler 1 Inlet Void Fraction	313 314	11VF-DT1 11VF-DT2		16
α_2	Boiler 2 Inlet Void Fraction	283 284	12VF-DT3 12VF-DT4		17
α_3	Pump 1 Outlet Void Fraction	2	21VF-DTZ		18
α_4	Pump 2 Outlet Void Fraction	124	4VF-DTZ		19
T_{B1-IN}	Boiler 1 Inlet Fluid Temp.	138	60T-D1	ºC	20
T_{B2-IN}	Boiler 2 Inlet Fluid Temp.	140	61T-D1		21
T_{B1-OUT}	Boiler 1 Outlet Fluid Temp.	139	60T-D2		22
T_{B2-OUT}	Boiler 2 Outlet Fluid Temp.	141	61T-D2		23
T_1	FES Temp.@top pin, middle HS13	442	208T-D12	ºC	24
T_2	FES Temp.@top pin, inlet HS13	433	208T-D3		25
T_3	FES Temp.@top pin, outlet HS13	444	208T-D14		26
T_4	FES Temp.@bot pin, outlet HS13	448	208T-D18		27
T_5	FES Temp.@top pin, middle HS8	424	203T-D12		28
α_5	HS5 Inlet Void Fraction	329	15VF		29
α_6	HS5 Outlet Void Fraction	328	16VF		30
α_7	HS13 Inlet Void Fraction	131	31VF		31
α_8	HS13 Outlet Void Fraction	130	32VF		32
$\Delta P_{HS13-HD5}$	DP from HS13 to HDR5	581	45Q-D1	kPa(a)	33
ΔP_{HS13}	DP Across HS13	579	32Q-D1		34
P_{SRG}	Pressure in Pressurizer*	177	26P-D1	MPa(a)	35
P_{B1}	Boiler 1 Drum Pressure*	105	1P	MPa(a)	36
ω_{P1}	Pump 1 Speed*	197	PM1-1Y	RPM	37
ω_{P2}	Pump 2 Speed*	200	PM2-1Y	RPM	38
Q_{BRK}	Break Discharge Mass Flowrate**			kg/s	39
W	Total System Power**			kW	40
M	Mass Inventory in Primary loop**			kg	41
W_{TH1}	Thermal Power Across Boiler 1**			kW	42
W_{TH2}	Thermal Power Across Boiler 2**			kW	43

* These are confirmatory variables, used to confirm that the simulations are performed under the correct conditions.

** These are variables that were not measured experimentally, but will aid in the code-to-code comparison.

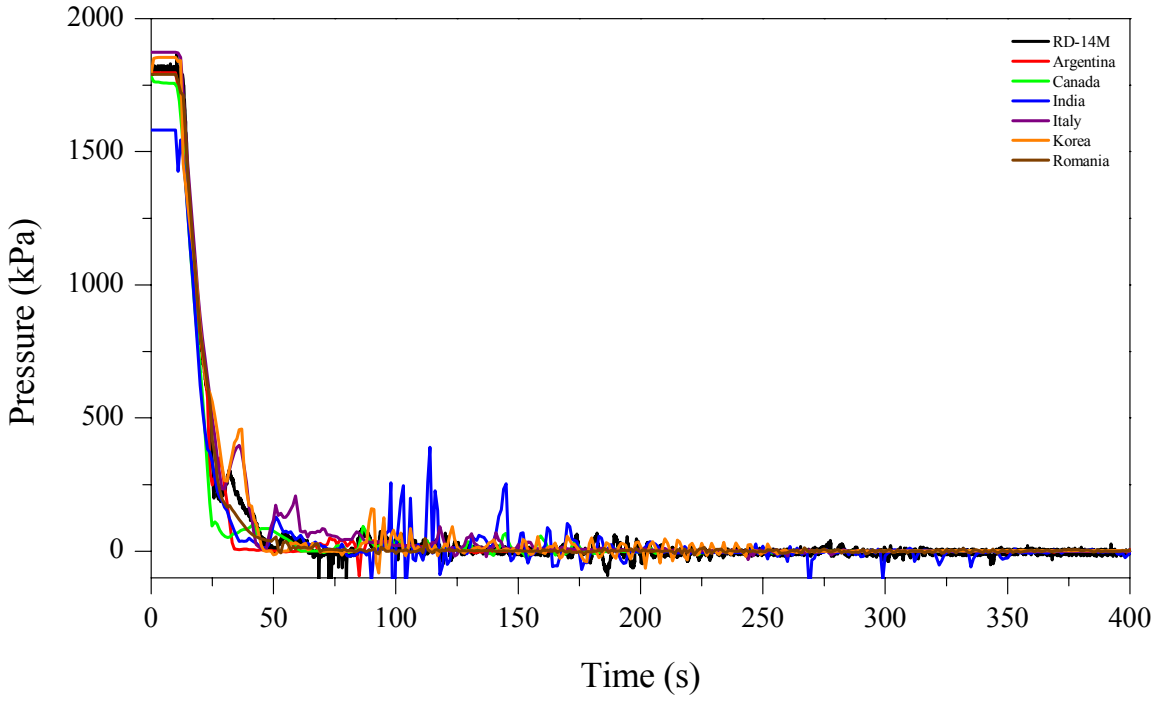

Fig. 5.1. Pump 1 Differential Pressure.

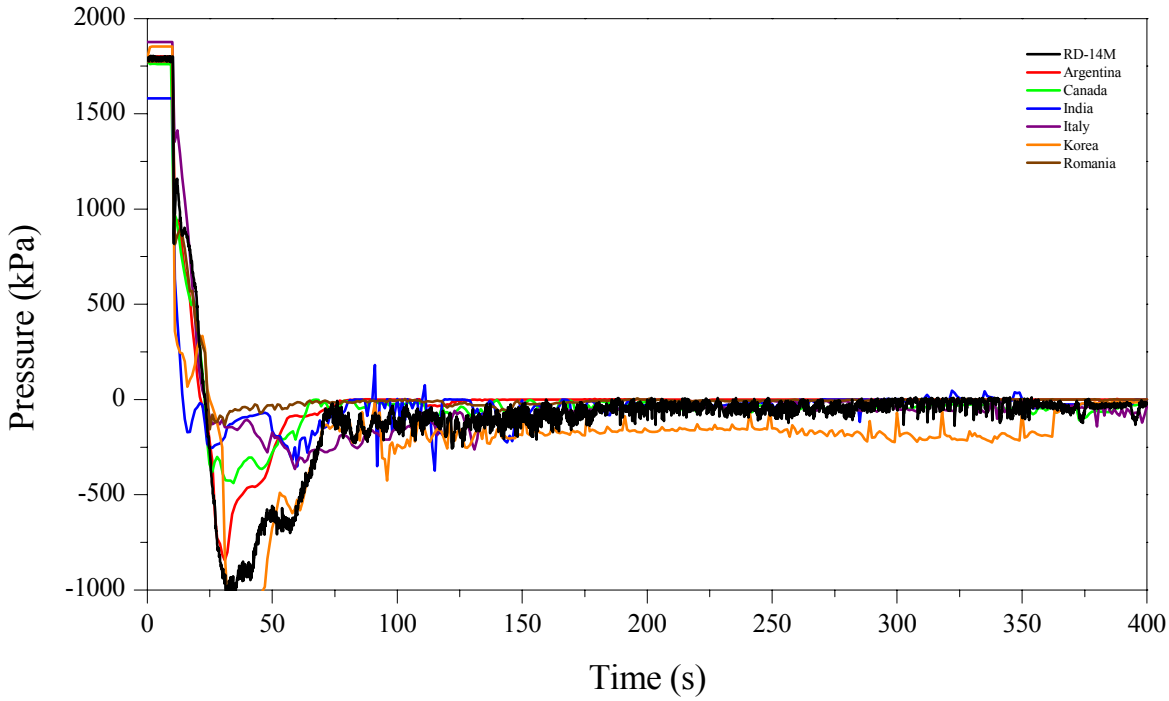

Fig. 5.2. Pump 2 Differential Pressure.

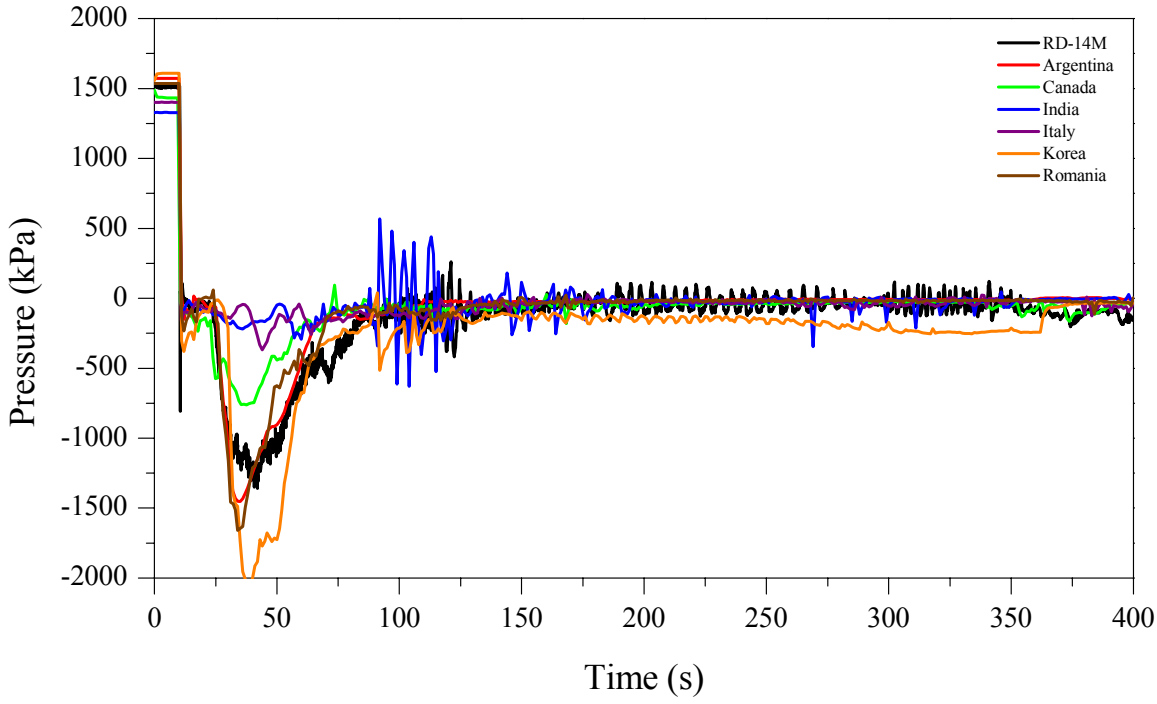

Fig. 5.3. Header 8 to Header 5 Differential Pressure.

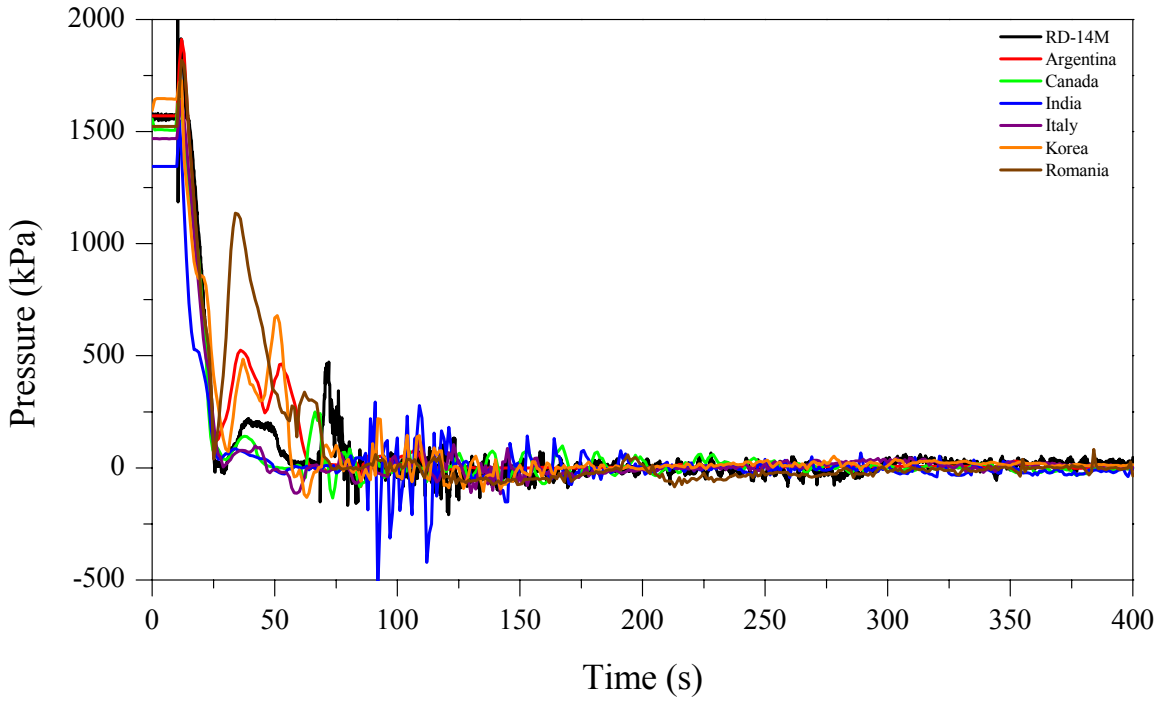

Fig. 5.4. Header 6 to Header 7 Differential Pressure.

5.3. Pressures at Header 8, Header 6 and Header 7, P_{HD8}, P_{HD6} and P_{HD7}

Header depressurisation is largely determined by break discharge rate. However, later it is affected by ECC injection. In test B9401, the ECC system was directed into four headers. Emergency coolant injection begins when the selected header pressure drops below the pre-determined injection pressure. Header pressures determine when and at what flowrate the ECC flow enters each header. Since header 8 is the broken header, it has the fastest depressurisation rate of the four headers during the blowdown. Header 6 is farthest from the broken header, and has the slowest depressurisation rate. Header 7 is an outlet header, and has a depresurisation rate between those of header 6 and header 8.

Figures 5.5 to 5.7 provide the code comparison to experiment. All participants captured the correct trend, with some participants predicting a more rapid depressurization in the first 100 s, and others predicting a less rapid depressurization.

5.4. Primary Pumps 1 and 2 Flowrates, Q_{P1} and Q_{P2}

Two primary pumps maintain coolant circulation in the primary loop. Apart from primary pump differential pressures, pump flowrate is another variable that can be used to determine loop flow direction changes during the transient. The flowrate measurement from the turbine flowmeters (TFM) in test B9401 is a volumetric flowrate, and is recorded in L/s.

Figures 5.8 and 5.9 provide the code comparison to experiment. In Figure 5.8 it is noted that two-phase conditions exist at the turbine flow meter early in the transient (Figure 5.17a), and as such the measurement is not reliable. The peak flow at about 75s was predicted by most of the participants. Pump 2 (Figure 5.9) “sees” two-phase flow at about 25s, and all calculations show correct trend until this time. It is noted that turbine flow meters are only reliable in single-phase flow. For this reason, Figure 5.9 only shows results to 25 s.

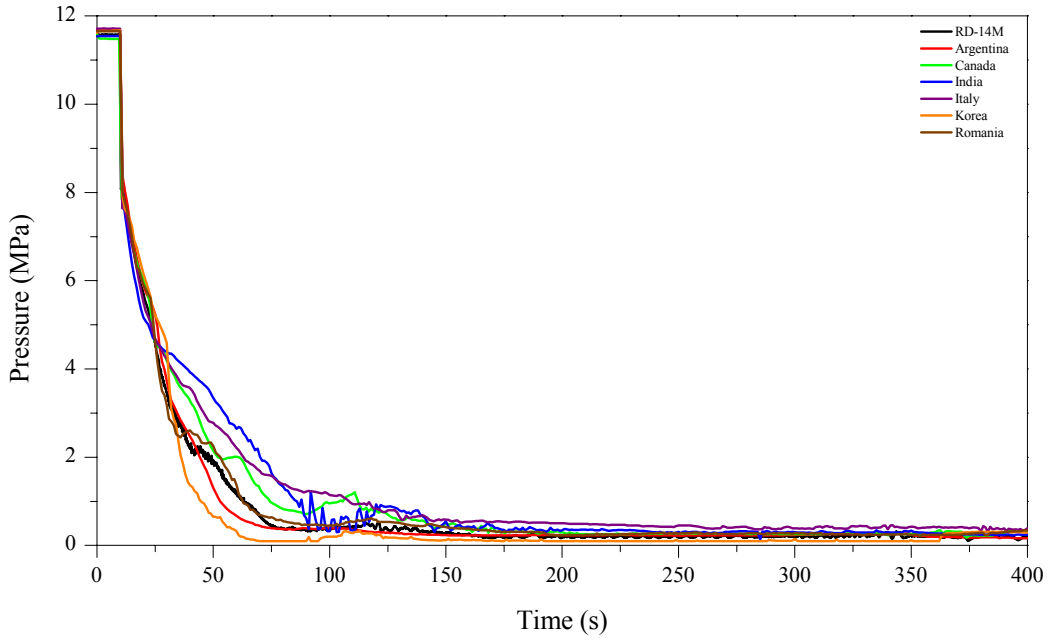

Fig. 5.5. Header 8 Pressure.

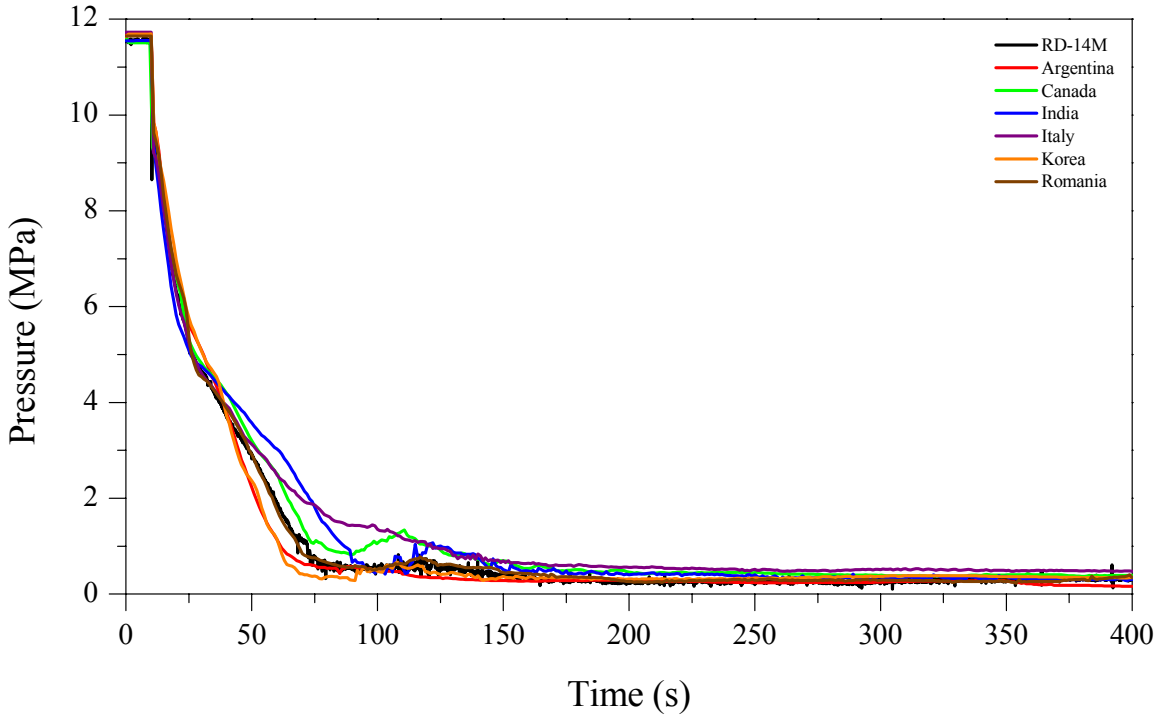

Fig. 5.6. Header 6 Pressure.

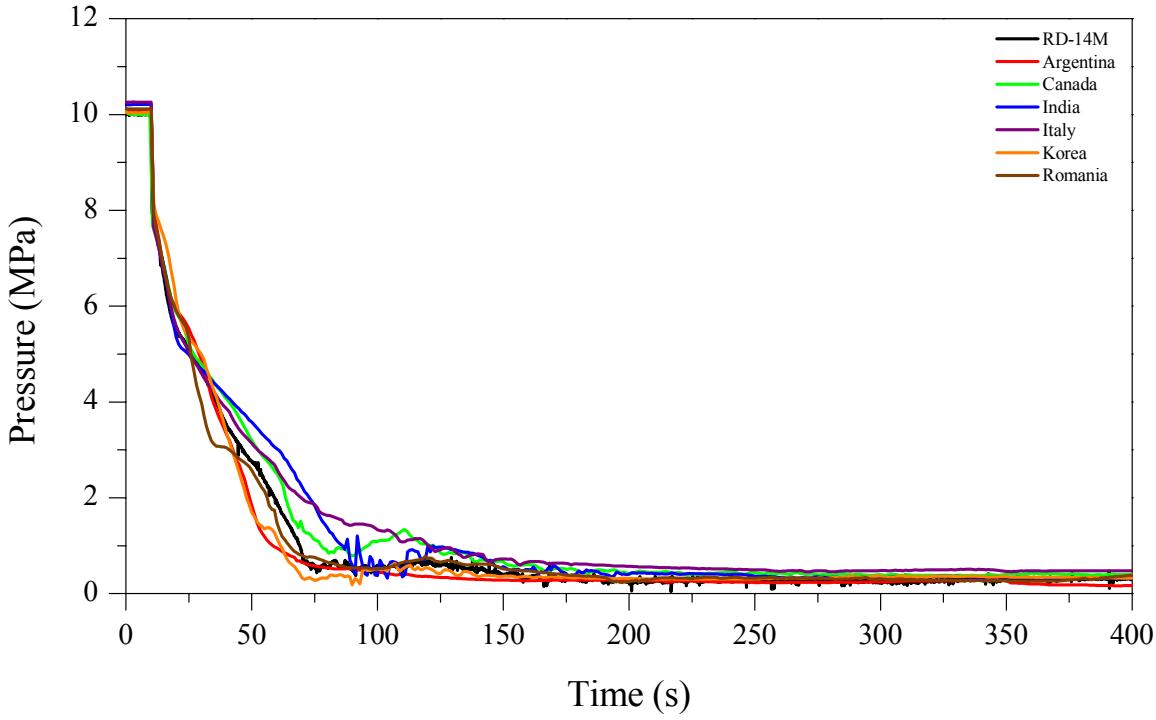

Fig. 5.7. Header 7 Pressure.

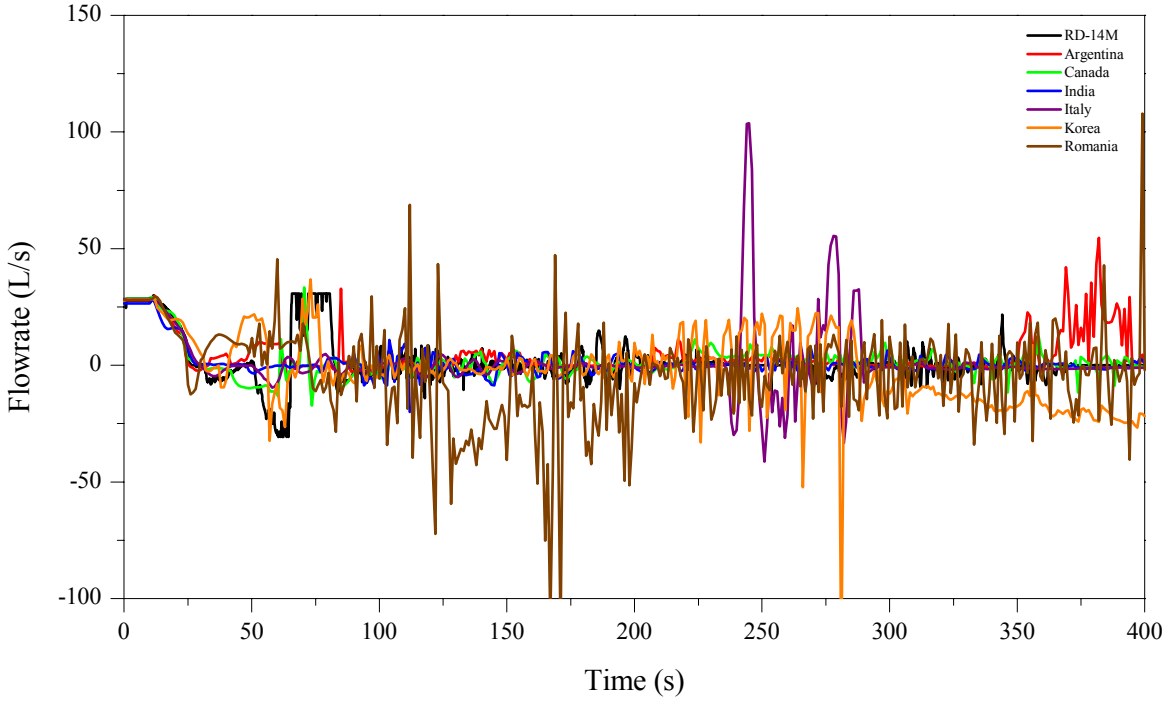

Fig. 5.8. Pump 1 Discharge Flowrate.

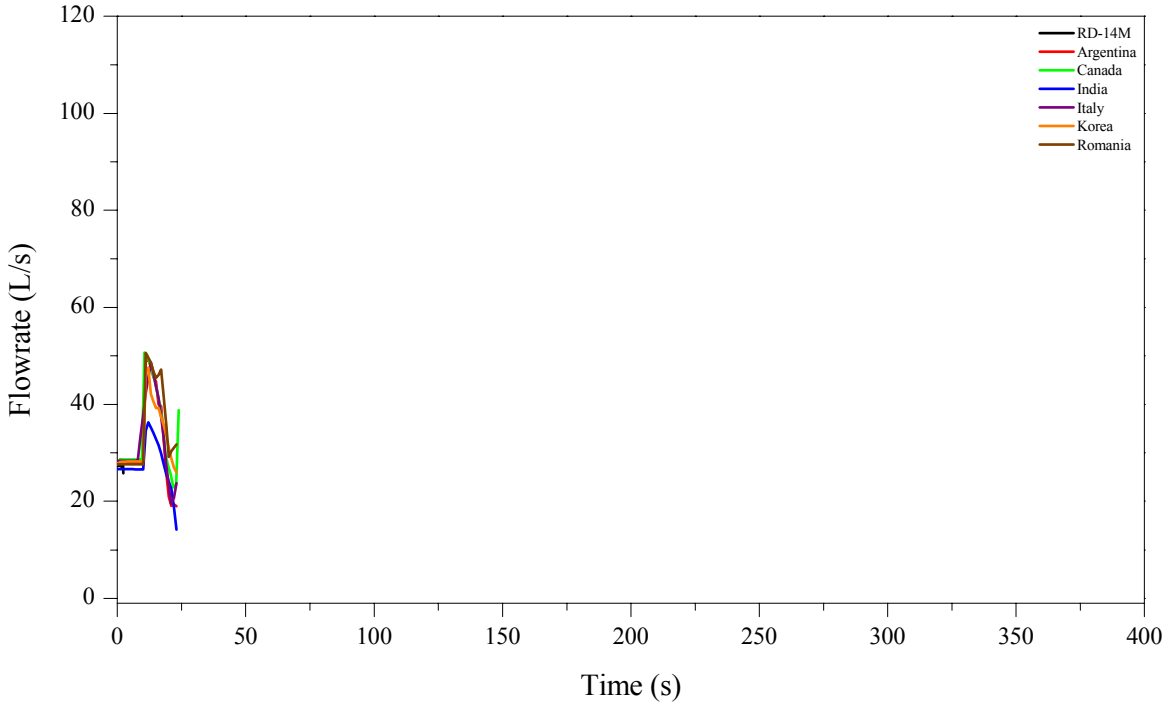

Fig. 5.9. Pump 2 Discharge Flowrate.

5.5. Header ECC Flowrates, Q_5 through Q_8

Since the depressurisation rates vary from header to header, the timing and flowrates of ECC to each header are different. ECC flowrates to each header (Q_5 through Q_8) are important for analysing ECC system behaviour, and more importantly, for analysing the fuel channel behaviour.

Figures 5.10 to 5.17 provide the code comparison to experiment. Emergency core coolant (ECC) is connected both to the broken & unbroken loops, and the codes all calculate this split. Some deviation is noted amongst participants, as ECC flows depend on the calculated pressure drop around the loop. It is noted that all participants predict the initiation of ECC flow accurately to Header 8 (break location). However, most calculations predict flow to other headers at a time before the experiment.

The participants noted that modelling of the ECC system was not always consistent with the experimental evidence. This was certainly true of the low-pressure ECC system, and this was resolved in an additional calculation. Further investigation was recommended by the participants. However, because overall system performance was predicted satisfactorily, no additional work was performed in this project.

5.6. Integral of ECC Flows, Q_{INT}

Integrated header ECC flowrates provides the total volume of fluid that comes from the ECC system to the primary loop. It is important since it has a direct impact on primary loop pressure, quenching of the fuel channels, FES sheath temperatures and mass inventory of the primary system.

Figure 5.18 provides the code comparison to experiment. All participants show excellent agreement with experiment during the high-pressure ECC, with India slightly under predicting flows during this time. Some differences are noted in the later part of low-pressure ECC (after 200 s), although this condition is specified as a boundary condition. It is not expected that these deviations would affect system behaviour significantly.

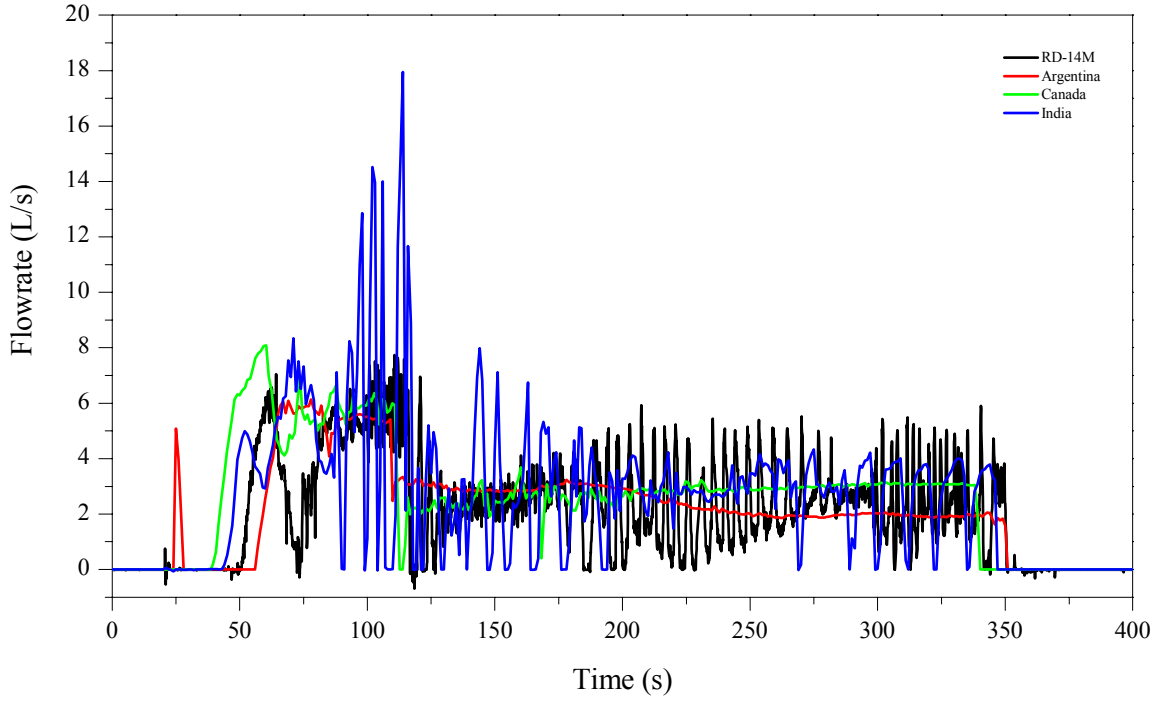

Fig. 5.10. ECC to Header 5 Flowrate.

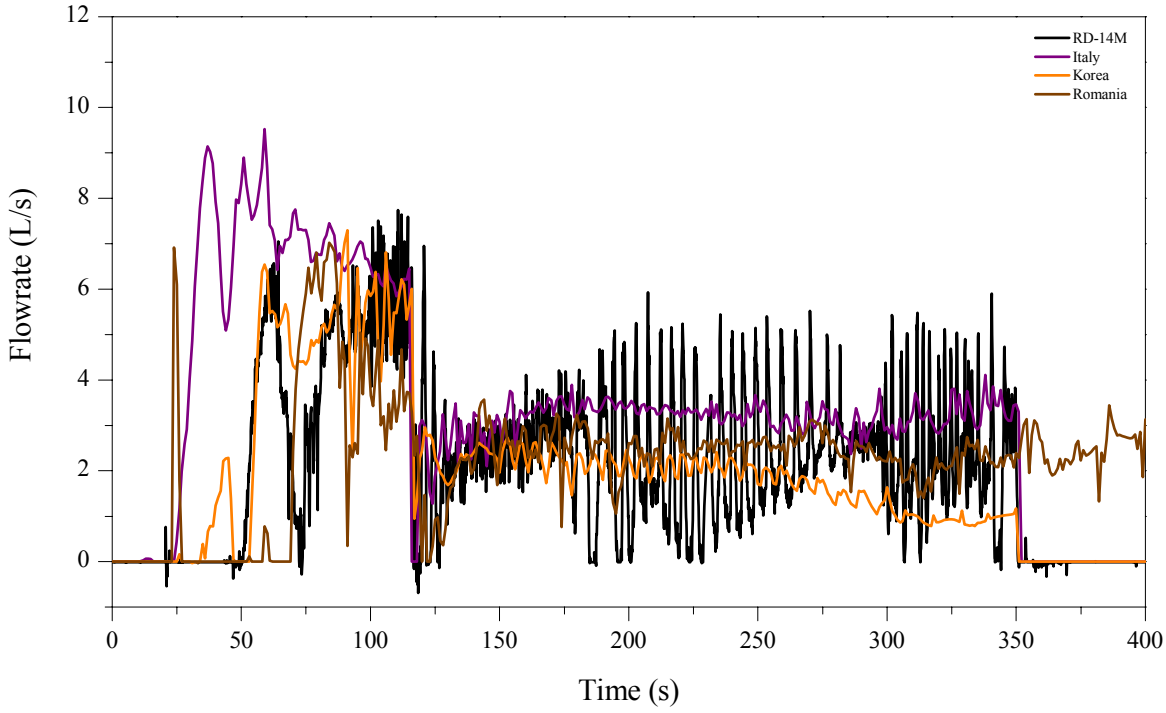

Fig. 5.11. ECC to Header 5 Flowrate.

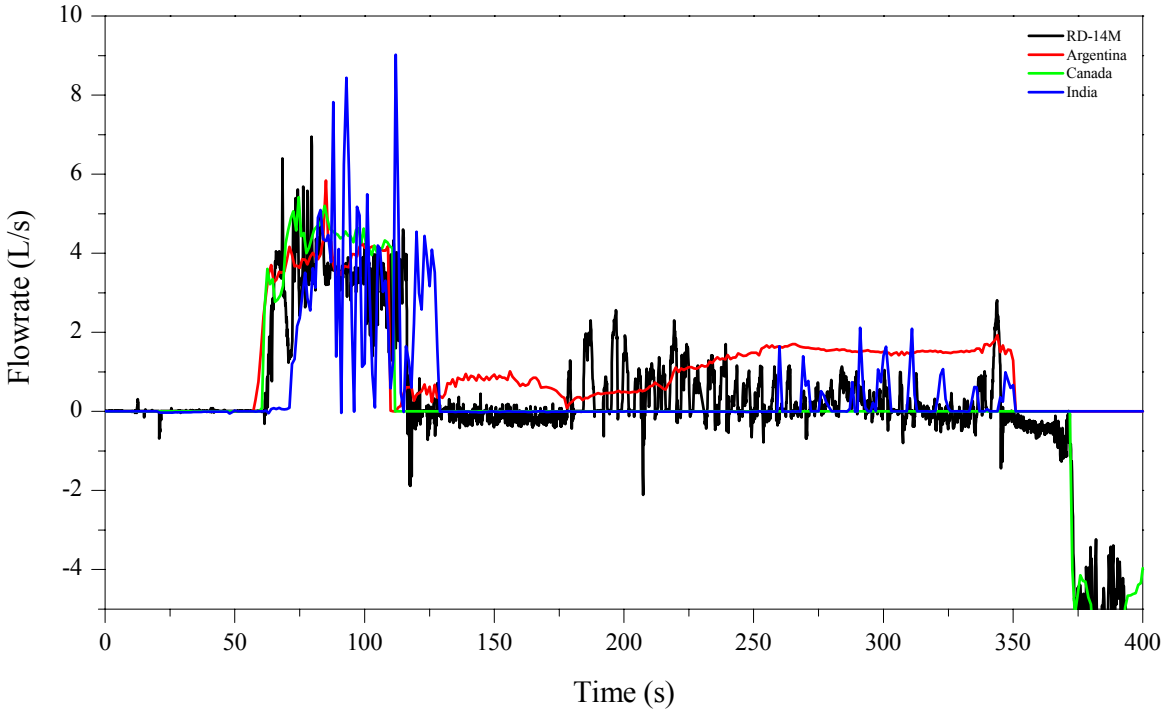

Fig. 5.12. ECC to Header 6 Flowrate.

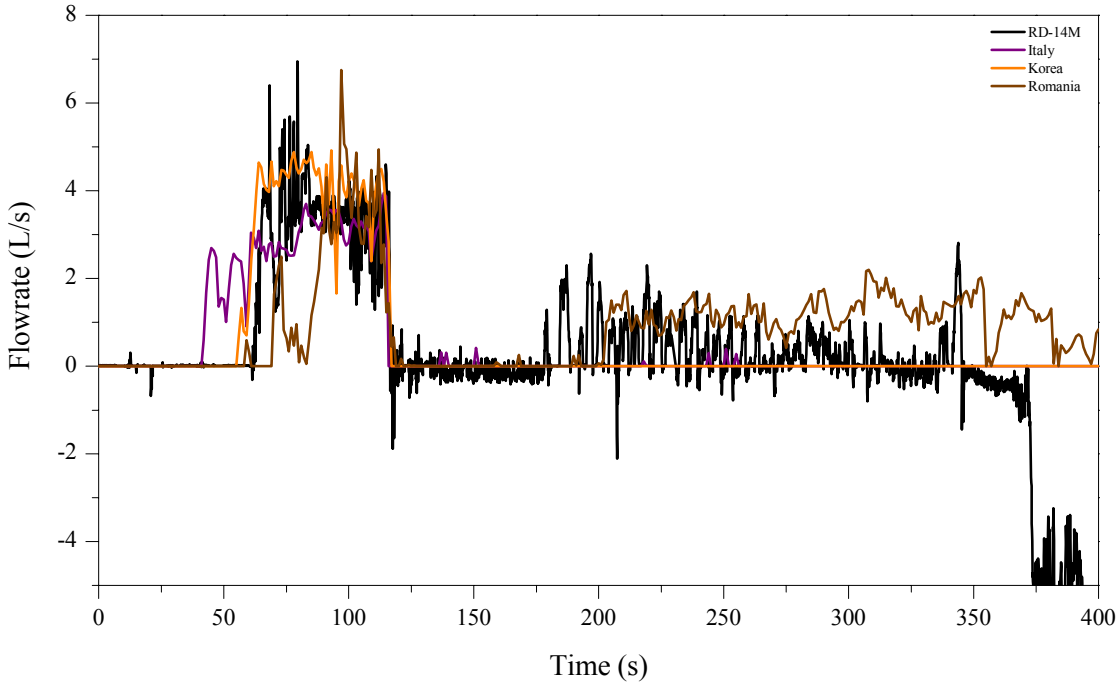

Fig. 5.13. ECC to Header 6 Flowrate.

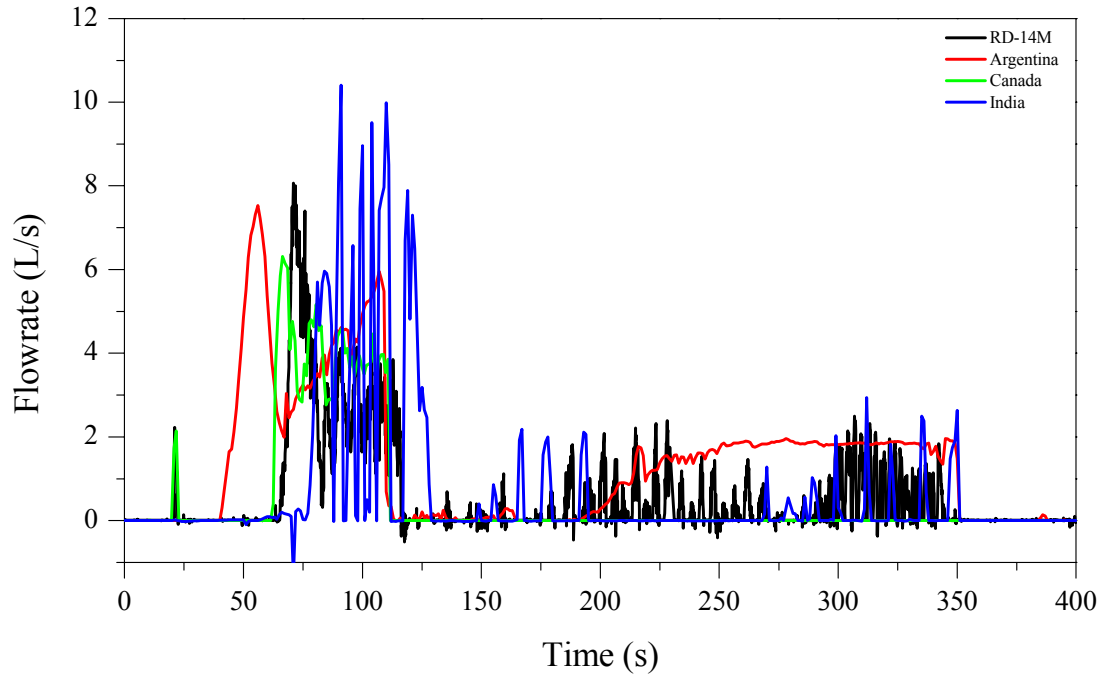

Fig. 5.14. ECC to Header 7 Flowrate.

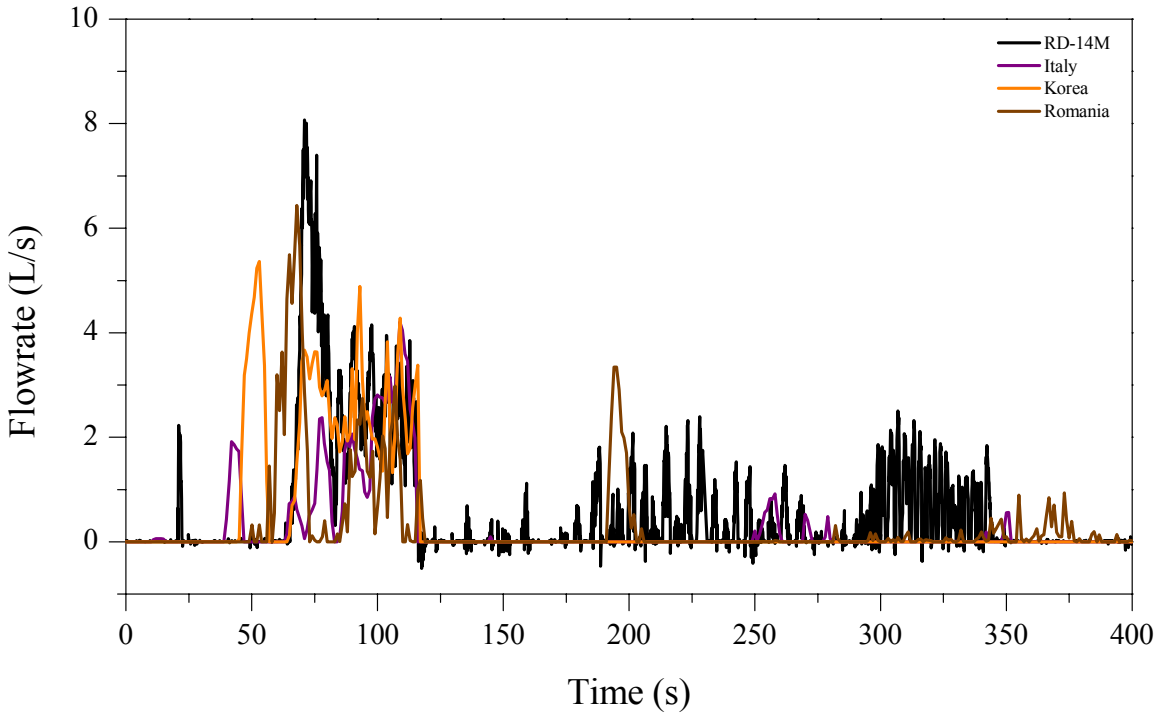

Fig. 5.15. ECC to Header 7 Flowrate.

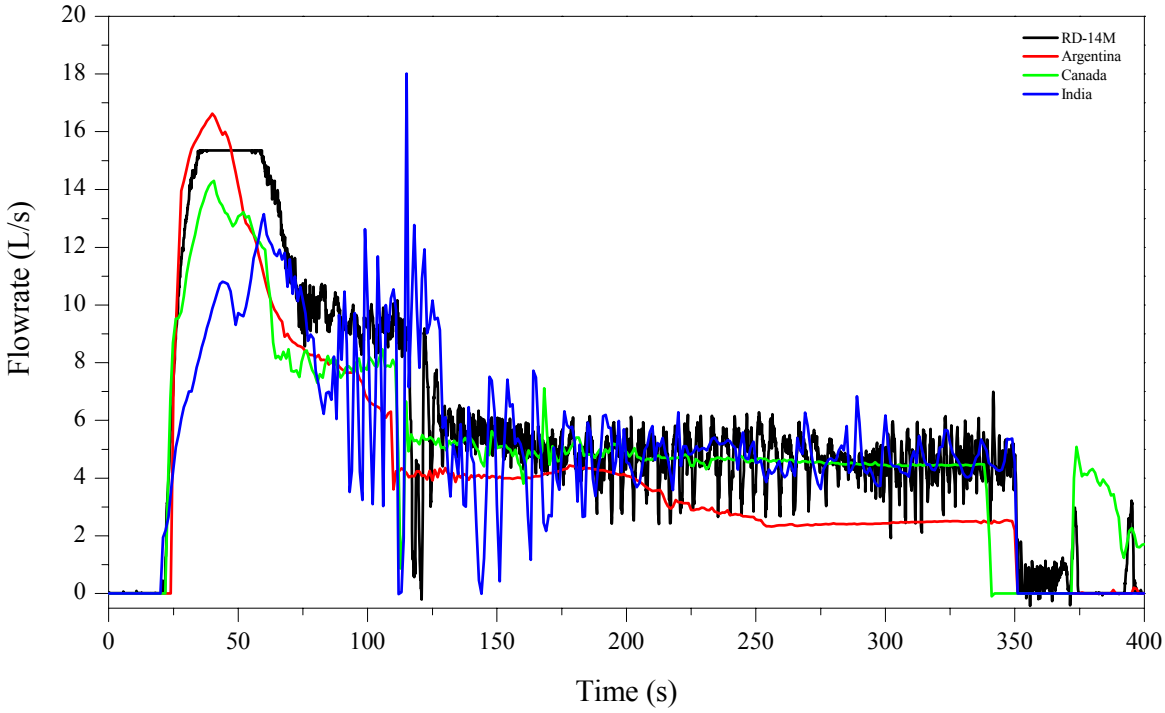

Fig. 5.16. ECC to Header 8 Flowrate.

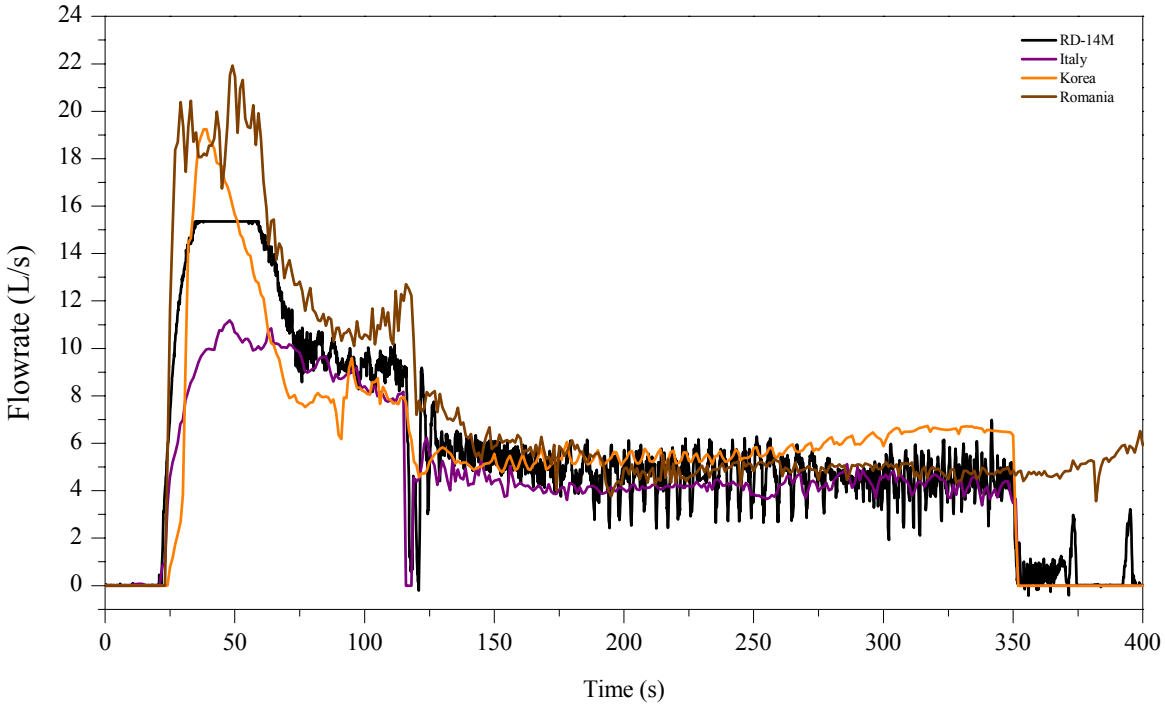

Fig. 5.17. ECC to Header 8 Flowrate.

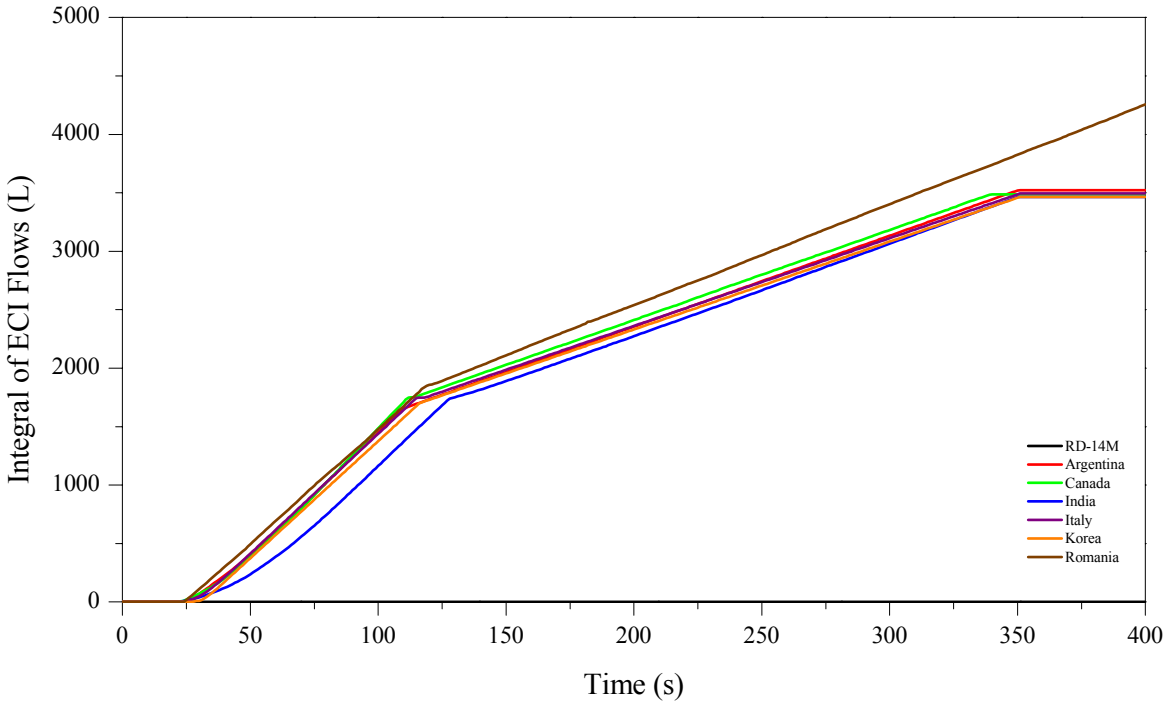

Fig. 5.18. Integral of ECI Flows.

5.7. Boiler 1 and 2 Inlet Void Fractions, α_1 and α_2

Boilers are heat sinks in a heat transport system under normal operation. However, they may behave as heat sources later in the transient. Void fractions at the inlets of the boilers (α_1 and α_2), combined with primary pump differential pressures, provide important information regarding ECC flow arrival to the primary heat transport system and subsequent voiding.

For all comparison of calculated void fraction with experiment, this comparison is made at a particular node and the experiment. Participants noted that in some cases, neighbouring nodes could have a significantly different void-fraction history — that provided better agreement with the experiment. One possible reason for these discrepancies could be the occurrence of choked flow in the feeders (specifically in the feeder orifices), and the inability of the codes to predict this behaviour correctly.

Figures 5.19 to 5.22 provide the code comparison to experiment. In Figures 5.19 and 5.20 all calculations show voiding by about 25 s. India, Republic of Korea, and Romania also correctly show the passage of a slug of water (at about 75 s in the experiment). In Figures 5.21 and 5.22 all codes show experimental trends adequately for the first portion of the transient (to 75 s). However, for the later part of the transient, some calculations showed significant void, in contrast to the experiment.

5.8. Primary Pump 1 and 2 Outlet Void Fractions, α_3 and α_4

Void fractions at the outlets of the primary pumps (α_3 and α_4) show voiding condition in response to sudden depressurisation of the primary heat transport system at the primary pump discharges, and they also show the timing of the ECC flow front movement.

Figures 5.23 to 5.26 provide the code comparison to experiment. In Figures 5.23 and 5.24, it is seen that all agree with experimental tends. All codes show the initial voiding correctly, with some disagreement after this point, ranging from total void to no void at all (Romania, India). Overall, a wide range of results can be expected – as driving forces are very small, and results can be affected. This can be seen in differences in Pump1 vs. pump 2, as one has higher DP. In Figures 5.25 and 5.26 all predictions are seen to be in good agreement, with the exception of a few calculations in the later part of the transient.

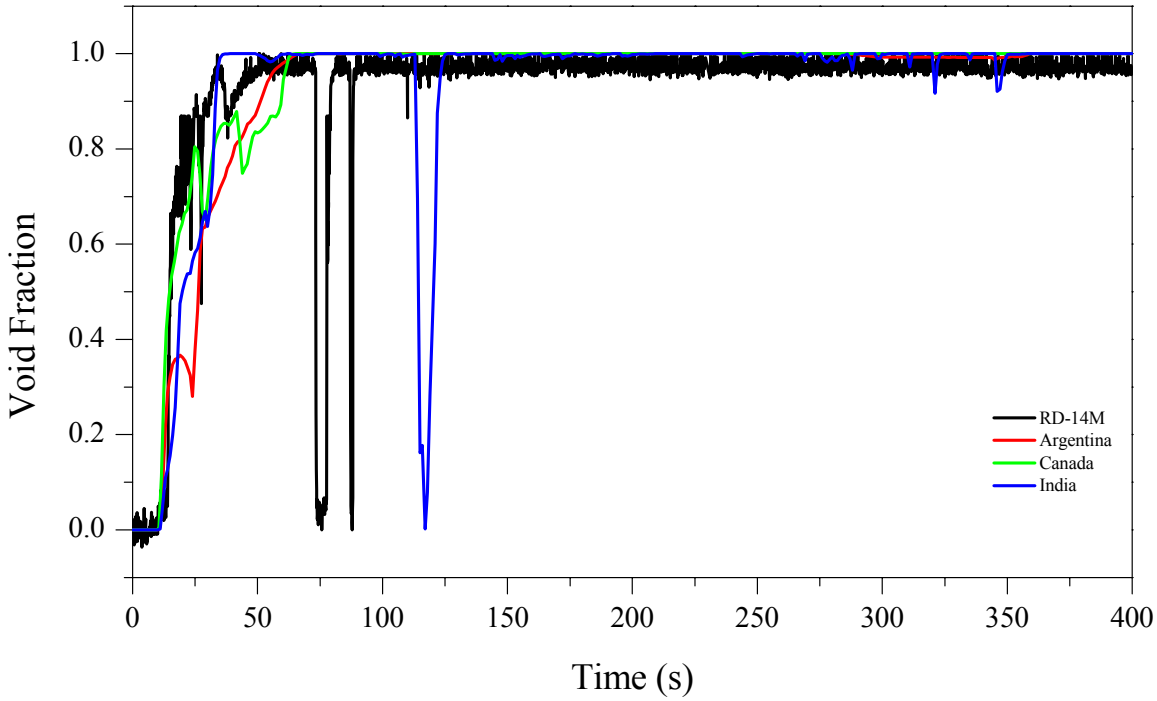

Fig. 5.19. Boiler 1 Inlet Void Fraction.

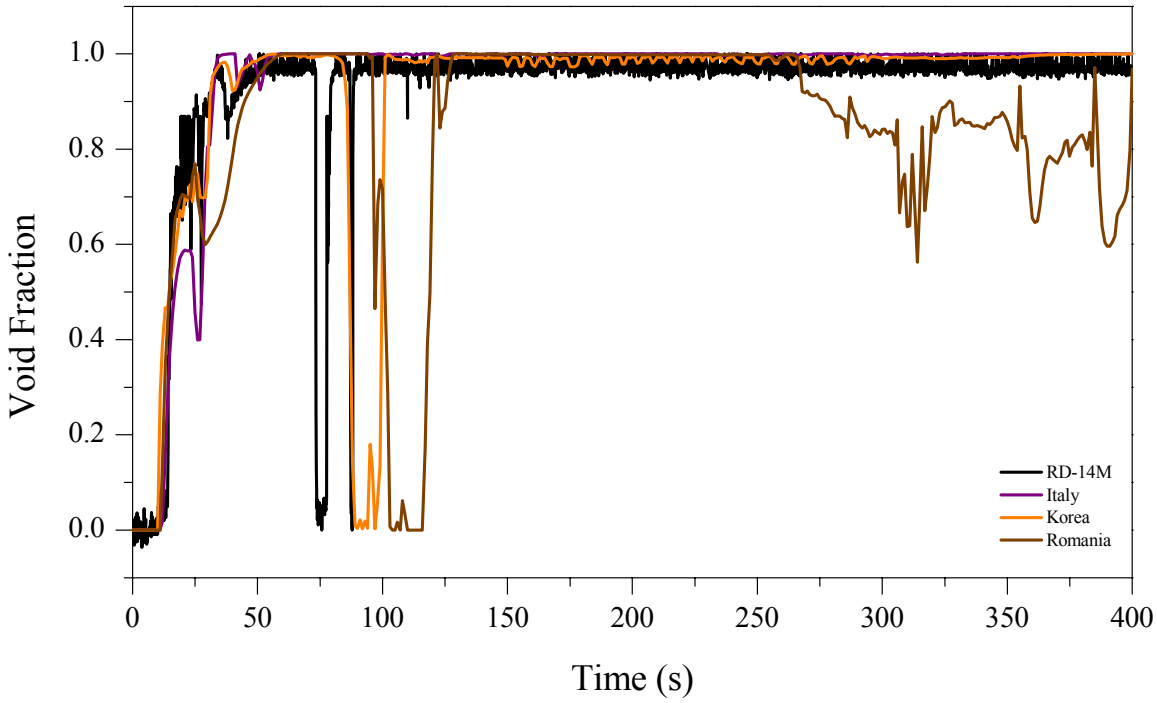

Fig. 5.20. Boiler 1 Inlet Void Fraction.

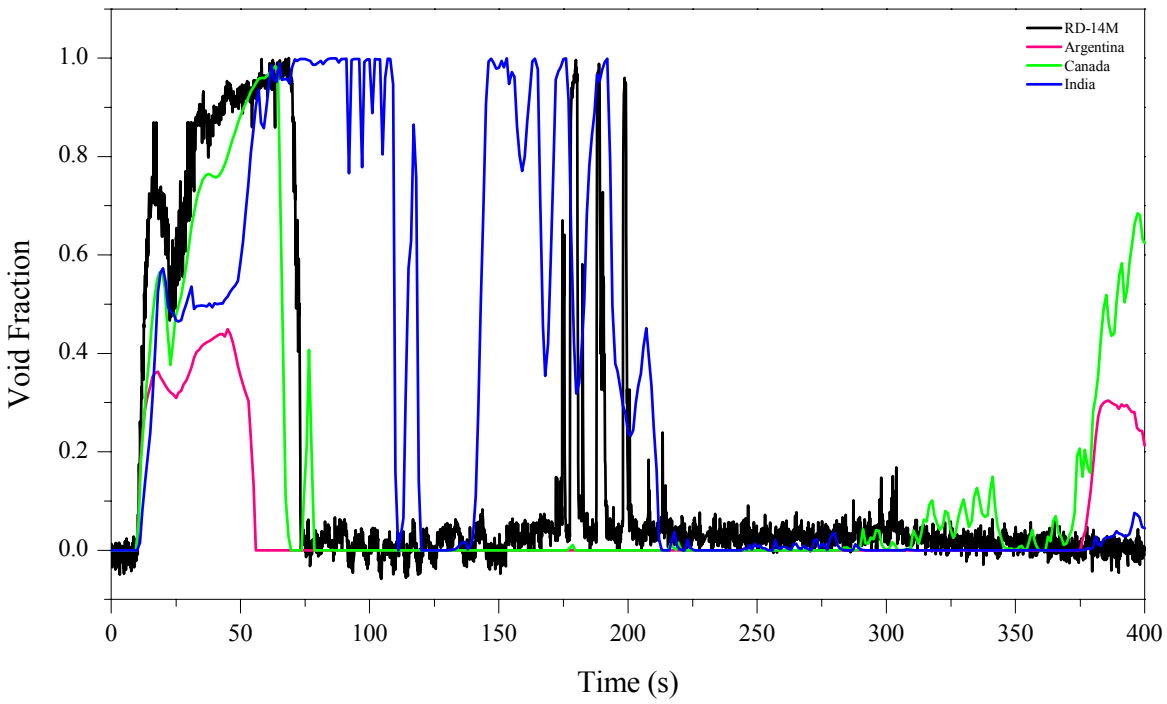

Fig. 5.21. Boiler 2 Inlet Void Fraction.

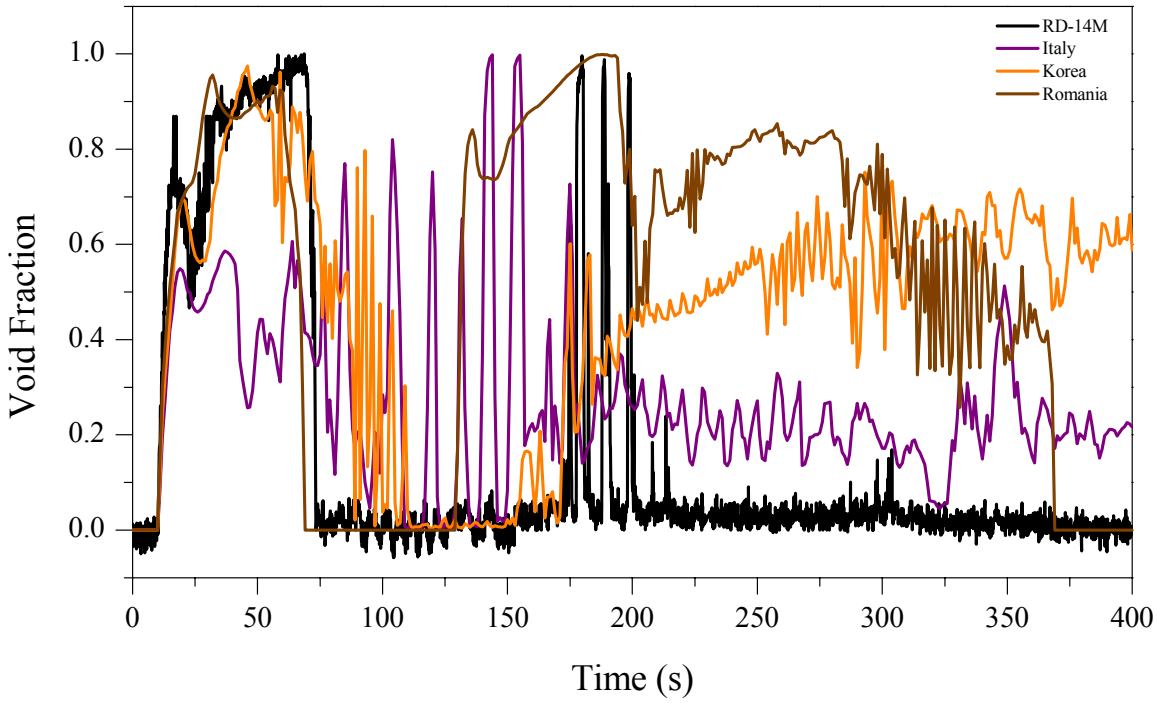

Fig. 5.22. Boiler 2 Inlet Void Fraction.

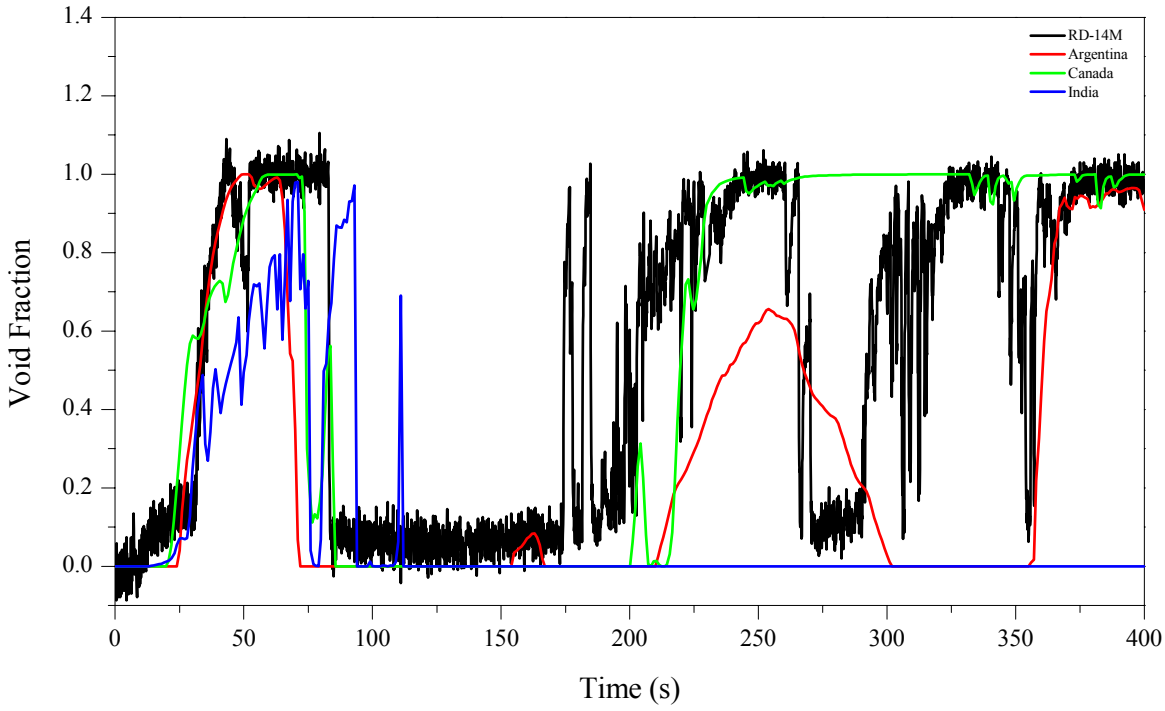

Fig. 5.23. Pump 1 Outlet Void Fraction.

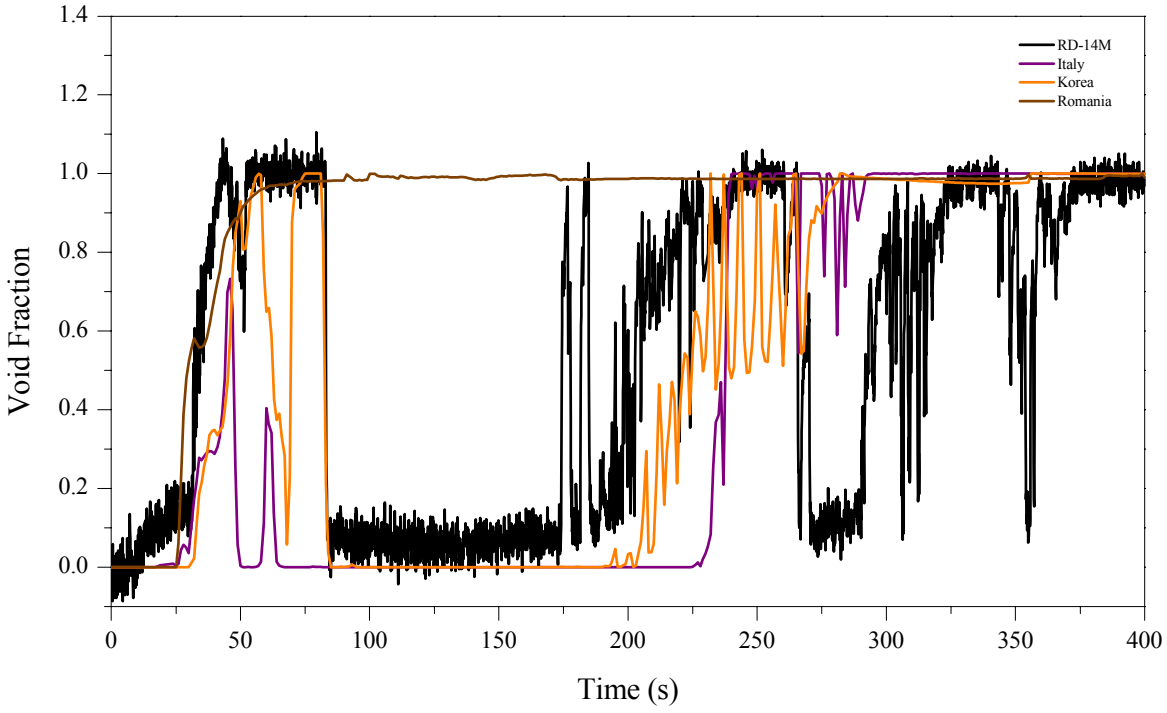

Fig. 5.24. Pump 1 outlet Void Fraction.

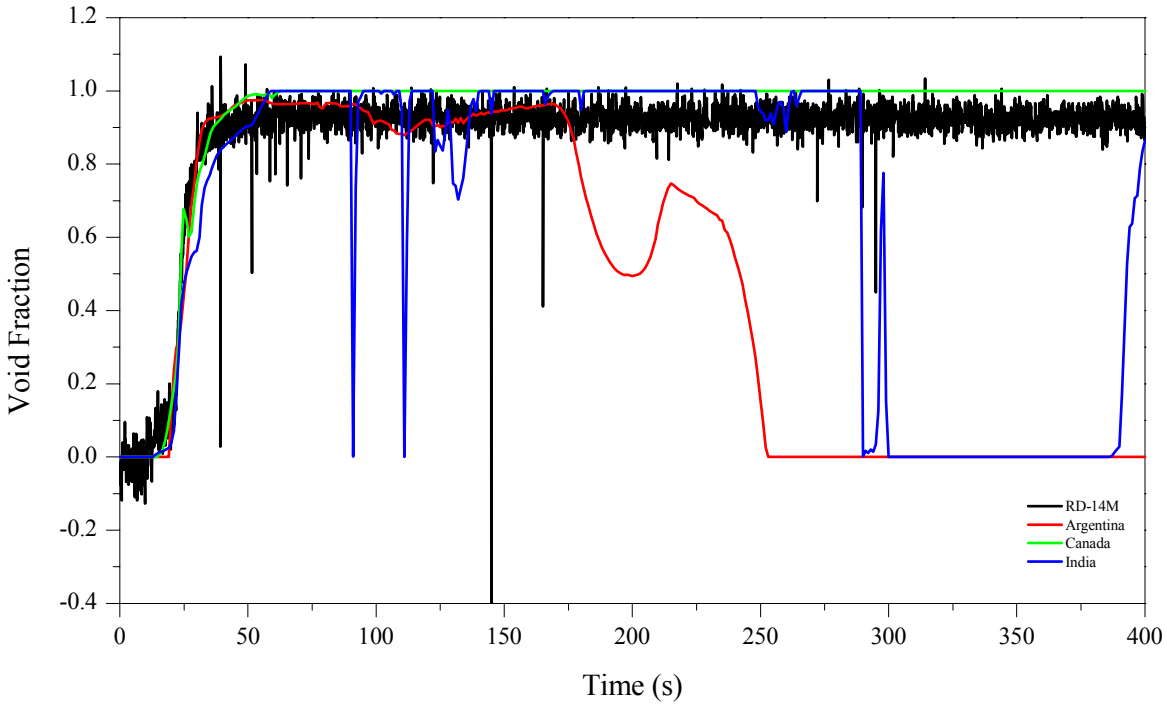

Fig. 5.25. Pump 2 Outlet Void Fraction.

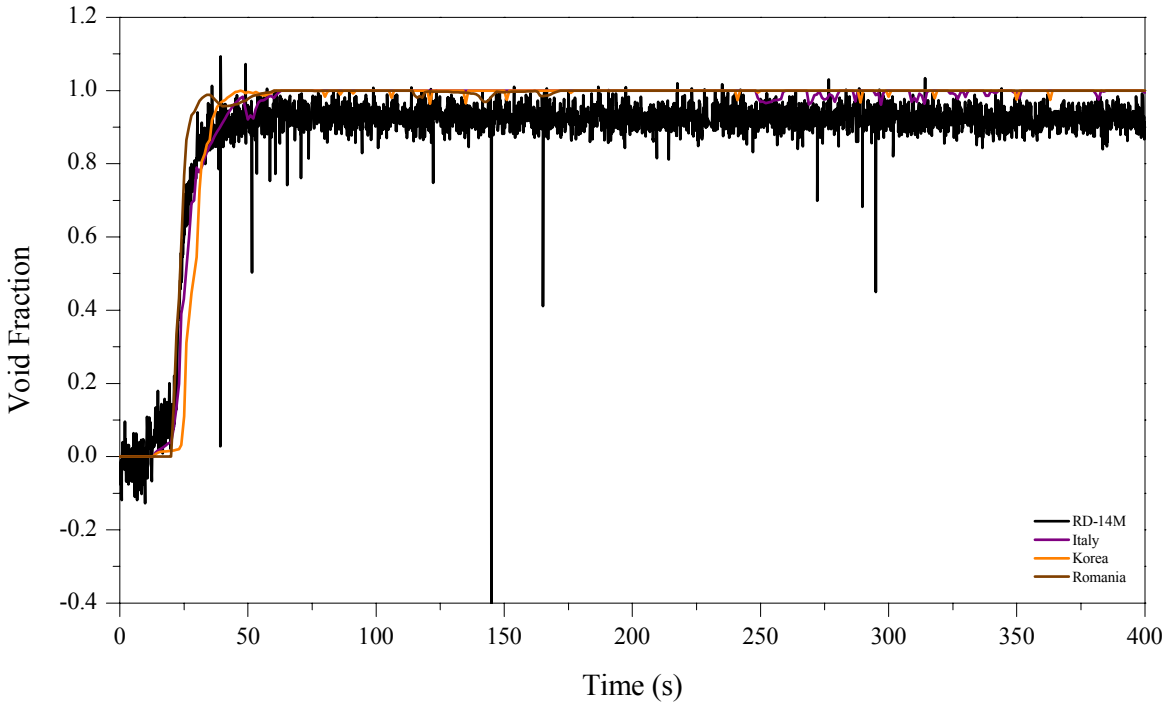

Fig. 5.26. Pump 2 Outlet Void Fraction.

5.9. Boiler 1 and 2 Inlet and Outlet Fluid Temperatures, $T_{B1\text{-}IN}$ through $T_{B2\text{-}OUT}$

Boiler inlet and outlet fluid temperatures provide local fluid temperature measurements in the primary loop, can be used as confirmatory data for simulations, and they provide information about heat removal/addition capability of the boilers during the blowdown transient.

Figures 5.27 to 5.30 provide the code comparison to experiment. All calculations show the correct experimental trend, and all agree reasonably well with experiment for about the first 50 s of the transient. The lower temperatures in some calculations are due to the arrival of low-temperature ECC flow. After that point, significant differences are noted.

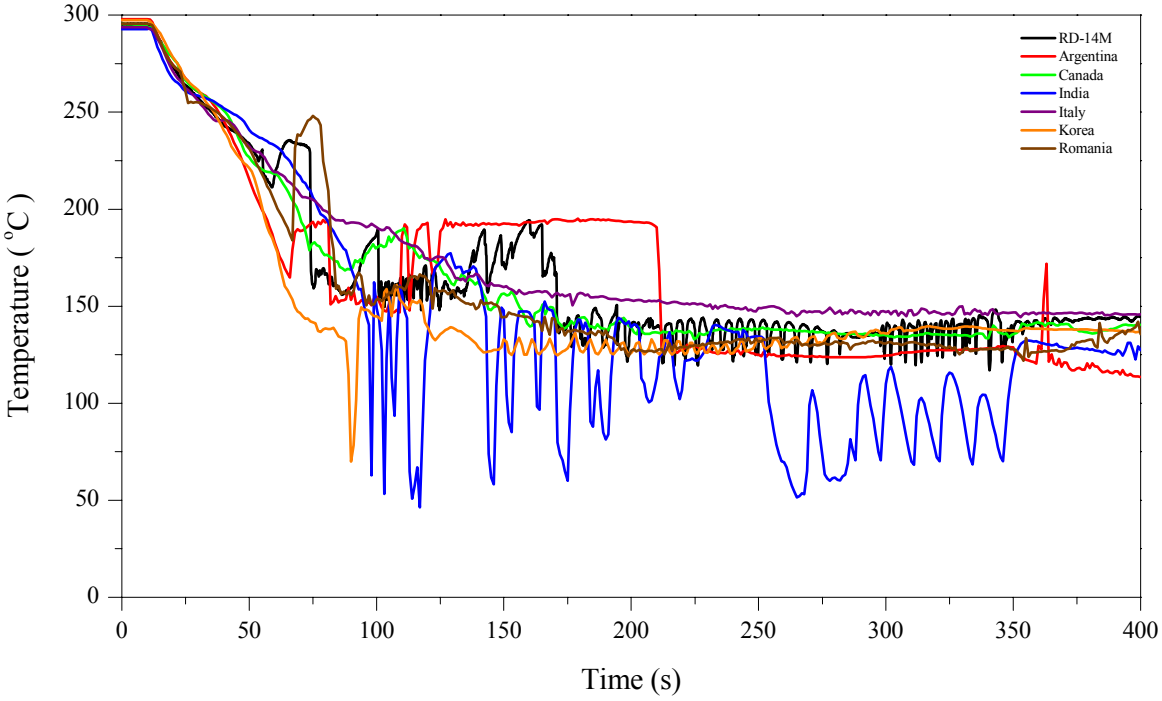

Fig. 5.27. Boiler 1 Inlet Fluid Temperature.

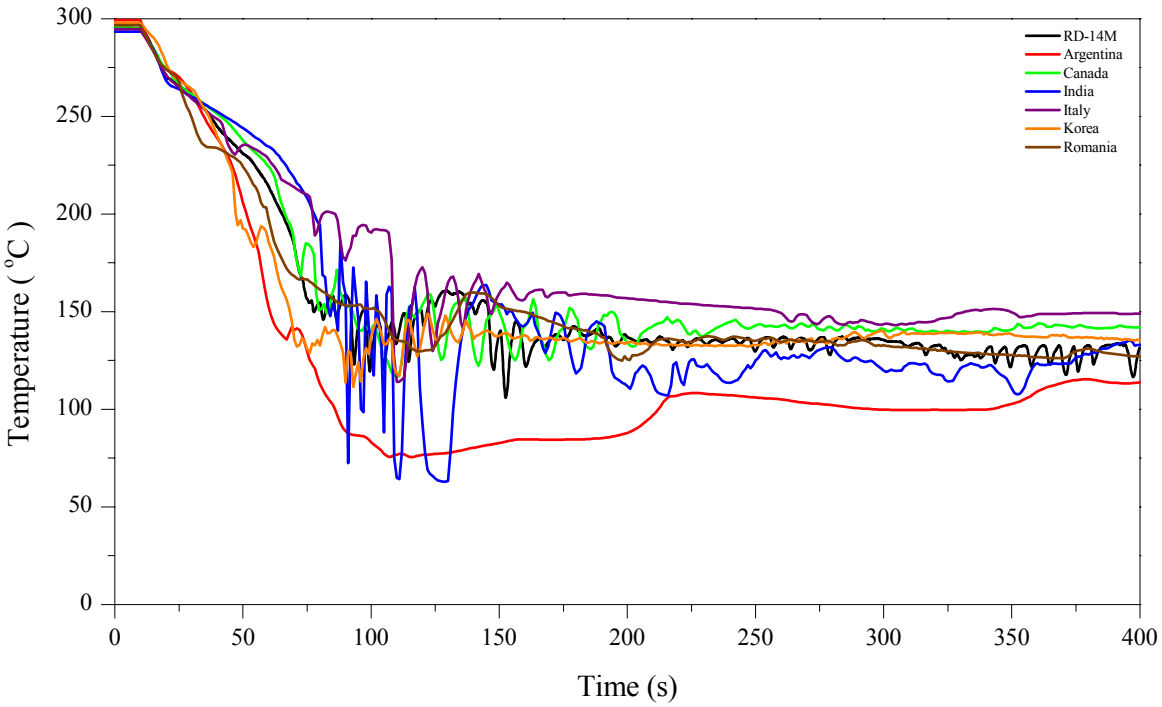

Fig. 5.28. Boiler 2 Inlet Fluid Temperature.

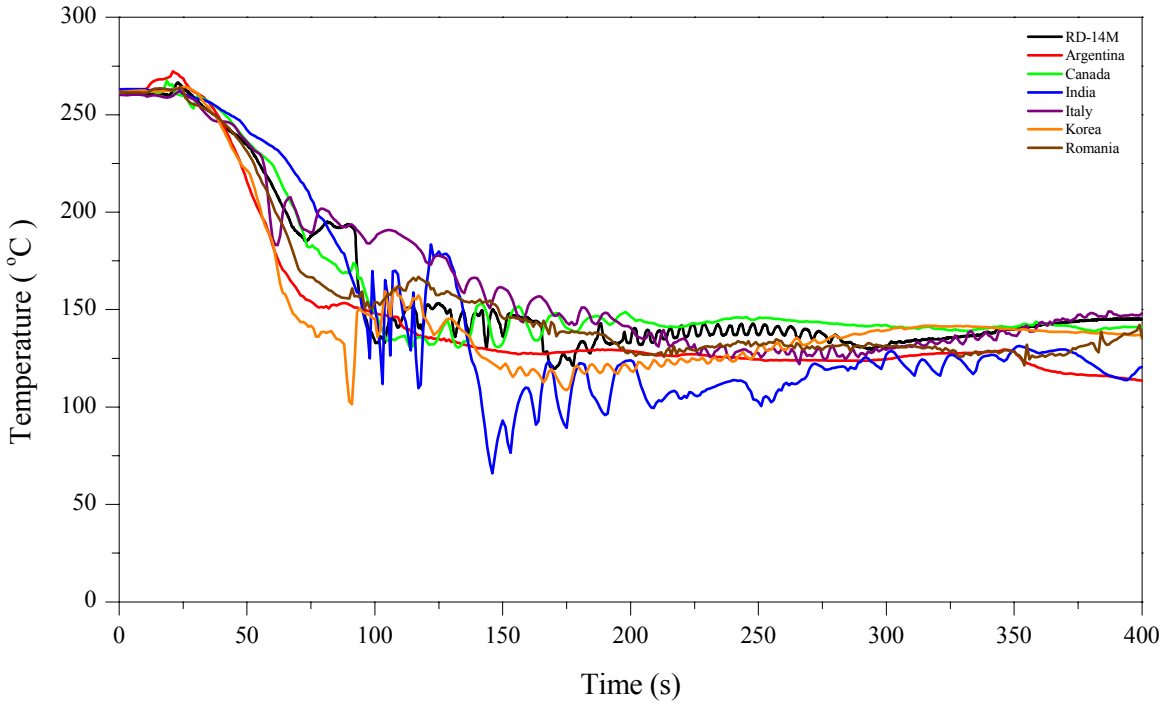

Fig. 5.29. Boiler 1 Outlet Fluid Temperature.

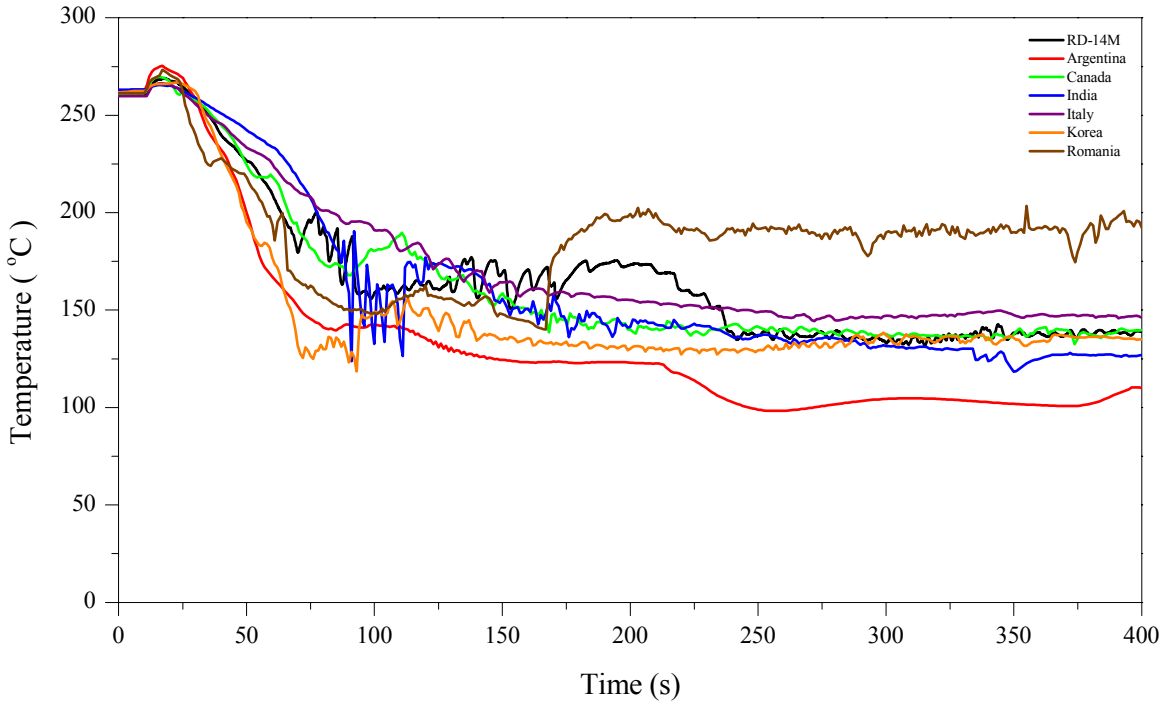

Fig. 5.30. Boiler 2 Outlet Fluid Temperature.

5.10. FES Sheath Temperatures in Heated Sections 8 and 13, T_1 through T_5

The terms "broken pass" and "intact pass" are used to distinguish the two halves of the RD-14M "figure-of-eight" primary circuit. For an inlet header break test, like B9401, the broken pass is that portion of the primary loop between the outlet of pump 2 and the inlet of pump 1, including the associated heated sections (10 through 14). The intact pass is that portion of the primary loop between the outlet of pump 1 and the inlet of pump 2, including the associated heated sections (5 through 9).

The maximum FES sheath temperature is often the most significant parameter in safety analyses. In test B9401, the maximum FES sheath temperatures occur in the high power channel of the broken pass, heated section 13 (HS13). The FES temperature excursions in HS13 began immediately upon initiation of the break as flow in this channel dropped significantly to a very low value (stagnated channel). The FES temperatures initially rose quickly and then slowed as the heated channel power was reduced to decay levels beginning at about 12 s. Shortly after the onset of the high-pressure ECC injection phase, quenching began as ECC water arrived at the channel. The measured maximum FES temperature (T_1) is that of the top pin in the middle of HS13.

Since the ECC flow entered header 5 and the quench front moved from header 5, through HS13, and towards the break on header 8, the outlet end of HS13 quenched more quickly than the inlet end. Top pin FES temperatures at the inlet and outlet end of HS13 (T_2 and T_3) are selected to demonstrate the difference.

When ECC flow enters the channel, significant time delays between quenching of bottom and top pins in the horizontally oriented heated sections can occur depending on the liquid flowrate. Top and bottom pin FES temperatures at the outlet of HS13 (T_3 and T_4) are chosen to show the flow stratification in this test.

No significant FES temperature excursions were recorded in the heated sections within the intact pass as channel flows remained high enough to maintain adequate cooling of the FES. Heated section 8 (HS8) was the high power channel in the intact pass. The FES temperature at the top pin in the middle of HS8 (T_5) was selected to compare with the FES temperature at the same location in HS13 (T_1)

Figures 5.31 to 5.35 provide the code comparison to experiment. All codes captured the temperature excursions, with mostly an over-prediction of peak temperature. It is noted that the Republic of Korea calculation tended to under predict peak temperatures, while the Romanian calculation showed a second temperature excursion for top pins. This is not unexpected, as the temperature excursions are limited and of short duration (predicted conditions are very near the critical heat flux (CHF)). For HS8 no major temperature excursions (above steady-state values) were predicted which is consistent with the experiment.

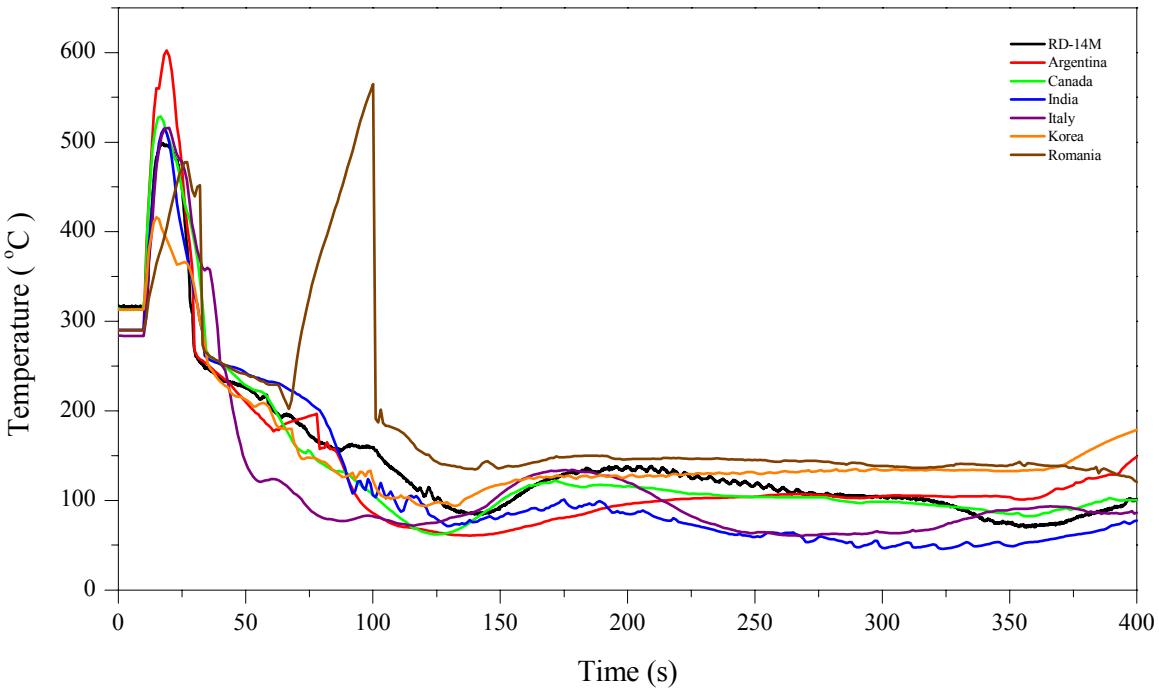

Fig. 5.31. FES Temperature at the Top Pin, Middle HS13.

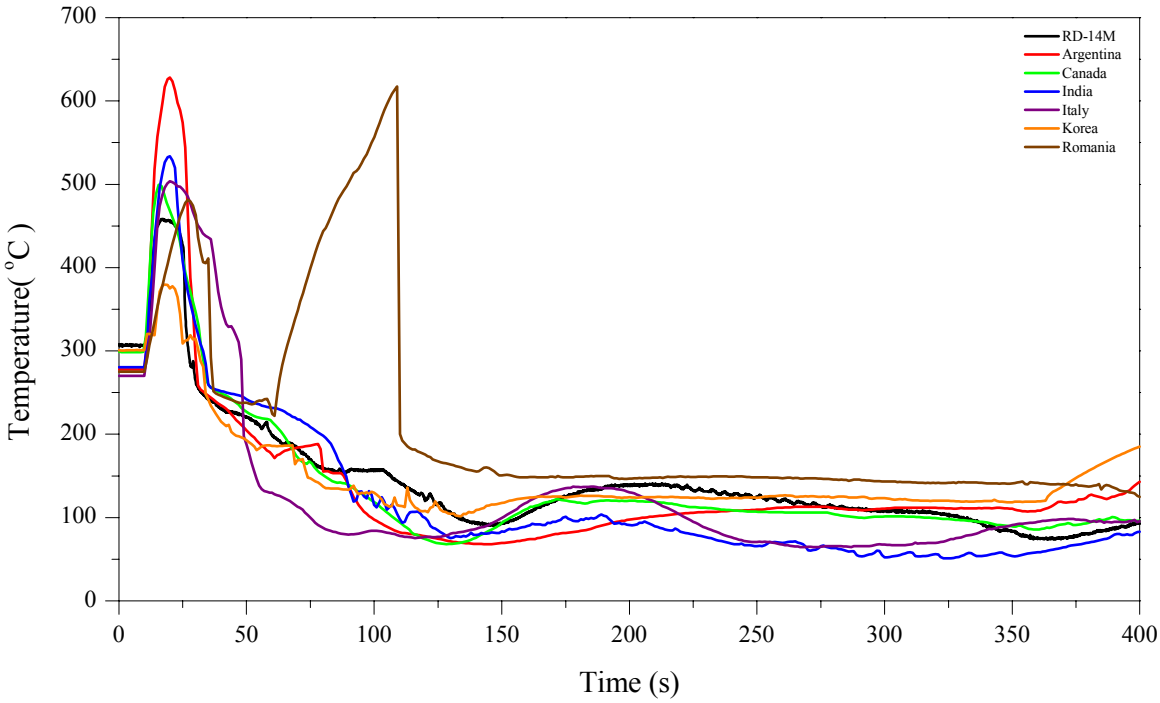

Fig. 5.32. FES Temperature at the Top Pin, Inlet HS13.

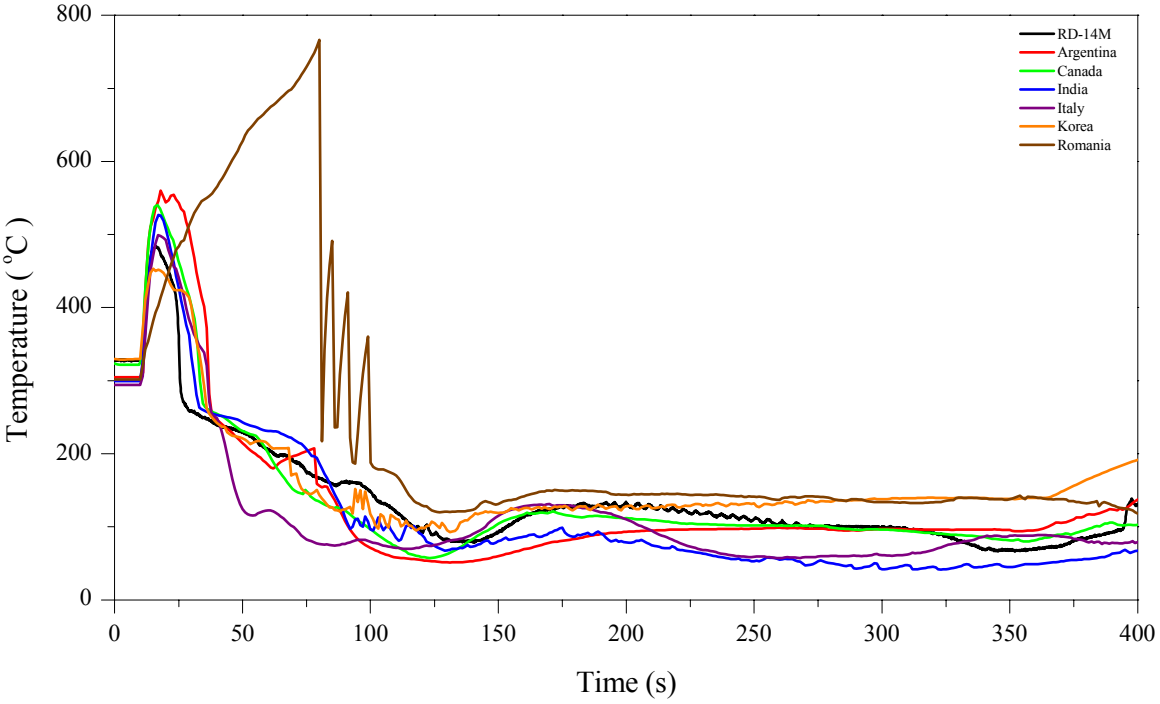

Fig. 5.33. FES Temperature at the Top Pin, Outlet HS13.

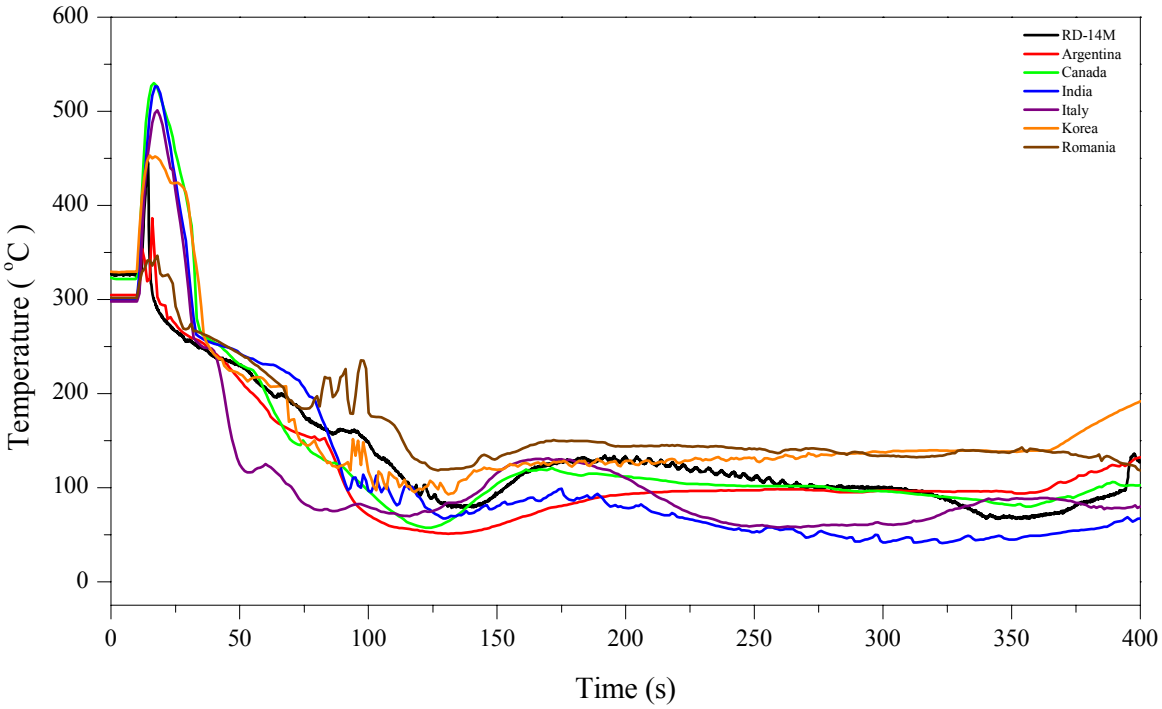

Fig. 5.34. FES Temperature at the Bottom Pin, Outlet HS13.

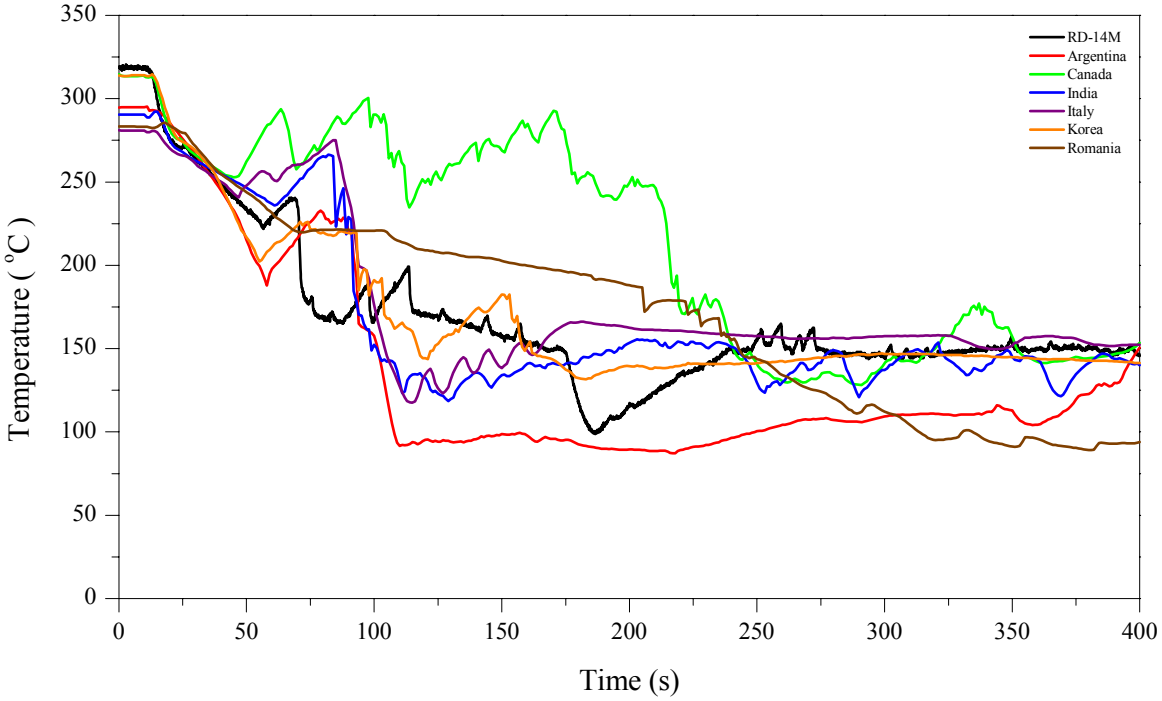

Fig. 5.35. FES Temperature at the Top Pin, Middle HS8.

5.11. Void Fraction at the Inlet and Outlet of Heated Sections 5 and 13, α_5 through α_8

Channel void fractions are important because they indicate the onset of channel voiding and the arrival time of the ECC to channels. This helps to explain the FES temperature behaviour in the heated sections. It should be noted that inlet and outlet void fractions of the heated sections were measured more than 2.0 m upstream and downstream of the heated section. In test B9401, rapid and nearly complete voiding of all the heated sections in the broken pass occurred upon initiation of the break at 10 s, whereas voiding of the heated sections in the intact pass occurred at about 40 s. The ECC flow from header 5 refilled the outlet end, then the inlet end of the heated sections in the broken pass. The ECC flow from header 6 refilled the inlet, then the outlet of the heated sections in the intact pass. Void fractions at the inlet and outlet of heated sections 5 and 13 (α_5 through α_8) are selected as representative of the channel voiding and refilling scenarios of the intact and broken passes.

Figures 5.36 to 5.43 provide the code comparison to experiment. All calculations show the initial voiding and refill being correctly predicted with differences noted between participants. These discrepancies were expected, and thought to be due to the modelling of the endfitting geometry with the various codes – noting the complexity of the endfitting geometry.

5.12. Pressure Drop across HS13, ΔP_{HS13}, and Pressure Drop from HS13 to HDR5, $\Delta P_{HS13\text{-}HD5}$

In test B9401, a flow split occurs in at least some of the heated sections of the broken pass following the break. During the initial stage of the flow split, single-phase liquid flows out

both ends of the heated section while rapid voiding of the channel occurs. The volumetric flow rates at the heated section inlet and outlet are measured using turbine flowmeters (TFM). The TFMs are calibrated only to measure single-phase liquid flow and they commonly become over-ranged during the blowdown when two-phase conditions are encountered. In test B9401, shortly after the break, void was detected by the gamma densitometer at the test section inlets and outlets near the turbine flowmeters and at the primary pumps. The flowrate measurements were no longer valid and could not be used for code comparison. Channel differential pressure (ΔP_{HS13}) provides an indication of the flow direction in HS13. Similarly, $\Delta P_{HS13\text{-}HD5}$ provides an indication of the flow direction in the outlet feeder of HS13.

Figures 5.44 to 5.46 provide the code comparison to experiment. The DP in Figures 5.44 and 5.45 determines the channel response. It is noted that all code calculations at steady state are greater than experiment. This is likely due to the inclusion of gravity head in the calculations. However, all calculations show the correct trend, with the maximum negative DP occurring at about 50 s. In Figure 5.46, all calculations show the correct general trend, with Argentina, Republic of Korea, and Romania showing the best agreement with the prediction of the negative DP at about 40 s.

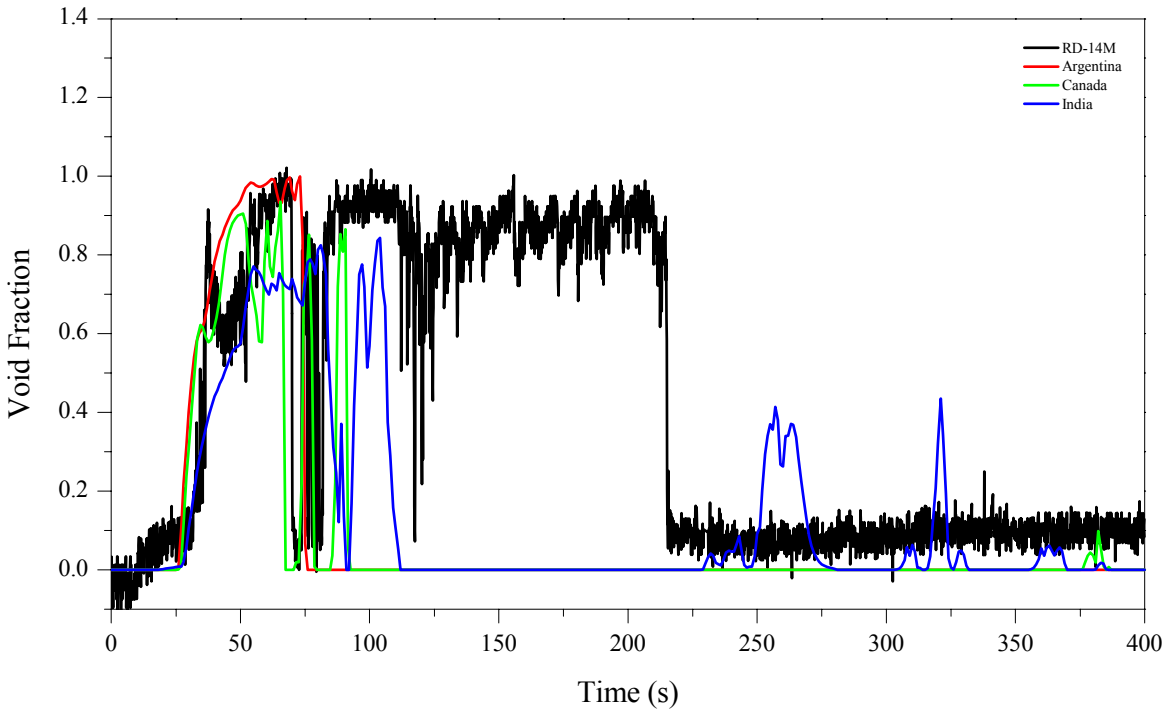

Fig. 5.36. HS5 Inlet Void Fraction.

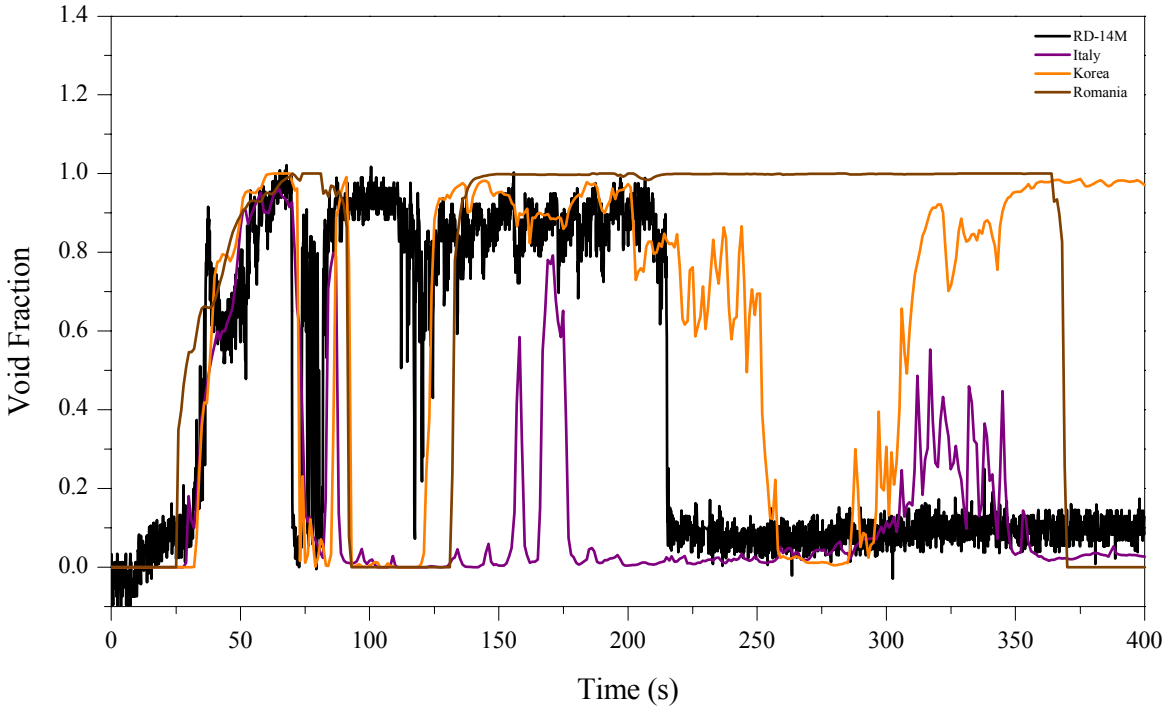

Fig. 5.37. HS5 Inlet Void Fraction.

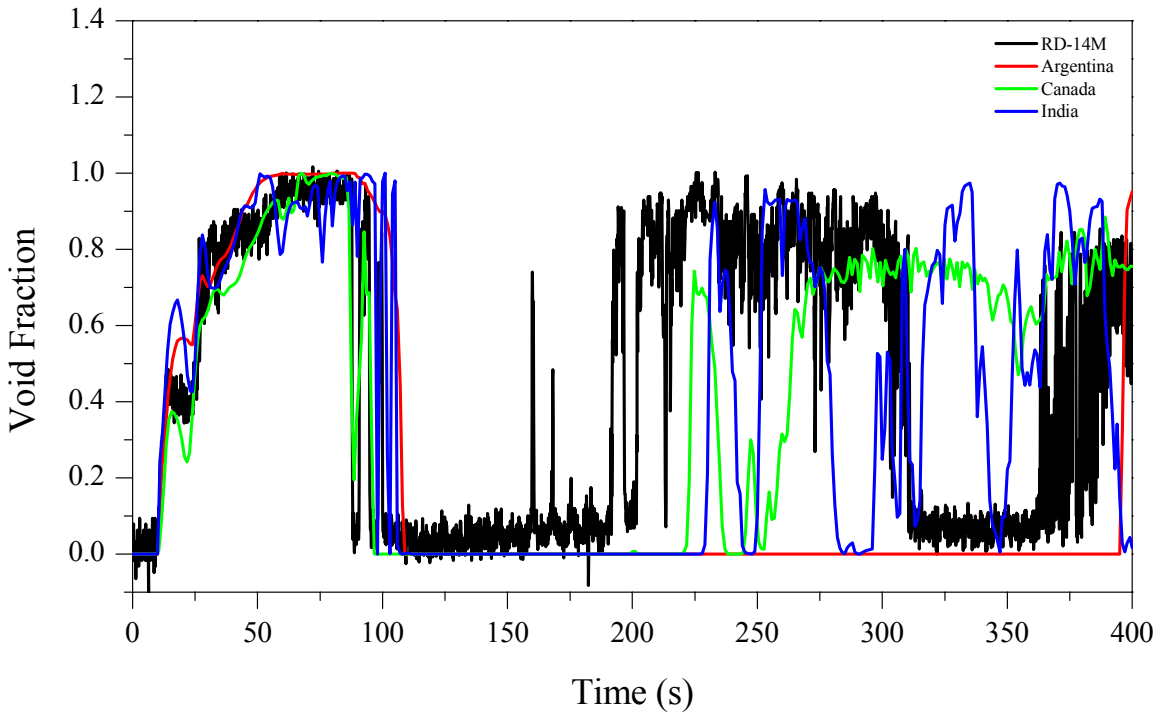

Fig. 5.38. HS5 Outlet Void Fraction.

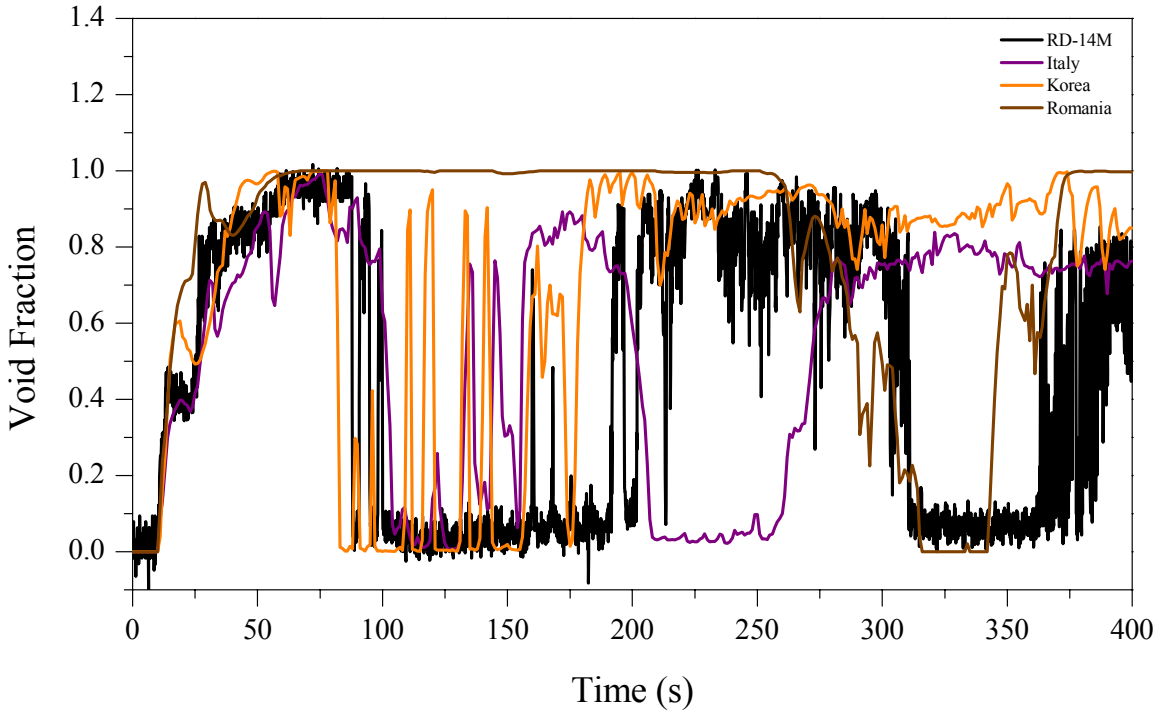

Fig. 5.39. HS5 Outlet Void Fraction.

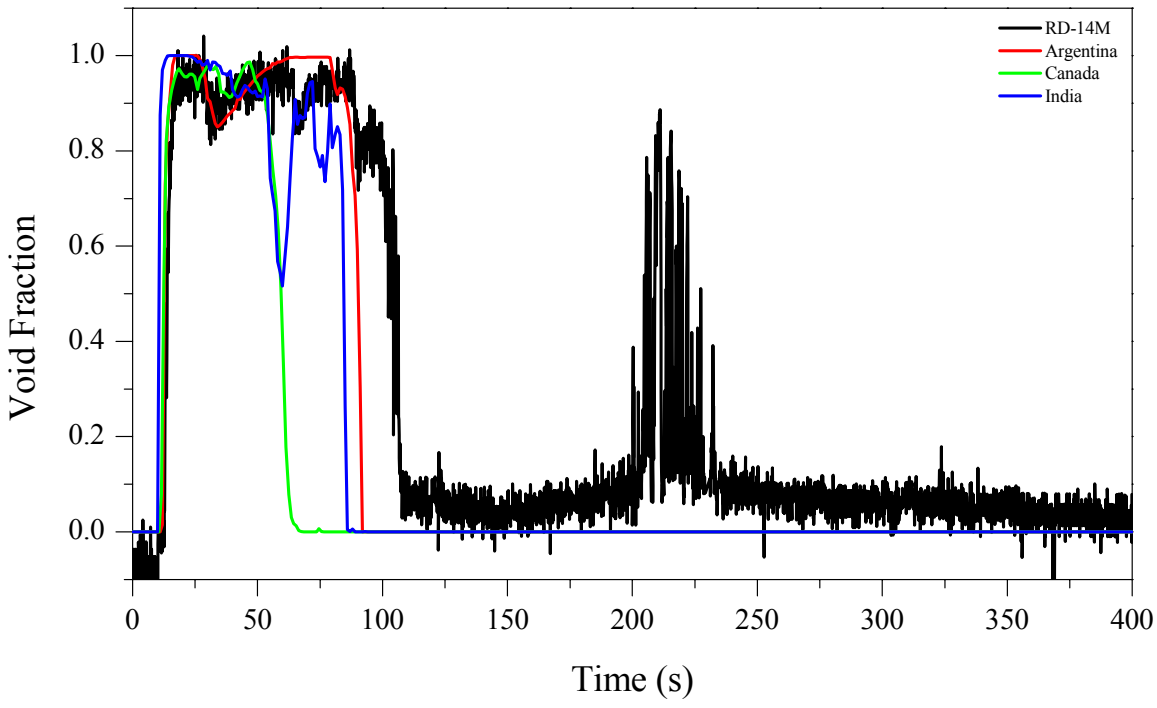

Fig. 5.40. HS13 Inlet Void Fraction.

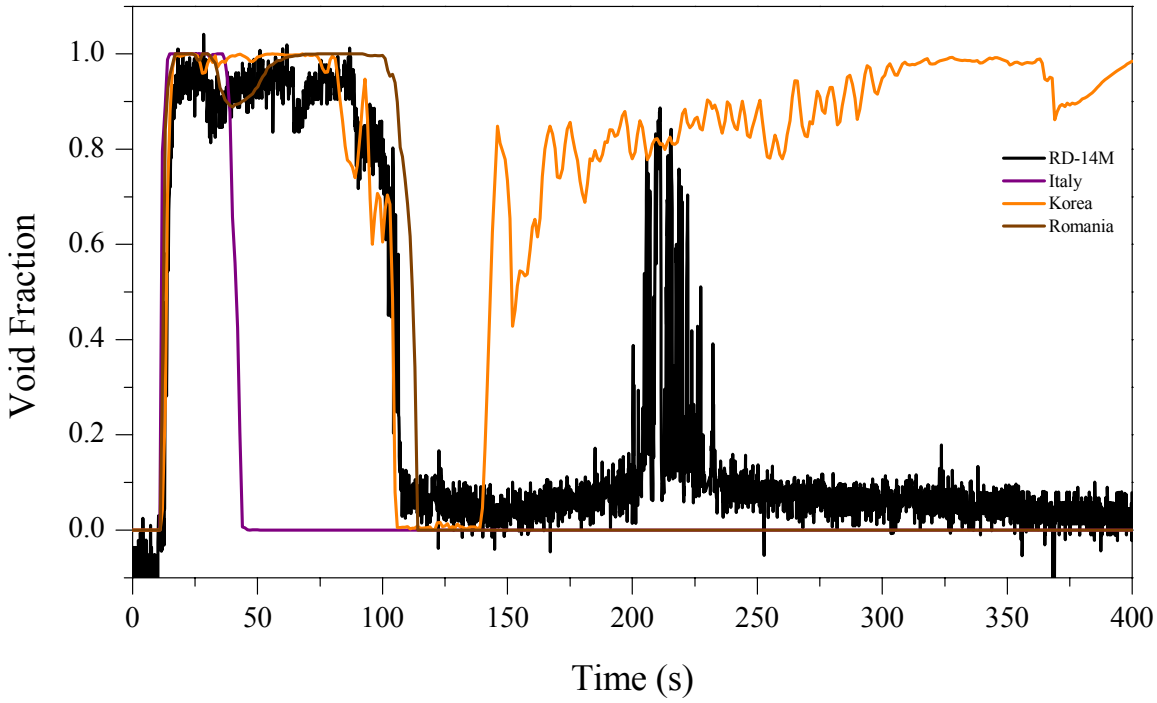

Fig. 5.41. HS13 Inlet Void Fraction.

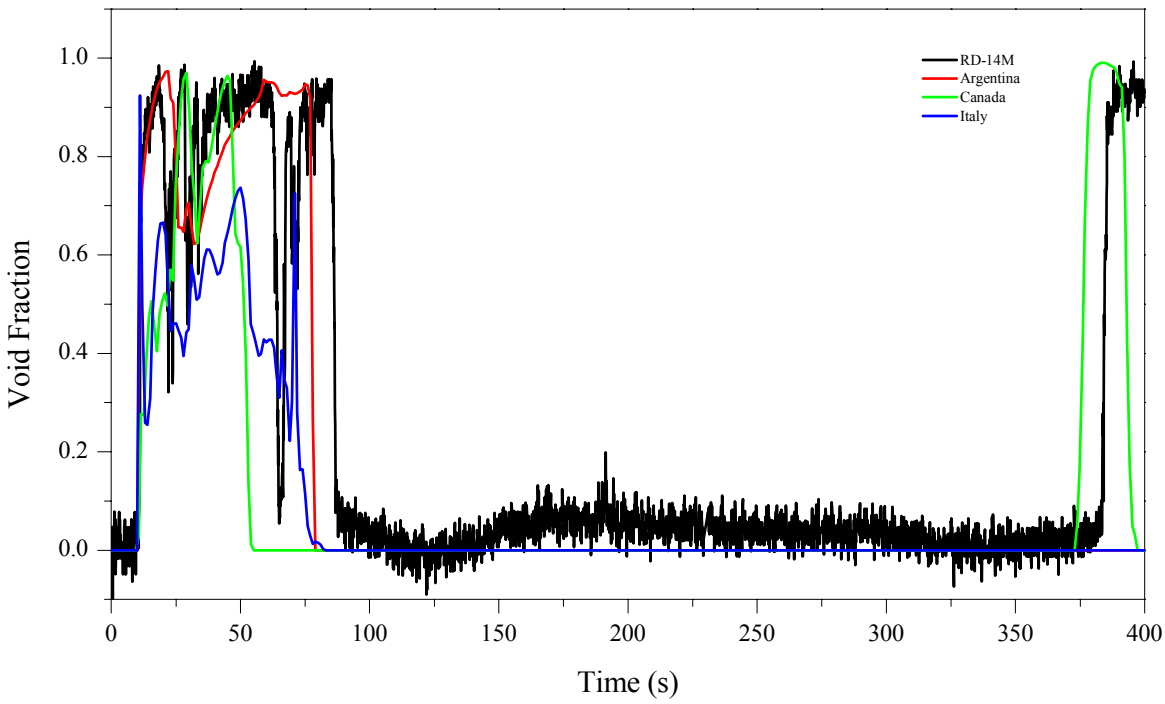

Fig. 5.42. HS13 Outlet Void Fraction.

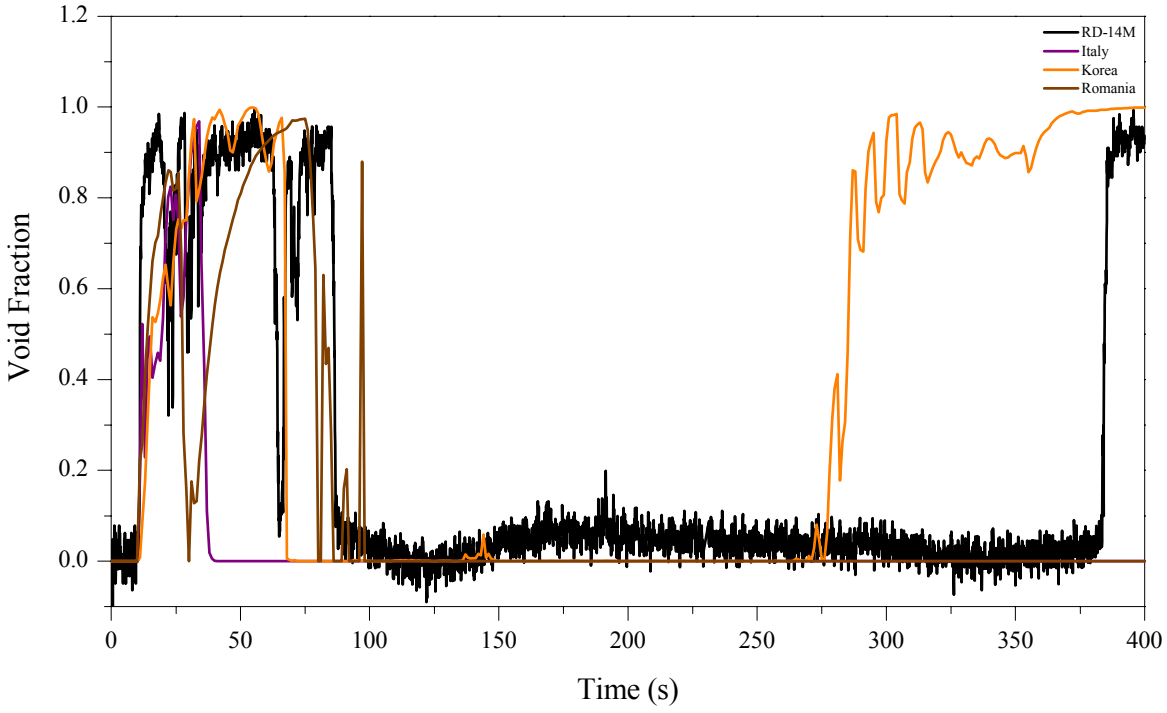

Fig. 5.43. HS13 Outlet Void Fraction.

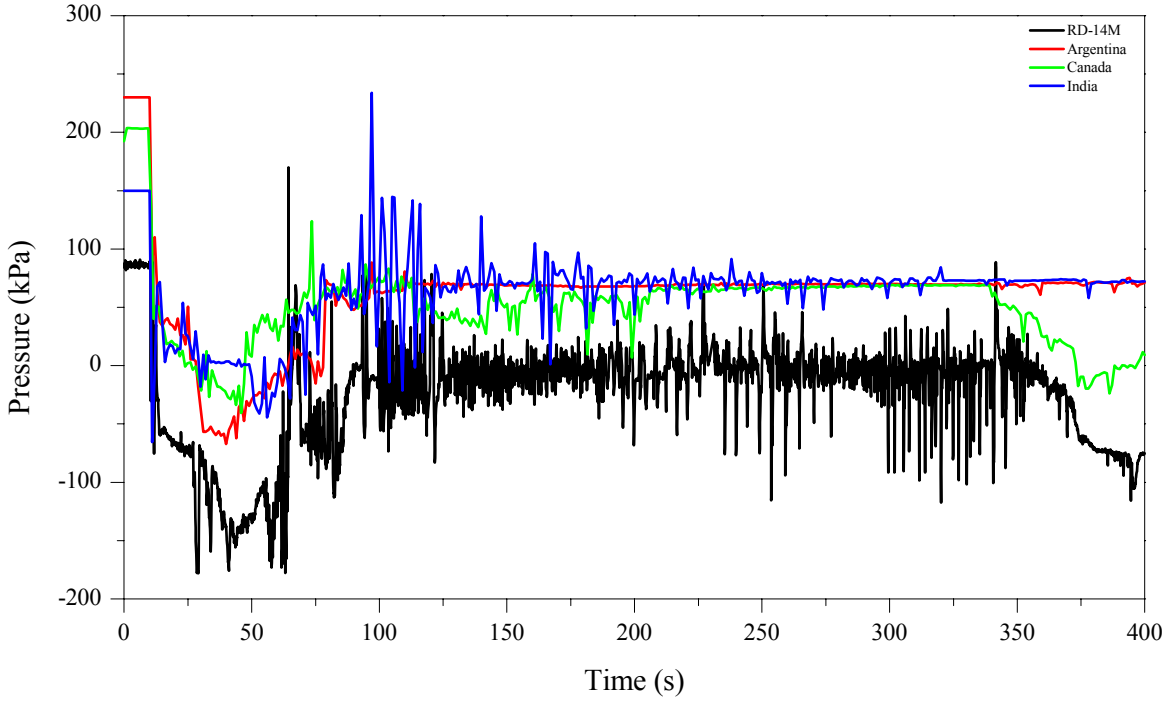

Fig. 5.44. Differential Pressure from HS13 to HDR5.

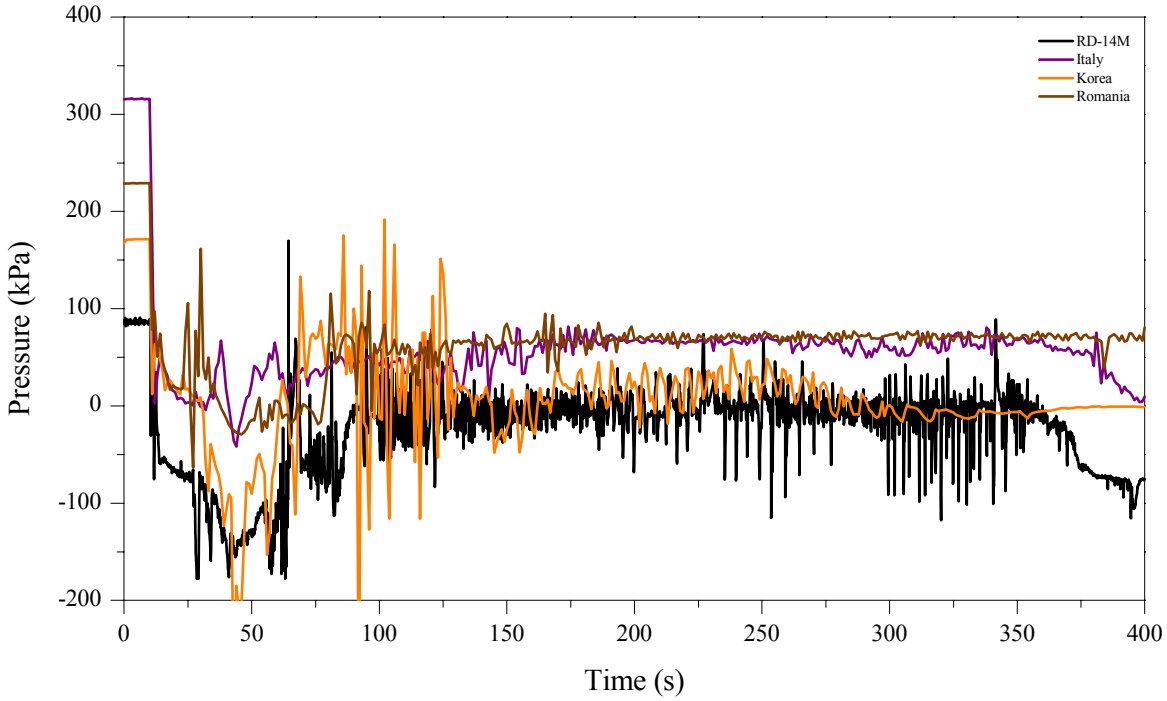

Fig. 5.45. Differential Pressure from HS13 to HDR5.

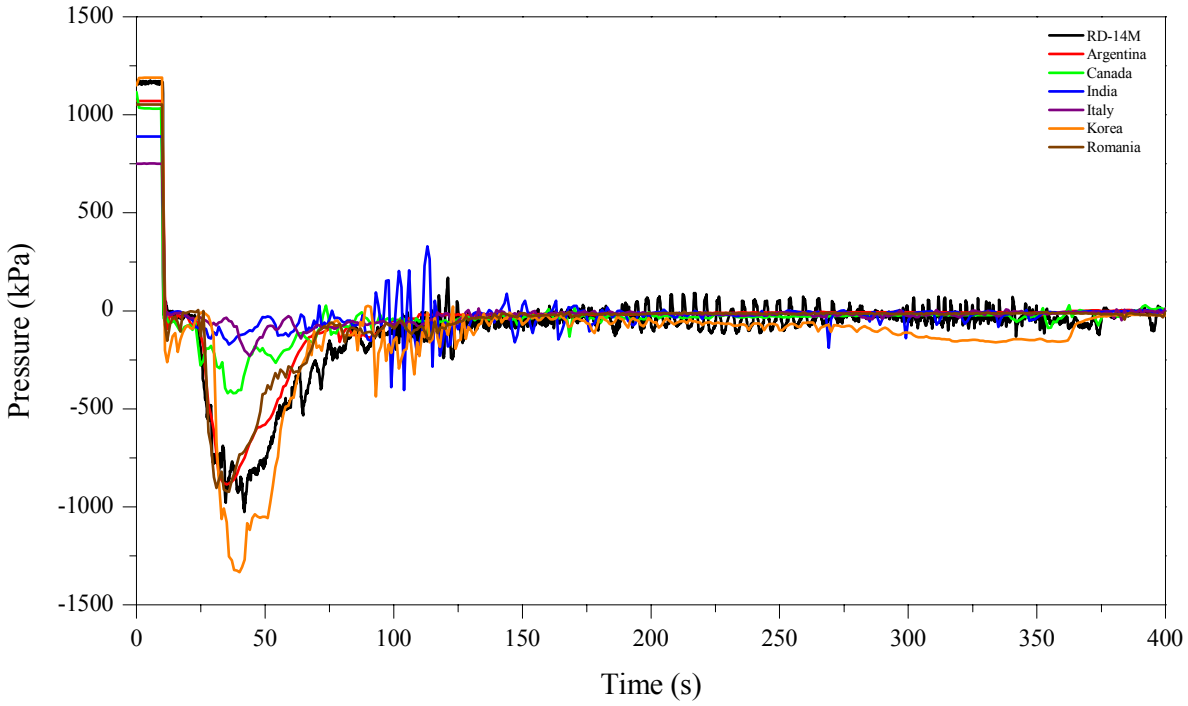

Fig. 5.46. Differential Pressure Across HS13.

5.13. Confirmatory Variables

The following are confirmatory variables and are used to ensure that the simulations are performed under the correct conditions.

- Pressure in the Pressurizer, P_{SRG}
- Boiler 1 drum pressure, P_{B1}
- Pump 1 speed, ω_{P1}
- Pump 2 speed, ω_{P2}

Figures 5.47 to 5.50 provide this information for each code.

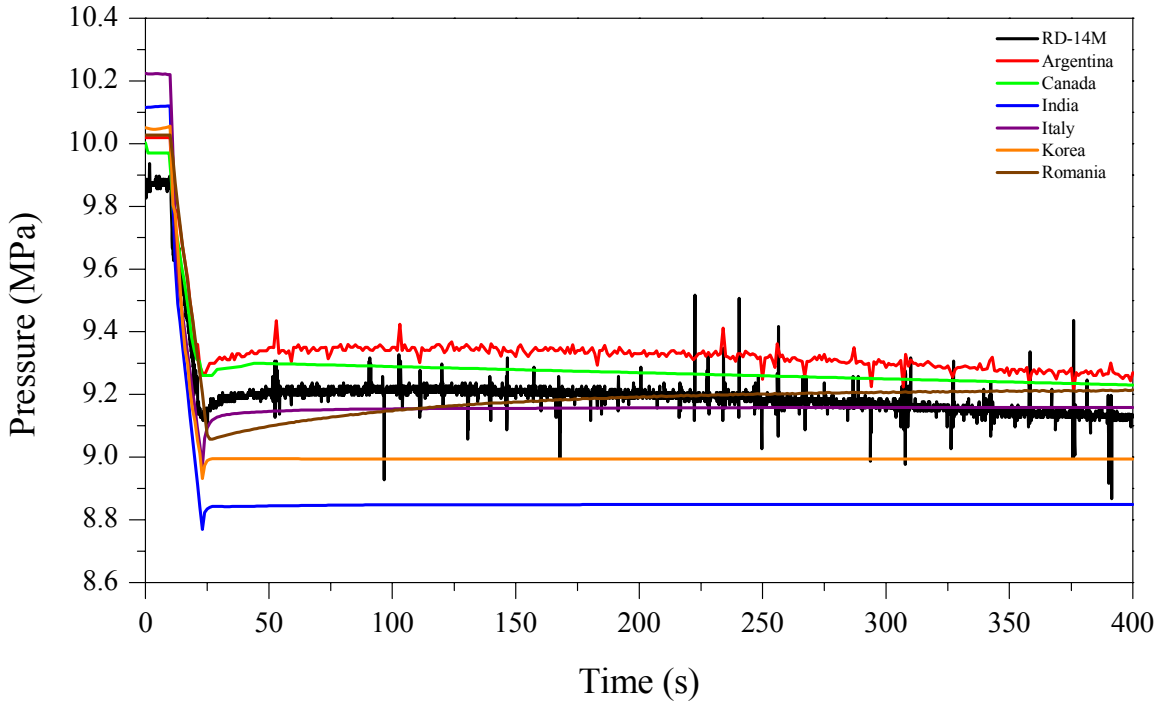

Fig. 5.47. Pressurizer Pressure.

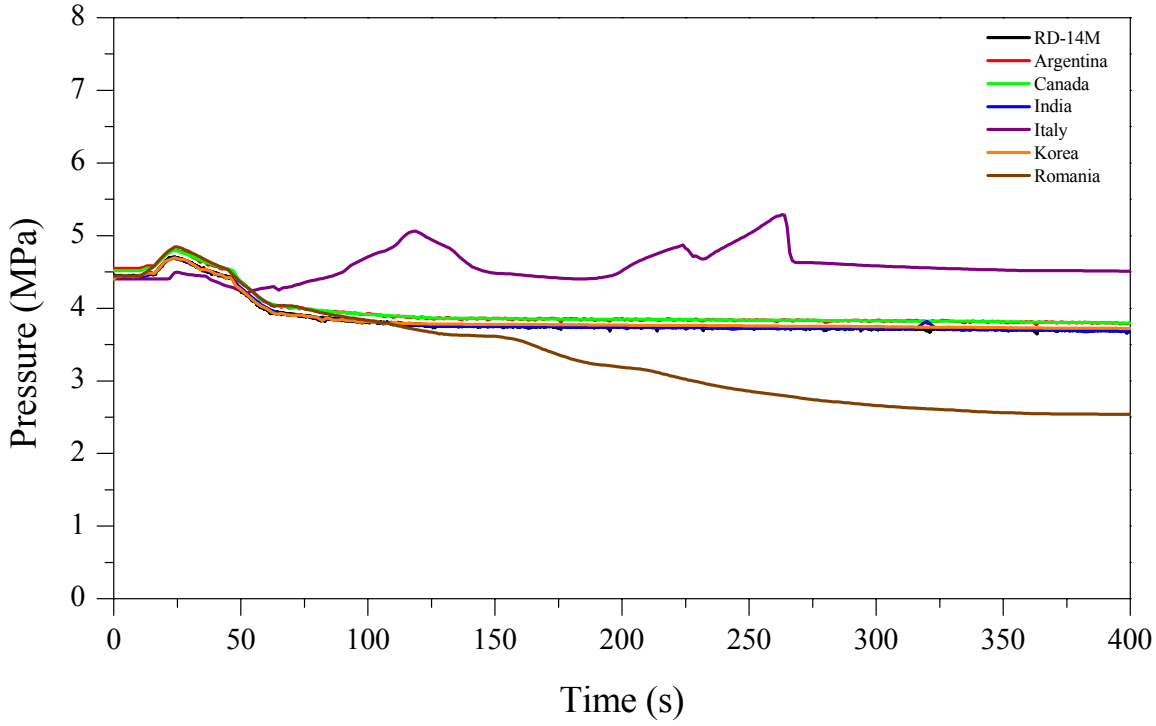

Fig. 5.48. Boiler 1 Drum Pressure.

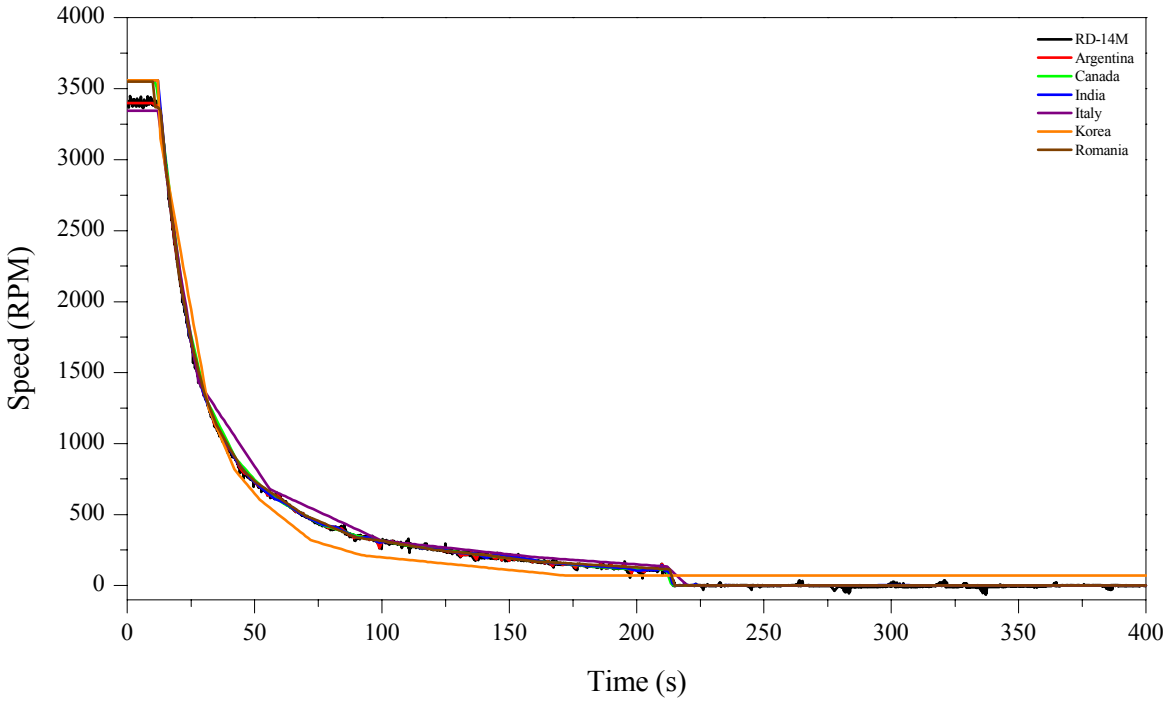

Fig. 5.49. Pump 1 Speed.

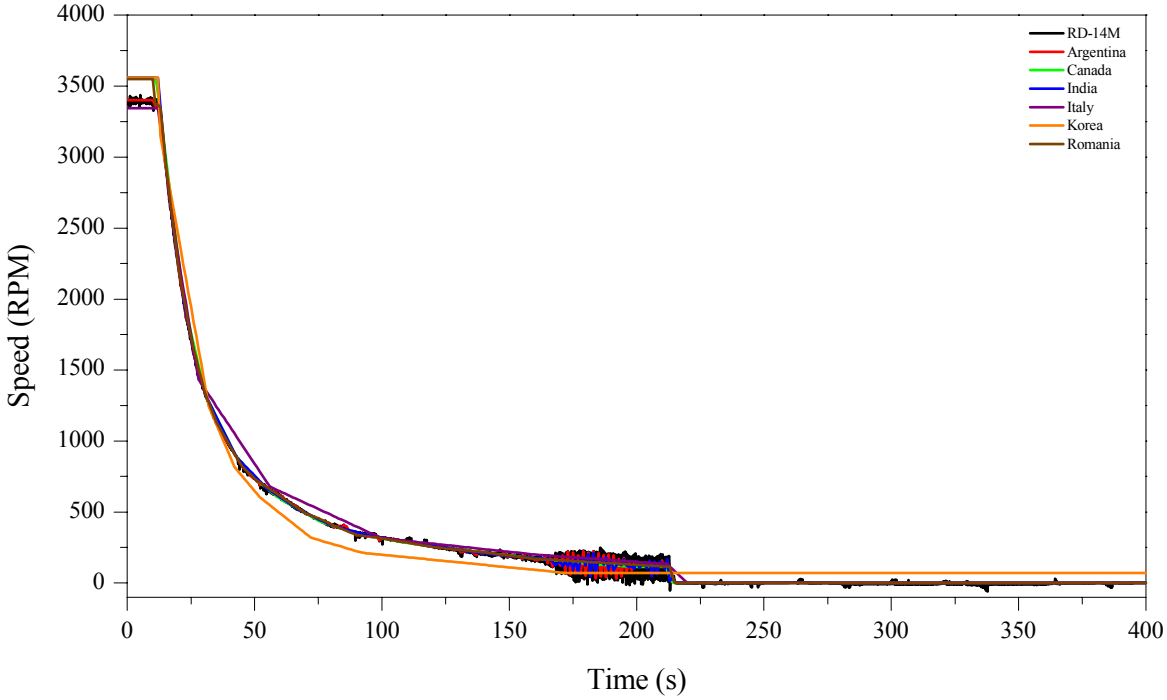

Fig. 5.50. Pump 2 Speed.

5.14. Variables to be Compared From Code-to-Code

The following variables are important for this code intercomparison activity. Unfortunately, there is no experimental data available in test B9401 to be compared to these variables. The only alternative is to compare the results predicted by each code. These variables are:

Break Discharge Mass Flowrate, Q_{BRK}

This variable is the mass flowrate history at the break location. Figure 5.51 provides the comparison of code results. All calculations show similar trends, with a peak discharge of about 50 kg/s, and a long-term discharge (200–350 s) of about 10 kg/s.

The total system power is the sum of the power to each heated section. Figure 5.52 provides the comparison of code predictions. All calculations show the correct trend. It is noted that the Italian contribution shows the thermal power to the fluid (from the FES) while the rest show the power applied to the heaters (an experimental boundary condition).

Mass Inventory in Primary System, M

This is the total mass in the primary system that does not include the mass in the ECC tank and the ECC system piping, and does not include the mass in the Pressurizer and the Pressurizer line. Figure 5.53 shows all calculations have a similar mass at steady state, and most calculations show the correct trend to about 100 s; however, significant differences are observed after this time.

It is noted that the RD-14M loop volume is approximately 1.01 m^3, and coupled with the density distribution in the loop, will determine the mass inventory. Thus differences in the participant's prediction at steady state are due to the modelling of the loop volume and the temperature / density distribution around the loop.

The Italian contribution shows a larger mass inventory in the period from 40 s to 100 s due to reduced discharge during this time. Again this could be caused by the incorrect calculation of choked flow in the feeder system. For the period from 100 to 400 s, the Romanian and Korean calculations show a lower system inventory — due to increased break discharge.

Thermal Power Across Boiler 1 and 2, W_{TH1} and W_{TH2}

The thermal power across a boiler is the total heat removed from (or added to) the primary side the boiler. Figures 5.54 and 5.55 provide the comparison of code results. All calculations show the correct trend.

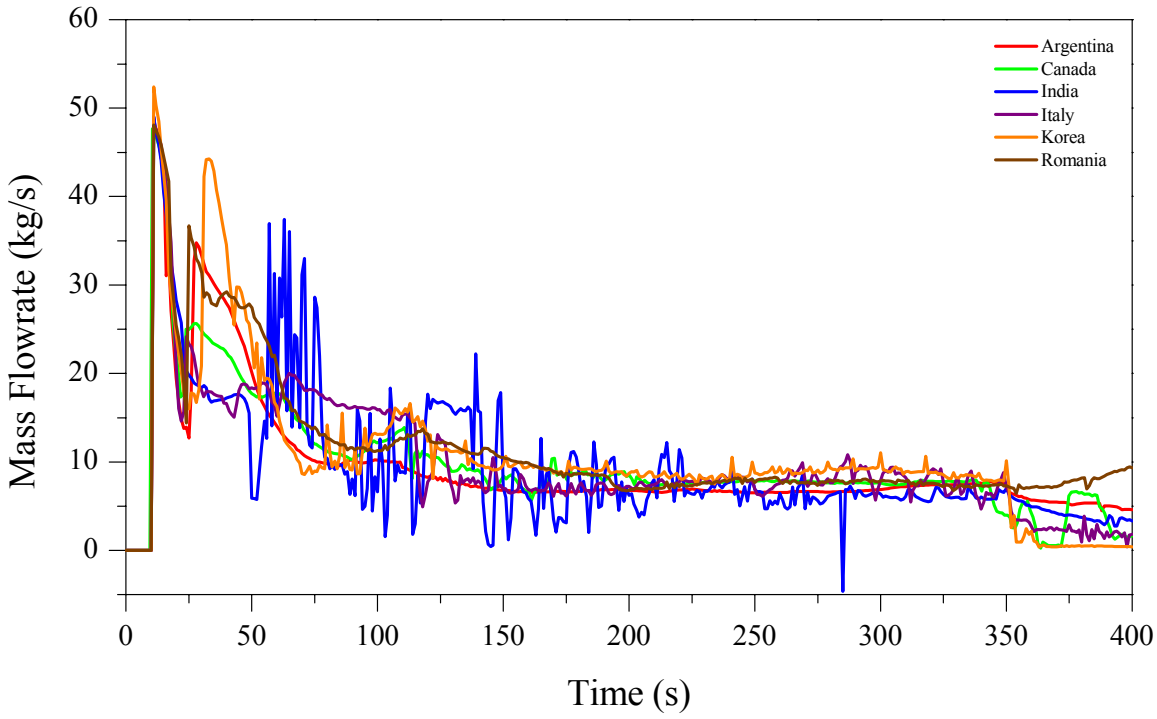

Fig. 5.51. Break Discharge Mass Flowrate.

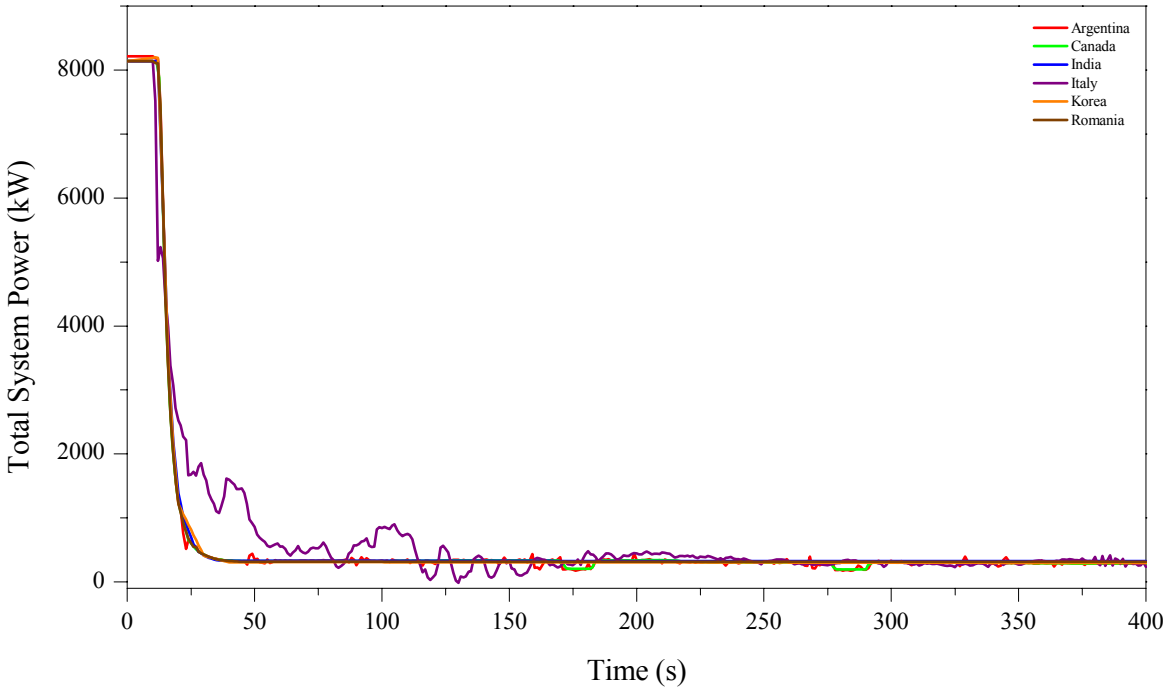

Fig. 5.52. Total System Power.

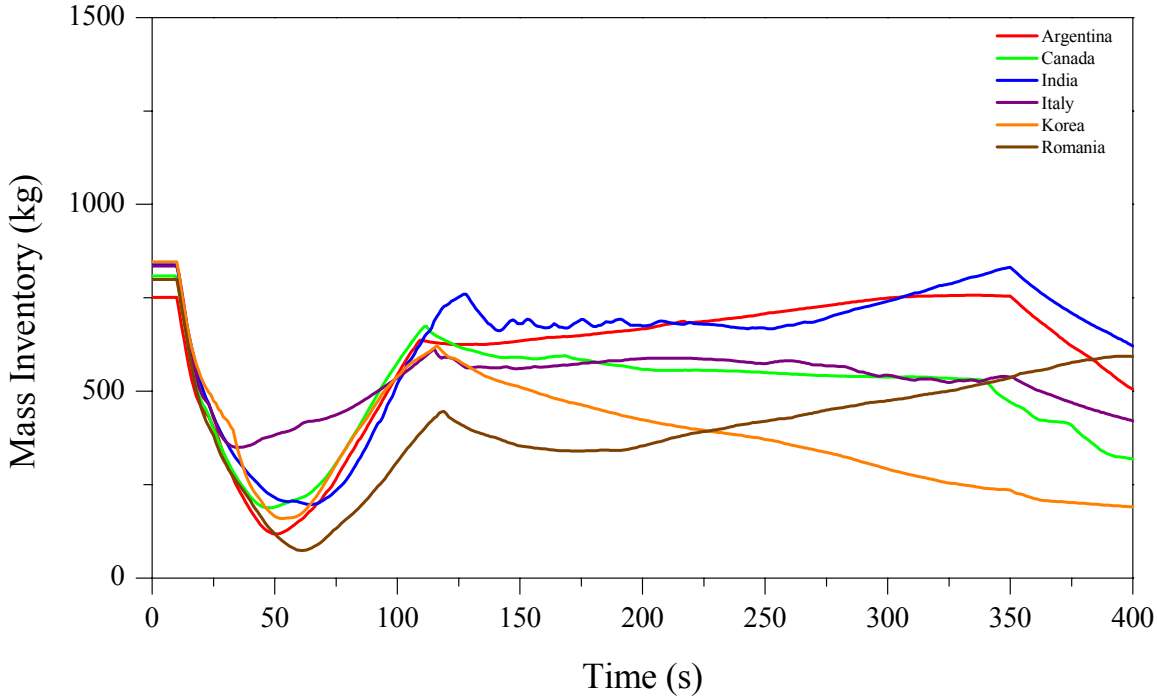

Fig. 5.53. Mass Inventory in Primary Loop.

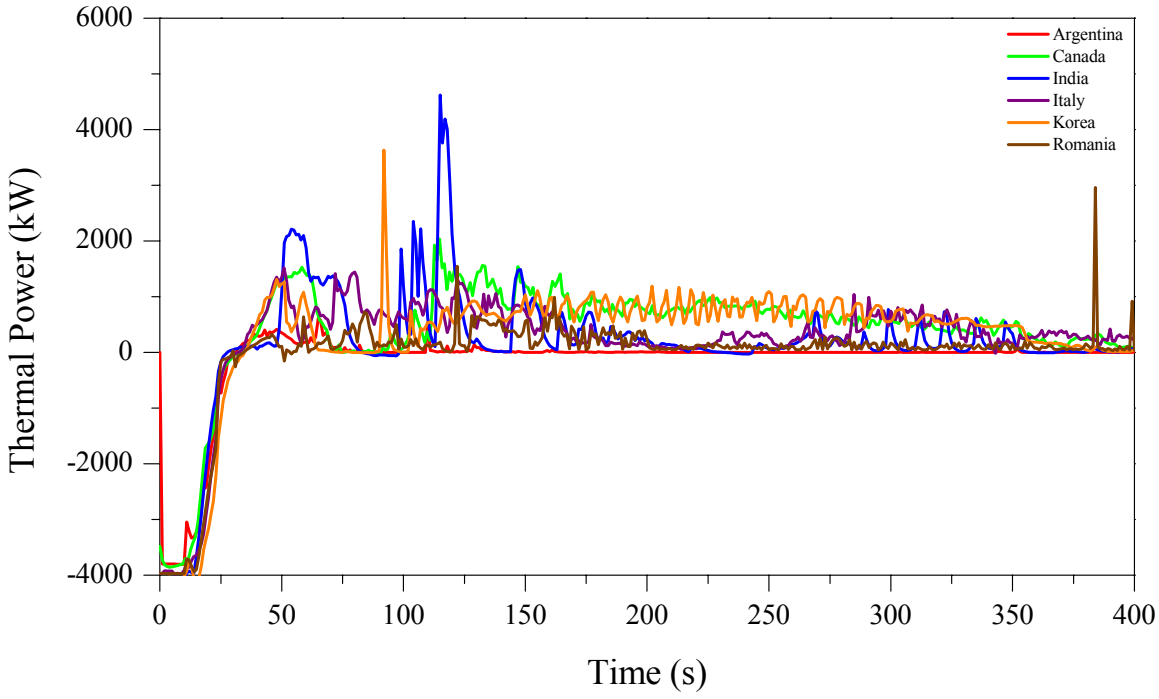

Fig. 5.54. Thermal Power Across Boiler 1

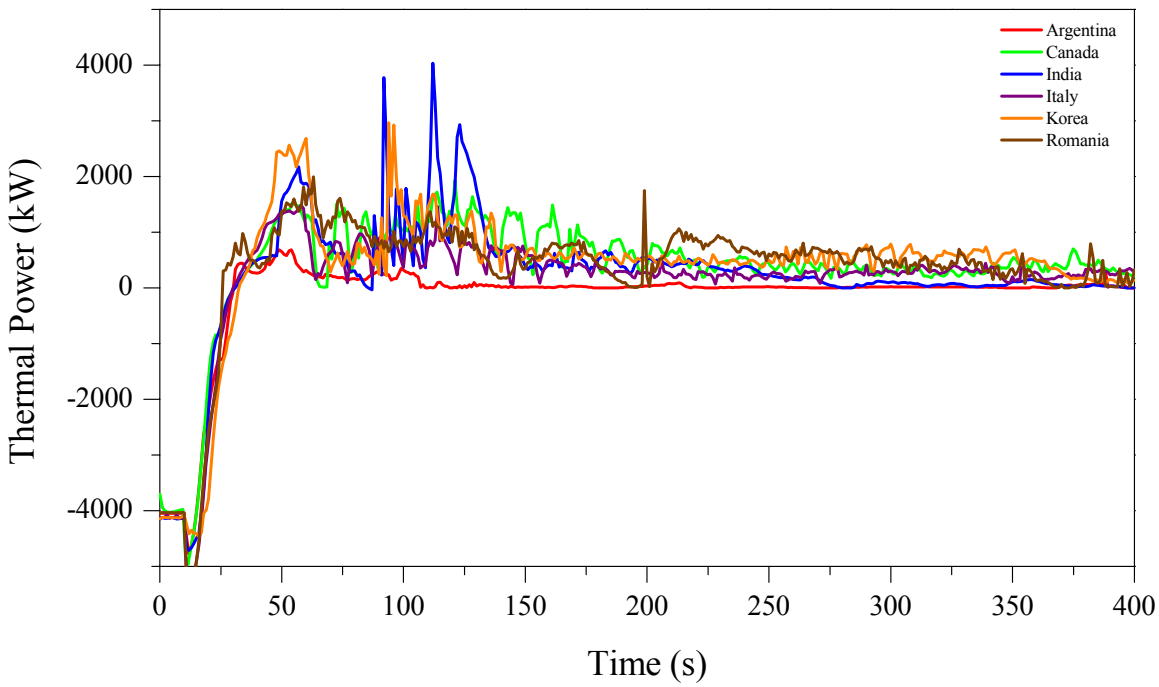

Fig. 5.55. Thermal Power Across Boiler 2

CHAPTER 6. EFFECT OF DELAYED ECC

6.1. Problem Description

RD-14M experiment B9401 was performed in a test facility subject to operating constraints such as maximum temperature. As a further test of the codes used in this exercise, a more challenging problem was devised — delaying the emergency core injection (ECC). This will result in higher FES temperatures, and a resulting refill of the channels at much higher temperatures. A further comparison of the codes used in this exercise was made with this problem. It is of course noted that no experimental data exists for this problem, and thus no comparisons with experiment can be made.

Initial Conditions:

The initial conditions for the problem are exactly the same as the first problem — for flowrates, pressures, temperatures, power history, etc

Boundary Conditions:

All boundary conditions remain the same as in the first problem (i.e. experimental conditions) – with the exception of ECC delivery. For this problem ECC injection is specified to start at 300 s (in the experiment it was at 20.6 s). When high-pressure ECC flow is terminated, low-pressure ECC is started and lasts for a period of 234.5 s.

6.2. Code-to-Code Comparison

For this problem a reduced set of calculated results is compared, and displayed in Figures 6.1 to 6.7:

- Pressure difference, Header 8 to Header 5,
- System pressure, Header 8,
- ECC flow to Header 8
- Integral of ECC,
- FES temperature at the top pin, middle of HS13,
- Flow, break discharge, and
- Mass inventory in Primary Loop

Five participants submitted contributions.

Figure 6.1 shows the comparison of Header 8 to Header 5 DP, and Figure 6.2 shows the pressure at Header 8. All calculations show similar trends. The Korean calculation shows somewhat lower flow during bout 400 s to 600 s, and this can be traced to the distribution of ECC flow during this period.

Figure 6.3 shows ECC flow to Header 8. Note that flow does not start to 300 s. All calculations show the proper trends. Again, differences between 400 s and 600 s are thought due to the distribution of ECC flow. Figure 6.4 shows the integrated ECC flow to all headers. Injection flow is terminated at approximately 600 s. All calculations show the same trends.

Figure 6.5 shows FES temperature at the top pin, middle of HS13. All calculations show the expected trends:

(1) the initial peak at about 25 s.,
(2) the heatup after about 150 s.,
(3) the quenching as ECC is delivered at 300 s, and
(4) a gradual rise at the end of the experiment.

Figure 6.6 shows the break flow, with all calculations producing similar results.

Figure 6.7 shows the Primary System inventory. All calculations show the proper trends of system emptying until ECC arrives, then an emptying again after ECC is terminated (~ 600 s.)

6.3. Conclusion

The results show that even with delayed ECC all codes predict that ECC is effective in cooling the channels, with no predicted asymmetry between channels. All major behaviours were similar between the codes.

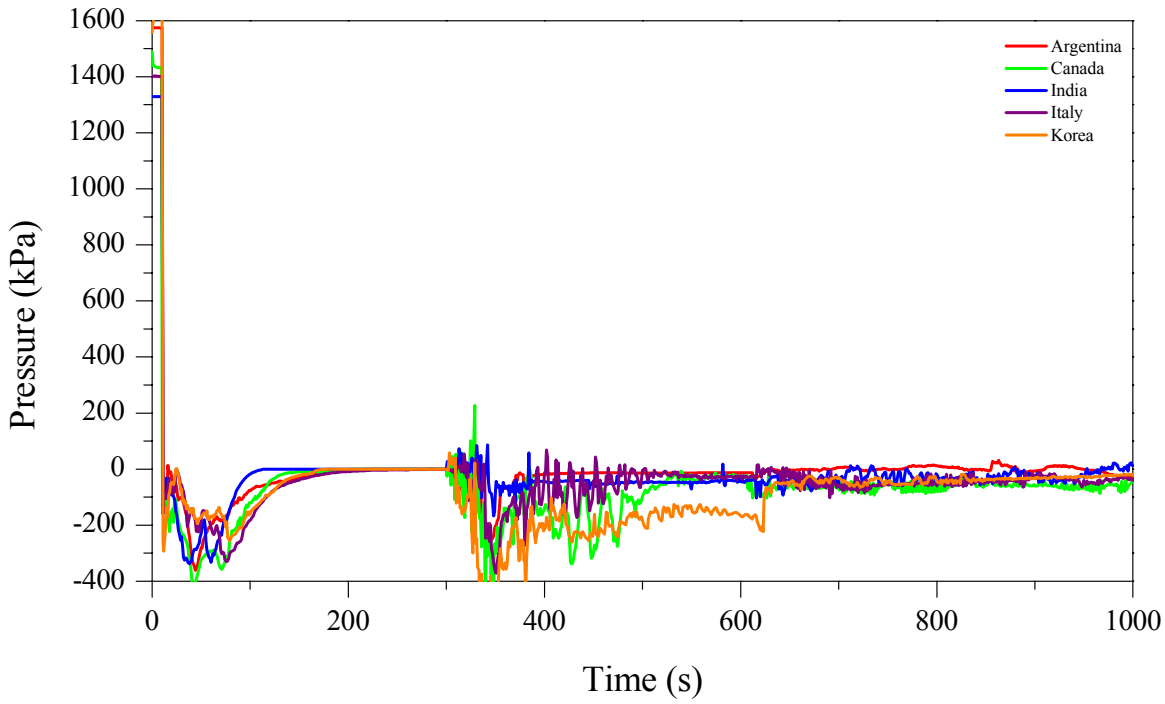

Fig. 6.1. Header 8 to Header 5 Differential Pressure, Delayed ECC.

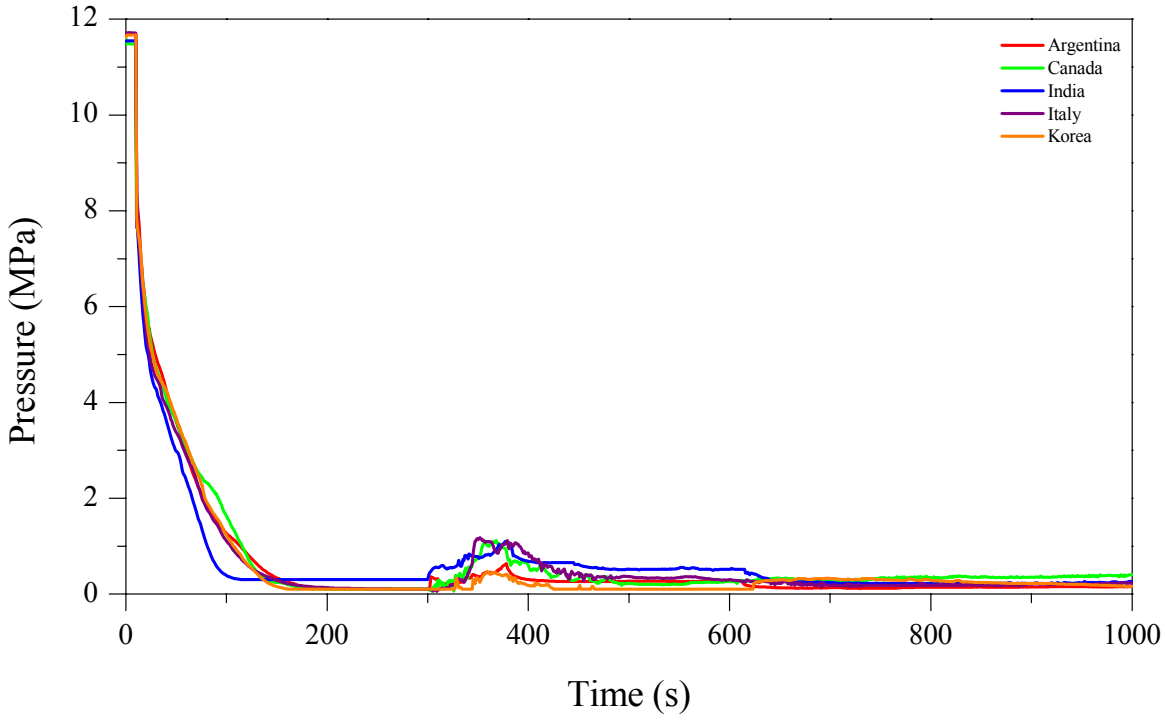

Fig. 6.2. Header 8 Pressure, Delayed ECC.

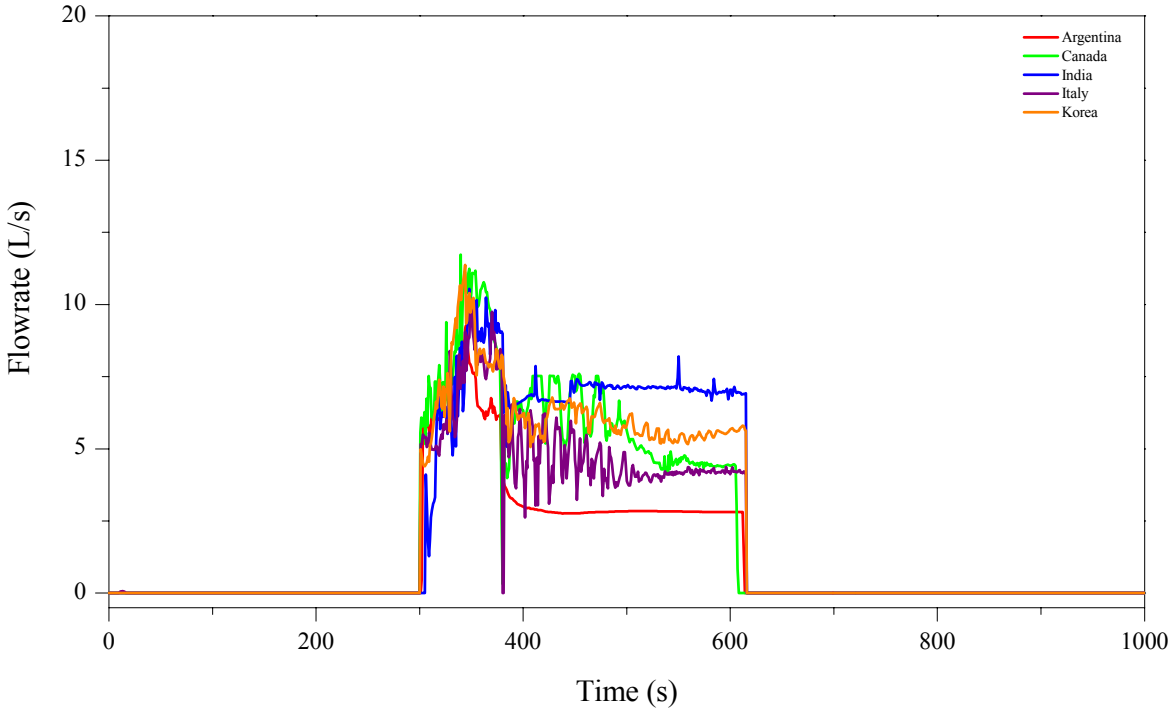

Fig. 6.3. ECC to Header 8 Flowrate, Delayed ECC.

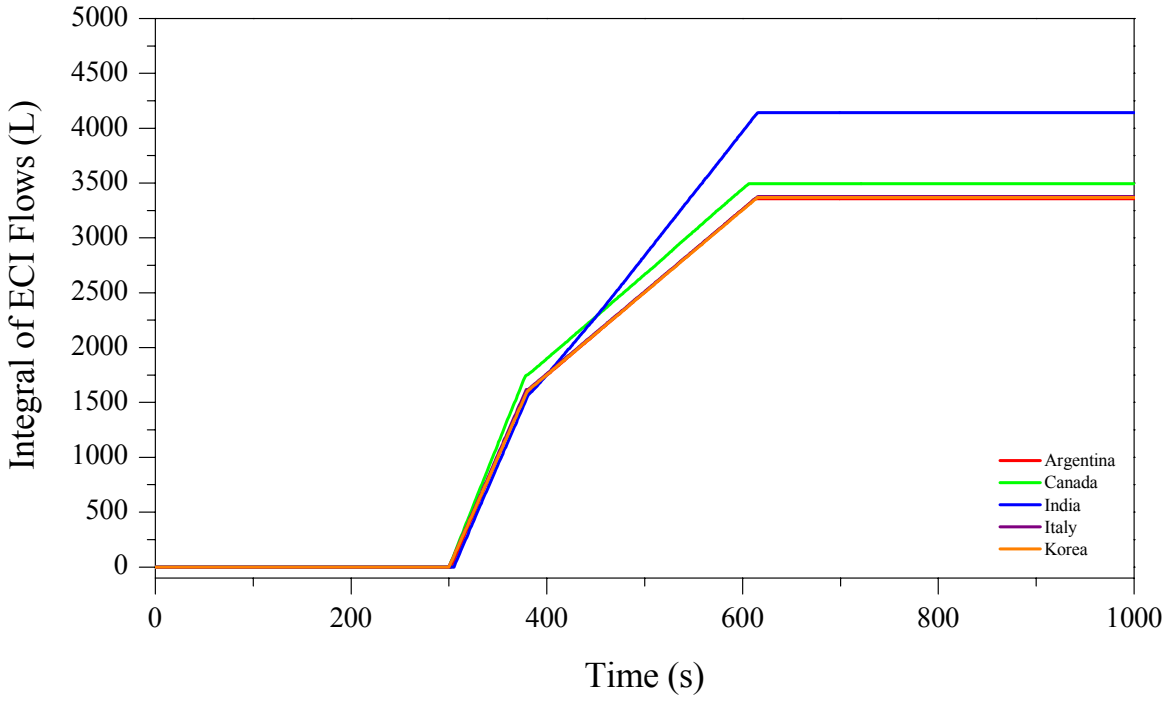

Fig. 6.4. Integral of ECI Flows, Delayed ECC.

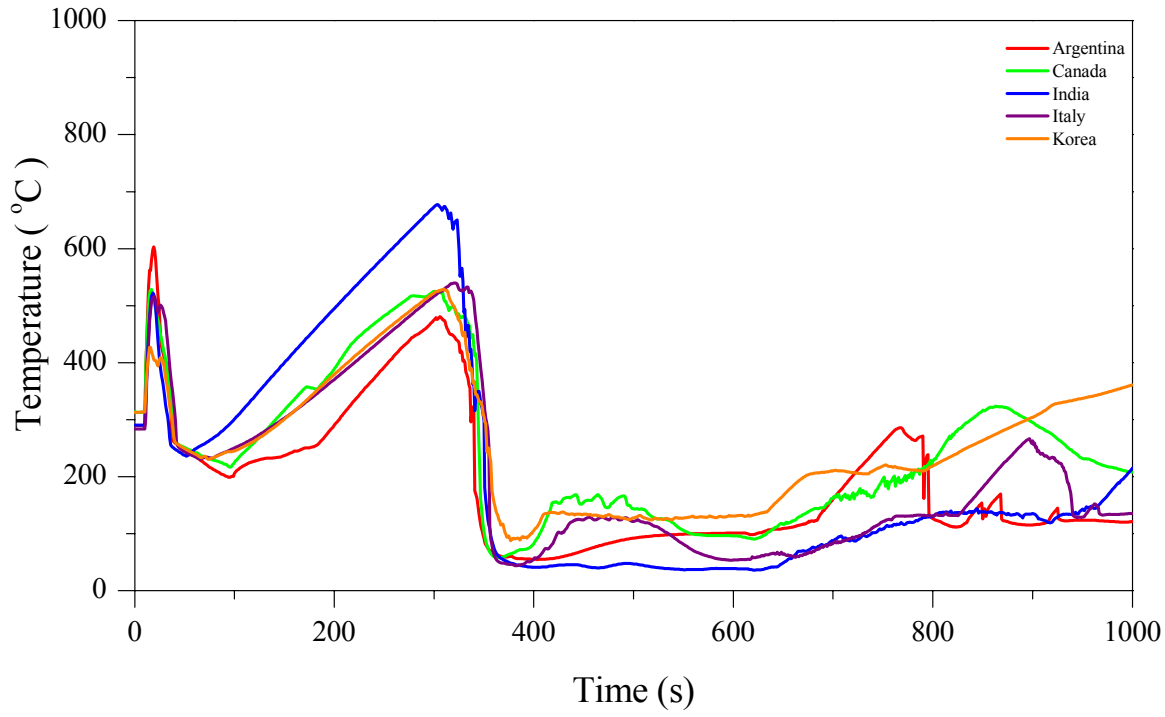

Fig. 6.5. FES Temperature at the Top Pin, Middle HS13, Delayed ECC.

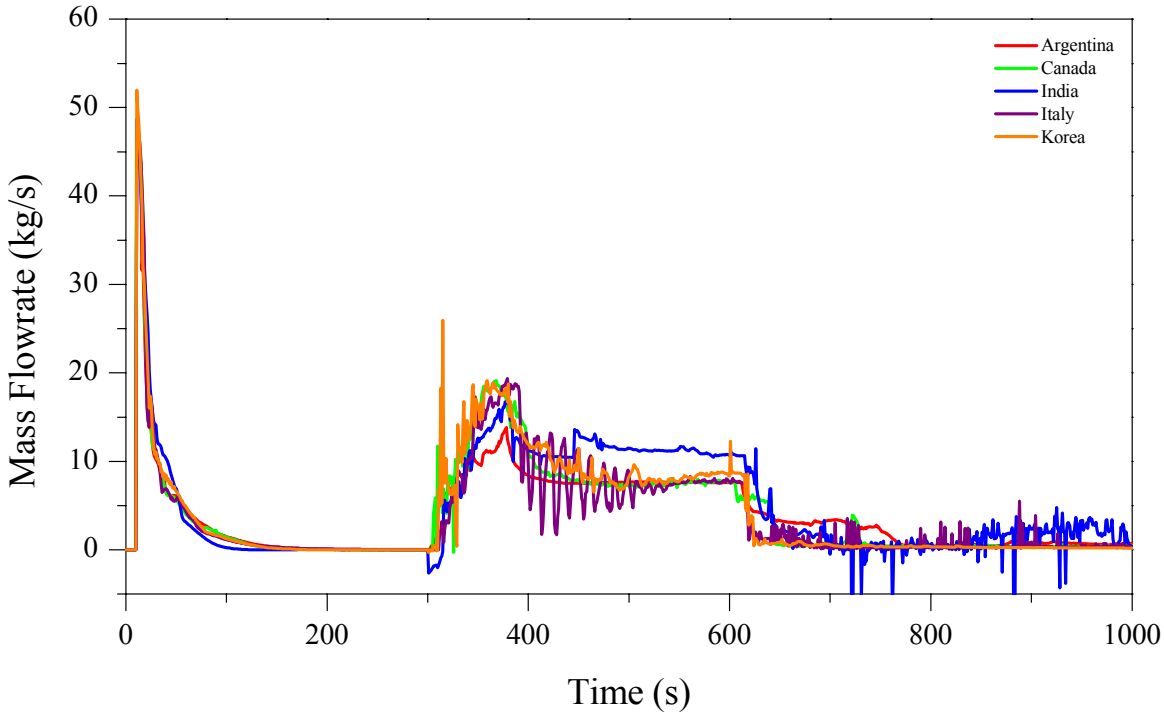

Fig. 6.6. Break Discharge Mass Flowrate, Delayed ECC.

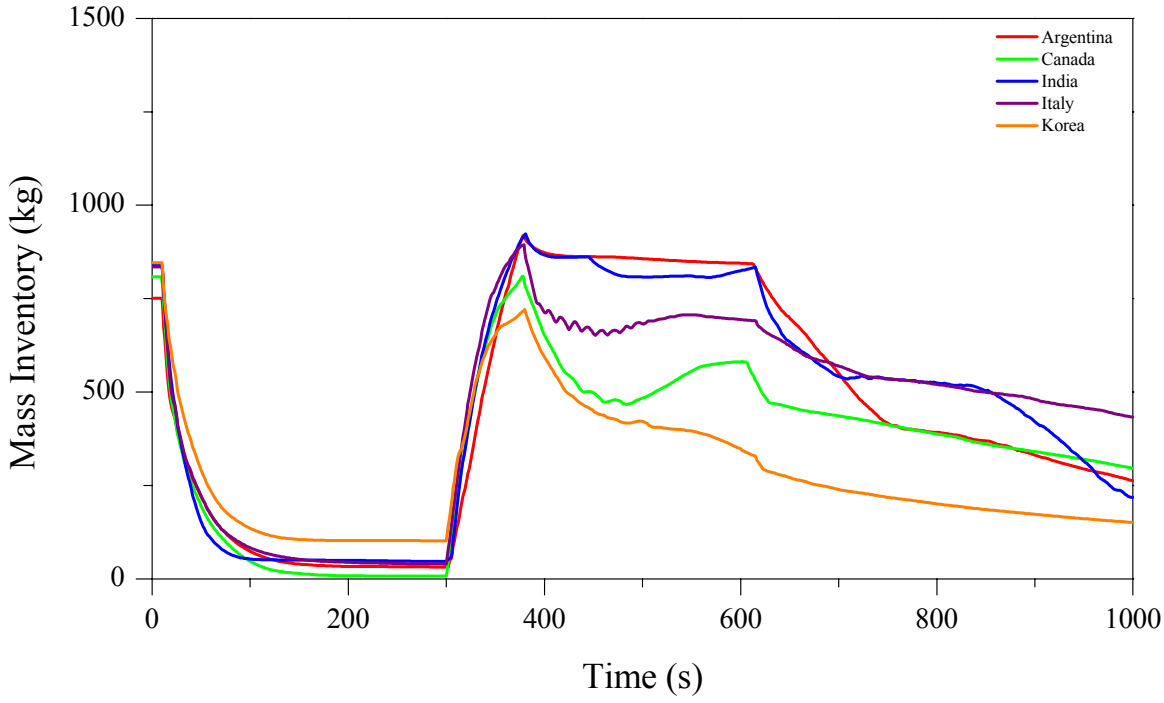

Fig. 6.7. Mass Inventory in Primary Loop, Delayed ECC.

CHAPTER 7. SUMMARY/CONCLUSIONS

The activity documented in this report deals with Large Break LOCA analysis in an HWR system. The reference experiment was performed in the RD-14M test loop located at the AECL Laboratories in Pinawa, Manitoba. This is the first international code to experiment exercise of this type in an HWR system and was made possible, within the framework of an IAEA project, by the availability of experimental data from AECL. The activity required significant resources from all participants and from the host institution (AECL, Chalk River) and was carried out in a manner similar to an ISP (International Standard Problem, within the OECD/CSNI framework).

The main features of the concerned RD-14M experiment, named B9401, are the limited temperature excursion shortly after the beginning of the LOCA (maximum rod surface temperature below 600 °C) and the demonstration that the ECC systems can fully recover the facility a few minutes after the occurrence of the break in one of the four headers. The geometric complexity of the concerned system represented a challenge for the adopted codes and the predictions: namely, the 'figure-of-eight' of the CANDU systems, the bends and the orifices inside the feeders and the configuration of the end fittings originated the main difficulties in the modeling. The transient pressure drops, the location of stagnation point, the possible occurrence of critical flow in orifices determined the fluid distribution into the loop and constituted the most difficult phenomena to be predicted.

Six different institutions adopting four different codes and six different idealizations (input decks) participated in the activity performing the post-test analysis of the B9401 experiment. It is worth noting that two codes, FIREBIRD and CATHENA have been originated within the HWR technology and two others, RELAP5/SCDAP and RELAP5/MOD3.2 (with the 'CANDU option' used by one participant), have been developed for Light Water Reactors. All codes are two-fluids six-equation codes, except FIREBIRD that is a three-equation code with the drift flux capability.

The following main conclusions can be derived from the exercise:

- All calculations were capable of achieving a steady state condition consistent with the experimental data apart from minor deviations that do not significantly affect the prediction of the transient scenario.
- All main phenomena (e.g. break discharge, system depressurization, temperature excursion and rewet in the heated sections) are qualitatively captured by the participants. Discrepancies in quantitative terms are observable and explainable but these do not affect the prediction of the overall system performance.
- The application of codes developed outside the HWR technology did not show any special deficiency in the comparison with the present experimental database. Therefore, it can be concluded that HWR systems do not need special tools for the analysis of benchmark experiments of this type.
- Notwithstanding the above, the existence of large spatial pressure gradients causes relevant void distribution effects including movements of liquid fronts that are un-typical in other systems. This requires special attention in the modeling.

- In addition, large discrepancies between measured and calculated trends of void fraction (e.g. Figures 5.36 and 5.37) derived from geometric complexities of some parts of the loop that cannot be simulated at a proper level of detail by currently available 1-D codes. However, it was found that such discrepancies were not significant in affecting the prediction of the overall system performance.
- The performed activity is relevant in assessing the capabilities of codes and permitted the quantification of the amount of discrepancy between measured and calculated values. This can be used to determine the uncertainty in predicting nuclear power plant scenarios.
- The need for qualified boundary and initial conditions is confirmed from the analysis of this experiment. An accurate representation of the ECC systems is necessary to correctly predict the fluid split among the various headers and consequently the fluid distribution into the system.
- The fluid stratification inside heated channels did not play an essential role in this experiment, although proper measurements were available (at different elevations in assigned horizontal channels) and codes have the capability to model gravitational effects inside horizontal channels (however, no proof was achieved of the quality of these models).
- No difference, at the overall system behaviour scale, could be characterized in terms of quality of prediction between six-equation and three-equation codes. This emphasizes the conclusion that stratification and non- equilibrium effects were not relevant in this accident scenario.
- The prediction of critical flow at the break and possibly at other locations (e.g. orifices in feeders or in end fittings) apparently causes deviations betwen measured and calculated trends of pressure and pressure drops.
- The exercise has not been immune from code user effects.

The participants received great benefit from the analysis of this experiment having had the opportunity of direct contacts with developers of HWR technology and the transfer of information that is not available in open literature. Moreover, they increased the confidence in the prediction capabilities by system codes and achieved a better understanding of physical phenomena related to HWR transient scenarios.

The exercise confirmed the importance of having built and operated complex facilities like RD-14M and showed, within an international context, the quality level achieved by some computational tools developed within the HWR technology. In addition, this was an opportunity for the AECL to assist scientists of HWR owner Countries in performing state of the art quality accident analyses.

Separate conclusions have been achieved from the analysis of an ‘extreme scenario’ designed on the basis of the B9401 experiment (i.e. delaying the time of ECC actuation). These conclusions are discussed in chapter 6 of this report.

CHAPTER 8. RECOMMENDATIONS

(1) The database constituted by the codes, the idealizations (input decks including sketches), the initial and boundary conditions (including the information about the RD-14M facility), the measurements and the calculation results, should be archived and will constitute a reference for future generations of codes and of scientists.

(2) Accuracy of the results should be quantified by applying tools aready available for this purpose to the database, including measurements and calculation.

(3) The experimental database should be used for qualifying HWR nuclear power plant nodalizations.

(4) It is highly recommended to repeat an activity like the one here documented. Areas of largest interest for future investigations include simulations of 'power-pulse' (i.e. following large break LOCA occurrence owing to positive power feedback) and of 'high' rod surface temperature (i.e. 1000°C in order to address code capabilities under such conditions).

REFERENCES

[1] R.S. SWARTZ, "An RD-14M Experiment for the Intercomparison and Validation of Computer Codes for Thermalhydraulic Safety Analyses of Heavy Water Reactors", Atomic Energy of Canada Limited Report, RC-2491, 2000 June.

[2] M.R. LIN, S. PRAWIROSOEHARDJO, "FIREBIRD-III MOD1 Program Description", AECL Internal Report, TDAI-373, 1984 November.

[3] B.N. HANNA, 1998, CATHENA: A thermalhydraulic code for CANDU analysis, *Nuclear Engineering and Design* **(180)** 113-131.

[4] J. KESTIN, J.V. SENGERS, B. KAMGAR-PARSI AND J.M.H. LEVELT, 1982, "Thermophysical Properties of Fluid H_2O", *Journal of Physical and Chemical Reference Data*, Vol. 13, No. 1, pp. 175-183.

[5] P.G. HILL, R.V. MACMILLAN AND V. LEE, 1981, "Tables of Thermodynamic Properties of Heavy Water in S.I. Units", Atomic Energy of Canada Limited Report, AECL-7531.

[6] K.E. CARLSON, R.A. RIEMKE, S.Z. ROUHANI, R.W. SHUMWAY, W.L. WEAVER, AND EDITORS: C. M. ALLISON, C.S. MILLER, N.L. WADE, *"RELAP5/mod3 Code Manual Volume I: Code Structure, System Models, and Solution Methods"*, US NRC NUREG/CR-5535, Washington (DC, USA) June 1990 (see also Vols. II to V).

[7] F. D'AURIA, G.M. GALASSI, *"Code Validation and Uncertainties in System Thermalhydraulics",* J. Progress in Nuclear Energy, Vol. 33 Nos. 1&2, 1998, pages 175-216.

[8] F. D'AURIA, N. DEBRECIN, G.M. Galassi, *"Outline of the Uncertainty Methodology Based on Accuracy Extrapolation",* J. Nuclear Technology, Vol. 109 No. 1, 1995, pages 21-38.

[9] R. BOVALINI, F. D'AURIA, G.M. GALASSI, *"Scaling of Complex Phenomena in System Thermalhydraulics"*, J. Nuclear Science and Engineering, Vol 115, Oct. 1993, pages 89-111.

[10] F.D'AURIA, G.M. GALASSI, M. LEONARDI, R. GALETTI, *"Application of the Fast Fourier Transform Method to Evaluate the Accuracy of SBLOCA Database",* NURETH-8 Int. Conf. Kyoto (J), Sept. 30 – Oct. 4, 1997.

[11] R. BOVALINI, F. D'AURIA, *"Scaling of the Accuracy of RELAP5/mod2 Code"*, J. Nuclear Engineering and Design, Vol 139, No. 2, 1993, pages 187-204.

[12] F. D'AURIA, G.M. GALASSI, P. VIGNI, A. CALASTRI, *"Scaling of Natural Circulation in PWR Systems",* J. Nuclear Engineering and Design, Vol 132, No. 2, 1992, pages 187-206.

[13] F. D'AURIA, G.M. GALASSI, *"Results from the Analysis of RD-14M Test B-9401 by RELAP5 and Proposal for Quantities to be Considered in the ComparisonRreport",* University of Pisa Report, DIMNP - NT 432(01), Pisa (I), April 2001. IAEA AGM on Intercomparison and Validation of Computer codes for Thermalhydraulic Safety Analyses of Heavy Water Reactors – Vienna (A), May 2-4, 2001.

[14] F. D'AURIA, G.M. GALASSI, *"Final Results from the Analysis by RELAP5 Code of the RD-14M Test B-9401",* University of Pisa Report, DIMNP - NT 471(02), Pisa (I), July 2002, IAEA Advisory Group on Intercomparison and Validation of Computer Codes for Thermalhydraulic Safety Analyses of Heavy Water Reactors – Vienna (A), Dec. 2-4, 2002.

[15] H.Q. ZHOU, "Intercomparison and Validation of Computer Codes for RD-14M Experiments B 9401: Variables to be Compared", RC-2600(Rev. 1), 2002 November.

CONTRIBUTORS TO DRAFTING AND REVIEW

Adam, N.	Karachi Nuclear Power Complex, Pakistan
Bedrossian, G.	National Atomic Energy Commission, Argentina
Cho, Y.J.	Republic of Korea Institute of Nuclear Safety, Republic of Korea
Cleveland, J.	International Atomic Energy Agency
D'Auria, F.	Universita Dedli Studi di Pisa, Italy
Galassi, G.M.	Universita Dedli Studi di Pisa, Italy
Gersberg, S.	CNEA, Argentina
Gupta, S.K.	Bhabha Atomic Research Centre, India
Istrate, R.	Cernavoda NPP Unit 1, Romania
Jifcu, P	Cernavoda NPP Unit 1, Romania
Lee, S.H.	Republic of Korea Institute of Nuclear Safety, Republic of Korea
Lyon, R.	International Atomic Energy Agency
Richards, D.L.	Atomic Energy of Canada Limited, Canada
Swartz, R.	Atomic Energy of Canada Limited, Canada
Zhou, H.	Atomic Energy of Canada Limited, Canada